NASA CONTRACTOR REPORT

NASA CR-933

A THREE-DIMENSIONAL HARD SPHERES THEORY OF SCATTERING OF GAS ATOMS FROM A SOLID SURFACE

by Frank O. Goodman

Prepared by
MASSACHUSETTS INSTITUTE OF TECHNOLOGY
Cambridge, Mass.
for

NATIONAL AERONAUTICS AND SPACE ADMINISTRATION • WASHINGTON, D. C. • NOVEMBER 1967

A THREE-DIMENSIONAL HARD SPHERES THEORY OF SCATTERING OF GAS ATOMS FROM A SOLID SURFACE

By Frank O. Goodman

Prepared under Grant No. NGR 22-009-021 by
MASSACHUSETTS INSTITUTE OF TECHNOLOGY
Cambridge, Mass.

for

NATIONAL AERONAUTICS AND SPACE ADMINISTRATION

For sale by the Clearinghouse for Federal Scientific and Technical Information
Springfield, Virginia 22151 – CFSTI price $3.00

A THREE-DIMENSIONAL HARD SPHERES THEORY OF SCATTERING OF GAS ATOMS FROM A SOLID SURFACE

By Frank O. Goodman

ABSTRACT

A three-dimensional model of the interaction of monatomic gases with solid surfaces is described. The solid surface is represented by similar, non-interacting, hard spheres, the centers of which form initially a regular two-dimensional array; an incident gas atom is represented by a hard sphere incident on this array. Collisions between the gas atom and the surface atoms obey the ordinary laws of classical hard spheres. The closely-related problems of (i) the detailed velocity distribution of the gas atoms reflected from the surface, (ii) the energy and momentum accommodation coefficients and (iii) the forces exerted on a target by a directed gas beam, are discussed and illustrated by means of a fairly comprehensive set of results.

ACKNOWLEDGMENTS

The calculations for this work were done in (i) The Department of Electronic Computing, University of Aberdeen, Scotland; (ii) the Computation Center of the Massachusetts Institute of Technology, Cambridge, Massachusetts, under problem number M4443 and; (iii) the Basser Computing Department of the School of Physics, University of Sydney, New South Wales.

The author wishes to thank all those at M.I.T. (especially Professors Leon Trilling and Robert E. Stickney) who were concerned with his invitation there as Visiting Professor during the year 1965-1966. Most of this work was done with the helpful encouragement of Professors L. Trilling, R.E. Stickney and H.Y. Wachman.

The author is indebted to the Government of the Commonwealth of Australia for the award of a Queen Elizabeth II Research Fellowship, during the tenure of which the work was completed.

INTRODUCTION

A three-dimensional (3D) model of the interaction of monatomic gases with solid surfaces is described; some preliminary results were presented at the Fifth International Symposium on Rarefied Gas Dynamics[1] in July 1966.

The solid surface is represented by similar hard spheres, the centers of which form initially a regular 2D array. These surface spheres are free and initially at rest and do not interact with each other in any way (the interaction potential between any pair is a constant). An incident gas atom is represented by a hard sphere (of a kind different from the surface spheres) incident on the array of surface spheres. The type, denoted by S, of this array is arbitrary, although only two have been used by the author; these are shown in Fig. 1.1 and are (i) a square array (S = square) representing, for example, the (100) face of a BCC or FCC crystal and (ii) an equilateral triangular array (S = triangular) representing the (111) FCC crystal face. The fundamental length, ℓ, of the surface array (that is, the side of the basic square or of the basic rhombus; see Fig. 1.1) is chosen to correspond to the surface of interest, as are the mass, m, and the radius, r_s, of a surface sphere. Similarly, the mass, M, and the radius, r_g, of the incident sphere are chosen to correspond to the gas of interest. In fact, the values of r_s, r_g, ℓ, M and m separately are unimportant, as only the dimensionless quantities $(r_s + r_g)/\ell$ and M/m enter the problem.

The gas atom must be sufficiently large so as to be unable to pass through the "holes" in the initial surface array (hence $r_s + r_g > \ell/\sqrt{2}$ for S = square and $r_s + r_g > \ell/\sqrt{3}$ for S = triangular) and it must be lighter than a surface atom. Collisions between the incident gas atom and the surface atoms obey the ordinary laws of classical hard spheres. A rule for the motions of the surface atoms subsequent to collisions must be invoked; this rule is that, immediately after a surface atom is struck by the gas atom, the surface atom is replaced in its initial position at rest. Hence, all collisions of the gas atom occur with surface atoms which are initially stationary and in their initial equilibrium positions. The incident gas atom may undergo several collisions with the surface atoms (but never two successive collisions with the same surface atom) before it is finally "reflected" from the surface.

The "aiming point" of the gas atom on the surface is defined by the coordinates, x and y, at which the initial path of the center of the incident gas atom intersects the plane containing the 2D array of surface atom centers. The center of one of the surface atoms is arbitrarily chosen as origin, and x and y are measured in rectangular (90°) axes for S = square, and in oblique (60°) axes for S = triangular, along the sides of the basic square and rhombus respectively; this is illustrated in Fig. 1.1.

The velocity of the gas atom is defined by its speed, v, and by the polar angles, θ and ϕ: $\phi = 0$ is taken along the x-axis (see Fig. 1.1) and θ is measured relative to the normal outward from the surface.

Eight parameters enter into the calculation of the interaction of the gas atom with the surface (that is, the calculation of the final velocity, defined by v, θ and ϕ, of the gas atom). These are

(1) The mass ratio,

$$\mu = M/m \tag{1.1}$$

(2) The distance, $r_s + r_g$, of closest approach of the centers of the gas atom and a surface atom, divided by the fundamental array length, ℓ,

$$R = (r_s + r_g)/\ell \tag{1.2}$$

(3) The type, S, of the array

(4-6) The initial velocity of the gas atom, defined by v_o, θ_o and ϕ_o, and

(7-8) the coordinates, x and y, of the aiming point, divided by ℓ,

$$X = x/\ell \quad \text{and} \tag{1.3a}$$

$$Y = y/\ell \tag{1.3b}$$

It is a property of the model that:

(a) v is directly proportional to v_o, and

(b) θ and ϕ are independent of v_o,

so we may set $v_o = 1$ with no loss of generality and calculate

$$V = v/v_o = v \tag{1.4}$$

Except for the rule about replacing surface atoms after collisions, the model is regarded as a "hard spheres limit" of other models (for example, the models of Refs. 2-6; the hard spheres limit is the limit as the initial speed of the incident gas atom becomes large). Because of this, some of the results have recently been used, with some success, by Goodman and Wachman[7].

The five parameters μ, R, S, θ_o and ϕ_o are chosen to correspond to the experimental geometry and to the gas-solid system of interest, and several trajectories are calculated for this choice of these parameters; the aiming points of these trajectories are uniformly distributed over the ranges $0 < X < 1$ and $0 < Y < 1$. The aiming point (p, q) is defined by the coordinates

$$X = (2p - 1)/2n \; ; \quad p = 1(1)n \tag{1.5a}$$

and

$$Y = (2q - 1)/2n \; ; \quad q = 1(1)n \tag{1.5b}$$

and the total number of points (trajectories) is n^2; n is regarded as another parameter as calculated values of accomodation coefficients depend (acs) in general on n for small n.

Two different types of calculations have been done using the model; these are labelled "microscopic" and "macroscopic" respectively.

MICROSCOPIC CALCULATIONS

2.1 Description of the Calculations

These are calculations of the detailed velocity distribution of the gas atoms reflected from the surface. For given n, these calculations give a maximum of information which is obtainable from the model. The reflected gas atoms are sorted into "boxes", each box defining an increment of velocity space. The possible ranges of V and cos θ (both 0-1) are each divided into 10 equal increments, and that of ϕ(0-360°) into 36 equal increments, giving a total of 3600 different boxes. Each box, therefore, covers an increment of solid angle of $\pi/180$ steradians and an increment of V of 0.1. N denotes the number of gas atoms reflected into a box and E their mean energy; the initial energy, E_o, and the mass, M, of a gas atom are set equal to unity and 2 respectively with no loss of generality:

$$2E_o = M = 2 \tag{2.1}$$

The mean energy of all the reflected gas atoms is denoted by $\mathcal{E}$:

$$\mathcal{E} = \overline{V^2} = \sum_{\text{boxes}} NE / \sum_{\text{boxes}} N = \sum_{\text{boxes}} NE/n^2 \qquad (2.2)$$

A great advantage of the model over other models[2-6] is that it enables a much larger number of trajectories to be calculated. It is found, in fact, that n = 100 (10000 trajectories) is not sufficiently large to obtain a "smooth distribution" in many cases; n = 150 (22500 trajectories) is chosen for the main series of calculations, although even with this number a smooth distribution is not obtained in every case (see below).

The main series of calculations is for the five gas-solid systems He, Ar and Xe on W and He and Ar on Ni, with S = square, ϕ_o = 20° and θ_o = 112.5° (22.5°) 180°. For each of these systems the sum, $r_s + r_g$, is estimated by equating it to a Lennard-Jones parameter, λ, appropriate to the gas-solid system; λ is defined by

$$W(u) = 4\varepsilon[(\lambda/u)^{12} - (\lambda/u)^6] \qquad (2.3)$$

where W(u) is the interaction potential of the gas and surface atoms when their separation is u. Therefore, using (1.2), we write

$$R = \lambda/\ell \qquad (2.4)$$

Values of μ are calculated from the atomic masses quoted in Ref. 8, and the method used for the estimation of R is described in the Appendix; the chosen values of μ and R appear in the Table. Only results for He, Ar and Xe on W at θ_o = 112.5°, 135° and 180° are discussed in this Report.

Results are presented in the form of "scans" over the reflected distribution; these scans are of two distinct types. The first type is over a plane, defined by the two ϕ-values ϕ' and $\phi' + 180°$, perpendicular to the solid surface, resulting in values of $N(\theta)$, $E(\theta)$, etc. at fixed ϕ; the second type is over the surface, defined by $\theta = \theta'$, of a cone, the axis of which is perpendicular to the solid surface, resulting in values of $N(\phi)$, $E(\phi)$, etc. at fixed θ. We ignore the speed distribution of reflected atoms for the moment. In order to get non-zero numbers of gas atoms scattered into the "planes" and "surfaces of cones", we consider those gas atoms scattered into certain ranges of ϕ and of θ respectively. When we scan over the half-plane, ϕ', we consider all gas atoms scattered into the 10° ϕ-range $\phi'-5° < \phi < \phi' + 5°$: when we scan over the surface, θ', of a cone, we consider all gas atoms scattered into the range of θ giving a range of 0.1 in cos θ and centered approximately at the

value $\theta = \theta'$. Results for $N(\theta)$ and $N(\phi)$ are presented in the form of histograms; the histogram increments in θ for the $N(\theta)$ results are those increments which give increments of 0.1 in $\cos\theta$, and the histogram increments in ϕ for the $N(\phi)$ results are each of 10°. Thus each histogram increment, both in the results for $N(\theta)$ and for $N(\phi)$, covers 1/10 of θ-space and 1/36 of ϕ-space, resulting in a coverage of a solid angle of $\pi/180$ steradians (the same as one of the above "boxes").

In the results for $E(\theta)$ and $E(\phi)$, it is assumed that the mean energy of the atoms scattered into each of the above histogram increments is that corresponding to atoms scattered exactly at the "center" of the increment. This center is calculated with respect to $\cos\theta$ and to ϕ respectively; for example, the center of the increment for which $0.2 < \cos\theta < 0.3$ and $10° < \phi < 20°$ is defined to be at $\theta = \arccos 0.25$, $\phi = 15°$. Straight lines are then used to join the resulting discrete points in the $E(\theta)$ and $E(\phi)$ plots.

Two planes are scanned in each case. For $\theta_0 \neq 180°$ (non-normal incidence), these are the "specular plane" and the "transverse plane" respectively; the specular plane is defined by the two ϕ-values $\phi = \phi_0 + 90° \pm 90°$ and the transverse plane by $\phi = \phi_0 \pm 90°$. [All the values $\phi \pm 360i°$ where i is any integer are considered to be identical.] For $\theta_0 = 180°$ (normal incidence), the two planes are (i) either of those parallel to a side of the basic square and (ii) either of those parallel to a diagonal; we choose the two planes $\phi = 90° \pm 90°$ and $\phi = 135° \pm 90°$.

One surface of a cone is scanned in each case. For $\theta_0 \neq 180°$, this is the "specular cone", defined by $\theta = 180° - \theta_0$. For $\theta_0 = 180°$, we choose the cone giving $\cos\theta = 0.7$ or $\theta \approx 45°$.

Very large values of n are required to get reasonably smooth distributions; n = 100 is insufficient in general and n = 150 is insufficient in some cases. A smoother distribution is obtained by halving the number of atoms scattered into twice the required range in each case. For example, to find $N(\theta)$ for the half-plane $\phi = 20°$ (defined here by the range $15° < \phi < 25°$), the number of reflected atoms in the range $10° < \phi < 30°$ is halved.

The results of scanning over the reflected distributions in the manner described above are shown for the systems He, Ar and Xe on W, in Figs. 2.1-2.7 for the scans over planes and in Figs. 3.1-3.5 for those over surfaces of cones. [Note that there is no scattering into the transverse plane when $\theta_0 = 112.5°$ for any of the systems and none when $\theta_0 = 135°$ for Xe-W.] For reasons of clarity in Figs. 2.1-2.7, θ is arbitrarily taken to be negative on one side of the surface normal and to be positive on the other;

these definitions are indicated in the figures.

The total number of gas atoms scattered into the particular plane or surface of cone under consideration is denoted in each figure by ΣN. As each histogram increment covers 1/360 of the hemisphere (see above), it follows that the value of $N(\theta)$ or of $N(\phi)$ averaged over all solid angles is about 0.28% in each of Figs. 2.1-2.7 and 3.1-3.5. Further, as each plane (two 10° ϕ-ranges) contains a solid angle equivalent to 1/18 of the hemisphere, the mean value $\overline{\Sigma N}$, of ΣN averaged over all planes is about 5.56% in each of Figs. 2.1-2.7. Similarly, each surface of a cone contains a solid angle equivalent to 1/10 of the hemisphere, so the value of $\overline{\Sigma N}$ for each of Figs. 3.1-3.5 is 10%.

The mean energy of the gas atoms scattered into the whole of the particular plane or surface of a cone under consideration is denoted by $\overline{E}$ in the figures; these values should be compared with the corresponding values, $\mathcal{E}$, of the mean energy of all the reflected gas atoms, defined by 2.2 and also shown in the figures.

We may note in passing that even with n = 150 and the "smoothing" procedure described above (halving the number of gas atoms in twice the required range), a smooth distribution is not obtained in Fig. 2.1a, for example, and in many others.

2.2 Summary of the Results of the Above and of Further Calculations

2.2.1- The surface is a strong speed selector. The fastest gas atoms are found in the forward tangential direction for non-normal incidence; as $\theta_o \to 180°$, the fastest atoms are still in the tangential directions, and the fastest of all move towards the corners of the basic square (see Figs. 2.4, 2.6, and 2.7). These results are generalized below in Section 2.2.5.

2.2.2- Many more gas atoms are scattered into the specular plane than the average ($\approx$ 5.56%) scattered into any pair of 10° ϕ-ranges, and these are scattered mostly into the forward direction for $\theta_o \neq 180°$. Similarly, there are many less than the average scattered into the transverse plane. Also, gas atoms scattered into the forward specular plane are the fastest (see Section 2.2.1 above).

2.2.3- Considering normal incidence ($\theta_o = 180°$) for the moment, except for the absence of scattering into tangential directions, the scattering as a function of θ of He is quite uniform; there are no obvious lobes. As the gas atoms become heavier, however, lobes begin to appear which move towards the tangential directions (see Section 2.2.6 below). When the

scattering is considered as a function of ϕ, most scattering takes place into the corners of the basic square, as one may expect. The lobes which result are quite small for He and increase in size as the gas gets heavier until, for Xe, they are quite large (see Section 2.2.6). Also, the mean energy of the gas atoms in the lobes (that is, scattered into the corners of the basic square) is considerably larger than that of atoms not in the lobes; this is particularly true for Xe (see Section 2.2.5).

2.2.4- Considering now scattering at non-normal incidence ($\theta_o \neq 180°$) as a function of θ, scattering lobes are obtained, the maximum, or peak, in a lobe being in the approximate vicinity of the specular direction. At very grazing incidence ($\theta_o \approx 90°$), of course, all scattering must be above the specular direction, whereas at normal incidence all scattering must be below the specular direction. The lobular maximum for light gases is always higher than that for heavy gases. For example, at $\theta_o = 135°$ the scattering maximum is just above the specular direction for He, just below it for Ar, and well below it for Xe (see Figs. 2.3a, 2.5a and 2.2b respectively). The fastest gas atoms are the forward tangential ones, and as the specular plane is scanned from $\theta = 90°$, $\phi = \phi_o$ through $\theta = 0$ to $\theta = 90°$, $\phi = \phi_o + 180°$, there is a definite fall in the average speed of the reflected gas atoms.

We next consider scattering at non-normal incidence as a function of ϕ. The maximum in a lobe is, as expected, in the specular direction (see Figs. 3.1-3.3); for very grazing incidence the lobes are quite narrow, and they broaden as the incidence becomes less grazing. The narrowest lobes are obtained with the heaviest gases, and the broadest lobes with the lightest gases. Thus, especially for heavier gases, many more atoms are scattered into the forward specular plane at grazing incidence than at larger angles of incidence. In fact, no scattering whatsoever is found for any of the systems into the transverse plane at $\theta_o = 112.5°$, and for Xe there is no transverse plane scattering even at $\theta_o = 135°$. Heavier gases experience less scattering out of the specular plane than do lighter gases; there is, for example, considerable scattering of He into the transverse plane at $\theta_o = 135°$ (see Fig. 2.3b). Also, the fastest gas atoms are found in the forward specular plane; the mean energy of atoms scattered into the forward specular plane is, in general, considerably larger than that of atoms scattered into other planes.

The results of this section are generalized in Sections 2.2.5 and 2.2.6.

2.2.5- The results in Sections 2.2.1 - 2.2.4 above on the dependence of gas atom speeds on direction of reflection may be collected together qualitatively under one general statement: "The average speed of reflected gas atoms travelling in a particular direction depends on the 'angular deviation' from the incident direction which the gas atoms have experienced on reflection; large deviations imply relatively low speed and small deviations relatively high." For example, on the average, the fastest reflected atoms are those which experience the least deviation from their incident direction; for grazing incidence these atoms travel in the forward tangential direction, but, as normal incidence is approached a smaller deviation (on the average) is experienced by those atoms reflected into the corners of the basic square.

Anticipating Section 2.2.7 and the definition (3.3) of the energy ac, a statement equivalent to that above (for our model) is: "The effective energy ac of reflected gas atoms is larger for large deviations from the incident direction, and smaller for small deviations." It should be noted that the two statements above are equivalent only when the effective temperature, $E_0/2k$, of the incident atoms is larger than the temperature of the solid (as it is for our model, for the model of Oman et al.[2-5], and for the experiments of Devienne et al.[9]), for then a large effective energy ac implies a small speed of reflected atoms. When the opposite is true (that is, when the temperature of the surface exceeds the effective temperature of the incident gas, as in the experiments of Smith[10], for example), then the two statements above have opposite meanings. It is impossible to conclude from our model which, if either, of the two statements holds under these conditions.

In any event, we observe no tendency for the average speed, or for the effective energy ac, of reflected atoms to be related in any way to the specular direction except, of course, for very grazing incidence. This tendency is reported from theory by Oman et al.[2,3] and from experiment by Smith[10] and by Devienne et al.[9], which work seems to indicate that the effective energy ac is greatest for those atoms farthest from the specular direction. [In the cases of Oman et al.[2,3] and Devienne et al.[9] this implies that the fastest reflected atoms travel in the specular direction, whereas in that of Smith[10] the slowest travel in this direction].

2.2.6- The results in Sections 2.2.3 and 2.2.4 above on the dependence of the form of the scattering lobes (both as functions of θ and of ϕ) on the gas being scattered may be collected together qualitatively under the following general statement: "Heavier gas atoms are deviated from their incident direction less, on the average, than lighter atoms." For example,

for non-normal incidence the scattering lobes in $N(\theta)$ for He are higher than those for Ar, which in turn are higher than those for Xe; also, for normal incidence, the heavier gases tend to scatter more into the tangential directions than do the lighter gases.

2.2.7- It is, in general, unnecessary to distinguish very carefully between "root mean square of speed" (= root mean energy; M = 2) and "mean speed" of gas atoms in the analysis, as the dispersion of speed present in the scattering into any one increment of solid angle is quite small. This is especially true for He, for which case the dispersion is always negligible. This dispersion is measured by the standard deviation, σ, of the speed:

$$\sigma^2 = \overline{V^2} - \bar{V}^2 \qquad (2.5)$$

For He, typical values of $\sigma/\bar{V}$ are less than 1%, even for the entire reflected beam. Attempts to show the variation of σ with θ and ϕ for Ar and Xe are made in Figs. 4.1 and 4.2. These results for $\sigma(\theta)$ and $\sigma(\phi)$ are plotted in the same manner as those for $E(\theta)$ and $E(\phi)$ (see Section 2.1 above); that is, it is assumed that the standard deviation of the speed of the atoms scattered into each of the histogram increments is that corresponding to atoms scattered exactly at the center of the increment. The standard deviation of the speed of the atoms scattered into the whole of the particular plane or surface of a cone under consideration is denoted for each case by σ' in the figures; the Σ quoted for each case in these figures is the standard deviation of the speed of all the reflected gas atoms for that case.

The dispersion of the speed is much larger for Xe than for Ar; this should be expected, although even for Xe at $\theta_o = 135°$ $\sigma/\bar{V}$ is only about 20% for the entire reflected beam. Values of σ tend to be larger for $\theta_o = 135°$ and smaller for more grazing and more normal incidences (see, for example, the quoted values of Σ in Figs. 4.1 and 4.2), although this tendency is reversed for certain values of θ and ϕ. Also, σ tends to be larger for $\theta = 45°$ (see Fig. 4.1). It is evident from both Figs. 4.1 and 4.2 that, for $\theta_o = 180°$, σ is considerably larger towards the corners of the basic square than at other values of ϕ. It seems a fairly general result for all θ_o that σ is larger at values of ϕ for which N and E are larger.

2.2.8- The model is a hard spheres (high incident speed) limit of other models, and is restricted to mass ratios, μ, less than unity. Because of these facts the results are not at present directly comparable with experiment, as experiments to date have been undertaken either at incident speeds considerably below those at which the hard spheres limit may be expected to apply[10-16] or for systems in which μ is not less than unity[9].

The lobes we obtain in the $N(\theta)$ plots are considerably broader than some of the narrow lobes obtained recently in the experiments of Smith and Saltsburg[11-13], although they seem quite comparable with other experimental lobes[10,14-16]. Also, it is not clear to what extent these narrower, low incident speed, experimental lobes will broaden at higher incident speeds. In any event, some of the more important experimental results are concerned with the dependence of the scattering patterns on incident gas speed and surface temperature, about which this theoretical model can say nothing. A theoretical model capable of dealing with these questions is being developed by Logan et al.[17,18]; this is mentioned again below.

We have observed that our theoretical lobes in $N(\theta)$ are broader than the recent narrower experimental lobes. It is clear that by taking $R = \infty$ our lobes become infinitesimally narrow, so the question arises: how do the theoretical scattering patterns change with increasing R? Our "realistic values of R" are chosen from a consideration of (2.4) and values of λ and ℓ from other sources (see Appendix); this seems a reasonable procedure, at least for high-speed incident gas atoms. Figs. 2.5a, 5.1 and 5.2a illustrate how the scattering of Ar-W in the specular plane with $\theta_o = 135°$ and $\phi_o = 20°$ is affected by increasing R from its originally-chosen value of 1.1 through the values 2, 4 and 6. [This investigation was made at the suggestion of Professor R.E. Stickney]. The lobes for $R = 2$ and $R = 4$ resemble more closely the sharper experimental lobes referred to above, although there may be no significance in this. [As described above, the values of $N(\theta)$ for, say, $15° < \phi < 25°$ are found by halving the values for $10° < \phi < 30°$ to obtain smoother distributions. For $R = 6$, nearly all the gas atoms are scattered into this range, so ΣN cannot be accurately evaluated for this case using this method. For example, if all the gas atoms were scattered exactly at $\phi = 20°$ (that is, $\Sigma N = 100\%$, as it is for $R = \infty$) the result we should obtain using the above method is $\Sigma N = 50\%$. The method is, of course, easily modified, although this has not been done.] The theoretical model of Logan et al.[17,18], referred to above, obtains good qualitative agreement with a considerable number of these experimental lobes by, effectively, taking $R = \infty$, although surface roughness is considered[18]. Account is taken of the velocity distribution of the incident atoms and of the thermal motion of the solid surface by using techniques based on those of Ref. 19. A much simpler theoretical model is advanced, also with some success, by

Hinchen and Shepherd[16]. This treatment also takes, effectively, $R = \infty$; a dispensable "energy accommodation coefficient" relating only to the normal component of the gas atom velocity is introduced. Good qualitative agreement with experimental data for Ar - Pt is obtained. Howsmon[20,21] uses a quantum mechanical model to describe the scattering patterns, again with some success. However, the whole question of these patterns is as yet unclear and considerable further work is required.

2.2.9- The effects of choosing smaller values of n are investigated. Figs. 5.2b and 5.3 contain $N(\theta)$ and $E(\theta)$ for the scattering of Ar - W into the specular plane with $\theta_0 = 135°$ and $\phi_0 = 20°$, taking n = 10, 20 and 100; these results should be compared with those for n = 150 in Fig. 2.5a. For n = 10 (100 trajectories) a very irregular distribution is obtained for $N(\theta)$, and even $E(\theta)$ is irregular. Even for n = 100 the $N(\theta)$ histogram is not "smooth", although $E(\theta)$ is quite smooth at n = 20. For n = 150 this particular distribution of $N(\theta)$ is smooth (see Fig. 2.5a), although, as observed above, in many cases the distribution of $N(\theta)$ is irregular even at n = 150. These results are quite general: a smooth distribution of $N(\theta)$ is not obtained until a very large number of trajectories is considered ($n \geq 150$, say), whereas smooth $E(\theta)$ curves are obtained with far fewer trajectories ($n \approx 20$, say). [Of course, the "smoothness" of any particular distribution depends on how fine-grained a scan is required; our remarks are, naturally, referred to the scans described in Section 2.1 above].

The remarks made in Section 3.2 below about the calculations of trajectories using integration of the full equations of motion of a gas atom and a more realistic model, typified by the calculations of Refs. 2-6, apply much more forcibly here. It is difficult to see how smooth scattering patterns will be obtained from these more realistic calculations (unless, of course, only very coarse-grained scans are required).

2.2.10- All results discussed so far have been for $\phi_0 = 20°$. In view of the results below on the independence of the acs on ϕ_0, we should not expect large variations of the detailed scattering patterns with ϕ_0 except for translation in ϕ-space of the entire pattern as ϕ_0 changes for grazing incidence. For normal or near-normal incidence these remarks are modified because, for normal incidence, the patterns are independent of ϕ_0. The variations for Ar - W at $\theta_0 = 135°$ are investigated in Figs. 2.5, 5.4 and 5.5 for $\phi_0 = 20°$, 0 and 45° respectively. The results are qualitatively similar, although a few differences are apparent. One of these is that at $\phi_0 = 45°$ (along a diagonal of the basic square) more atoms are "channeled" into the specular plane than at $\phi_0 = 0$ or 20° and, accordingly, fewer appear in the transverse plane. At the same

time there is more "backscatter" ($\theta > 0$ in Fig. 5.5a) for $\phi_o = 45°$, and these backscattered atoms have quite low energy (on account of their large deviations from their incident direction; see Section 2.2.5). The mean energy of atoms scattered at any particular direction relative to the incident direction is independent of ϕ_o. However, the appearance of scattered atoms in certain directions and their disappearance in others as ϕ_o varies result in small changes in the mean energies with ϕ_o. For example, the appearance of a number of backscattered atoms of low energy for $\phi_o = 45°$ results in a mean energy, $\bar{E}$, in the specular plane less (although negligibly so) than that at $\phi_o = 0$ or 20°.

MACROSCOPIC CALCULATIONS

These are calculations of the macroscopic parameters of gas-surface interactions, in which details of trajectories of gas atoms are hidden by averaging procedures. Examples of such macroscopic parameters are (i) acs and (ii) forces exerted on targets by gas beams.

3.1 Accommodation Coefficients

3.1.1- Definitions and description of the calculations. The thermal (energy) ac, the tangential momentum ac and the normal momentum ac are denoted respectively by α_e, α_t and α_n. The acs are all defined in a similar manner[19]:

$$\alpha_q = \frac{\bar{Q}_o - \bar{Q}}{\bar{Q}_o - \bar{Q}_s} \tag{3.1}$$

where $\bar{Q}_o$ and $\bar{Q}$ are the average values per gas atom of some scalar property, Q, of the gas in the incident and reflected gas beams respectively, and $\bar{Q}_s$ is the value $\bar{Q}$ would have if the gas were reflected as a thermal (Maxwellian) beam (3D here) at the temperature, T_s, of the solid surface. For our model $T_s = 0$ and this means for α_e, α_t and α_n that $\bar{Q}_s = 0$; our definition of α_q reduces, therefore, to

$$(T_s = 0) \qquad \alpha_q = 1 - \bar{Q}/\bar{Q}_o \tag{3.2}$$

which is the origin of equation (9) of Ref. 1. Therefore, in the above notation

$$\alpha_e = 1 - \overline{v^2} = 1 - \mathscr{E} \tag{3.3}$$

$$\alpha_t = 1 - \overline{v \cos(\phi - \phi_o) \sin\theta} \; \mathrm{cosec}\theta_o \tag{3.4}$$

and $$\alpha_n = 1 + \overline{V \cos\theta}\ \sec\theta_o \qquad (3.5)$$

where the averages are over the entire reflected beam (remember that $\sec\theta_o < 0$). [The error in equation (11) of Ref. 1 was pointed out to the author by Mr. D.P. Jackson of the University of Toronto; the correct equation (3.4) was used for the calculations, however]. In general (see Section 3.1.2 below) far fewer trajectories are needed for the macroscopic calculations than for the microscopic and, for the great majority of cases, either n = 10 or 20 is chosen. In the following, "α" stands for "α_e, α_t and α_n".

The main series of calculations is on α as functions of μ, R, S, θ_o and ϕ_o for different combinations of μ = 0.001, 0.1(0.2) 0.9; R = 0.9(0.1)1.3; S = square, triangular; θ_o = 112.5°(22.5°) 180°; ϕ_o = 0(15°)45° for S = square and ϕ_o = 0(10°)30° for S = triangular.

Results for S = square are summarized in Figs. 6.1 - 6.36. As indicated below by (3.6)-(3.8), results for S = triangular are very similar to those for S = square and it does not seem worthwhile to show them all in full; one example of each of $\alpha(\mu)$, $\alpha(R)$, $\alpha(\theta_o)$ and $\alpha(\phi_o)$ for S = triangular is shown for comparison in Figs. 6.1a, 6.11a, 6.21a and 6.29a respectively. Most of the ac results are obtained with n = 10 or 20, but in a few cases it was found that n = 100 is necessary to get smooth curves; the most troublesome curve of all was the $\alpha_t(\theta_o)$ of Fig. 6.22 (see also Fig. 7.1 and Section 3.1.2 below). The maximum in $\alpha_t(\theta_o)$ for $\theta_o < 180°$, exhibited by this curve and some others, seems to be real; this seems to be confirmed by the results at θ_o = 120° and 160° shown in Fig. 7.1, for which n ≈ 50, 100 and 110 all produce the same result.

At the risk of stating the obvious, we may mention that considerable help may be obtained in drawing these curves by remembering some of their simpler properties:

(i) $\mu \to 0$ implies $\alpha_e \to 0$.
(ii) $\theta_o \to 90°$ implies $\alpha_e \to 0$, $\alpha_t \to 0$ and $\alpha_n \to -\infty$.
(iii) All curves of $\alpha(\theta_o)$ have zero gradients at $\theta_o = 180°$.
(iv) All curves of $\alpha(\phi_o)$ have zero gradients at $\phi_o = 30i°$ for S = triangular and at $\phi_o = 45i°$ for S = square where i is any integer.

It is fairly clear from Result (iv) above that there cannot be much variation of α with ϕ_o; this is confirmed below by (3.6)-(3.8).

The ranges of μ and R considered in this Report are, approximately, $0 < \mu < 1$ and $0.9 < R < 1.3$; for the smaller values of μ and R in these ranges, approximate qualitative

correlation of the results is obtained by the following equations:

$$\alpha_e(\mu,R,S,\theta_o,\phi_o) \approx 3.6\ \mu(-\cos\theta_o)/(1+\mu)^2 \qquad (3.6)$$

$$\alpha_n(\mu,R,S,\theta_o,\phi_o) \simeq A(\mu,R) - B(\mu,R)(-\sec\theta_o) \qquad (3.7)$$

and

$$\alpha_t(\mu,R,S,\theta_o,\phi_o) \simeq C(\mu,R)(-\cos\theta_o) \qquad (3.8)$$

where

$$A > B > 0 \quad \text{and} \quad C > 0 \qquad (3.9)$$

Note that the factor, 3.6, in (3.6) is to be considered as giving only approximate correlation of α_e. This factor is interesting, however, and arises because the ratio of α_e for a gas beam incident normally on the solid surface and α_e for a head-on collision between gas and surface atoms is about 0.9. It is encouraging, although probably fortuitous, that Oman[5] reports a similar ratio of 0.894.

It must be emphasized that the "correlation equations" (3.6)-(3.8) apply only to the smaller values of μ and R in the stated ranges, and do not hold at larger values of μ or R; at $R = \infty$, for example, we have

$$\alpha_e(\mu,\infty,S,\theta_o,\phi_o) = 4\mu\cos^2\theta_o/(1+\mu)^2 \qquad (3.10a)$$

$$\alpha_n(\mu,\infty,S,\theta_o,\phi_o) = 2\mu/(1+\mu) \qquad (3.10b)$$

and

$$\alpha_t(\mu,\infty,S,\theta_o,\phi_o) = 0 \qquad (3.10c)$$

The correlation equations (3.6)-(3.8) may be compared with the four "pictures" generally used in discussions of scattering results; these are the four possible combinations of cosine and specular reflection with $\alpha_e = 0$ and $\alpha_e = 1$ (in the author's opinion, it is inconceivable that specular reflection with $\alpha_e=1$, or cosine reflection with $\alpha_e=0$ should occur). In an obvious notation, where for example α_{tcl} means α_t with cosine reflection and $\alpha_e = 1$, the results for α for our model ($T_s = 0$) from these four pictures are as follows.

$$\alpha_{ecl} = \alpha_{esl} = \alpha_{tcl} = \alpha_{tsl} = \alpha_{tco} = \alpha_{ncl} = \alpha_{nsl} = 1 \qquad (3.11a)$$

$$\alpha_{eco} = \alpha_{eso} = \alpha_{tso} = \alpha_{nso} = 0 \qquad (3.11b)$$

$$\alpha_{nco} = 1 - (2/3)(-\sec\theta_o) \qquad (3.11c)$$

Comparing (3.11) with Figs. 6.1 - 6.36, it is clear that these simple pictures are useless for a description of our model.

3.1.2 Dependence of α on choice of n- It is possible to obtain misleading results in some cases by a combination of bad luck and a value of n insufficiently large; sometimes a smooth curve which is apparently correct is obtained which, after choosing a larger value of n, remains smooth but changes its form. This happens very infrequently (about three times during this analysis), but is sufficiently annoying (and serious!) to be pointed out. Even after being convinced that the results are all right, one is sometimes still left with the feeling that perhaps a larger value of n would modify them. An example of this situation is illustrated in Fig. 7.1 where $\alpha(\theta_o)$ are plotted as functions of n for a special case (note that in both Figs. 7.1 and 7.2 the discrete points at which each of α is calculated are joined by straight lines). A "smooth" curve may be drawn for $\alpha_t(\theta_o)$ for each of n = 2, 6 and 10; in these cases one would probably guess that $\alpha_t(180°) \approx 0$. It is not until n = 50 is tried that the "true" shape of $\alpha_t(\theta_o)$ becomes apparent; this is very rare, however, and this case is the worst experienced of about three. In general, very few trajectories are needed to get a good α_e curve; even n = 2 (only 4 trajectories) is sometimes sufficient (see Fig. 7.1), although n = 6 is much better and nearly always sufficient. It is clear from Fig. 7.1 that all the curves get progressively "better" as n is increased.

The troubles associated with insufficient trajectories are clearly experienced by Oman[2-5]. The reason why he does not always obtain smooth curves (Figs. 1 and 2 of Ref. 4 for example) is probably that he uses a grid of only 18 trajectories. To illustrate this important point, the case corresponding to Fig. 2 of Ref. 4 ($\alpha(\phi_o)$ for μ = 0.5, R = 1.06, S = square and θ_o = 135°) is calculated here for n = 2, 4, 6 and 10, and the results appear in Fig. 7.2. Oman's calculations "correspond" roughly to n = 4, and it is clear that very much smoother curves will be obtained with n = 10. However, it must be remembered that Oman's calculations are fully integrated trajectory calculations, requiring about 1 minute of IBM 7094 time per trajectory, whereas the greatly simplified calculations presented here require only about 0.01 second per trajectory. These remarks do not detract from the value of Oman's work, which is the only published work of this nature; one does not expect smooth ac curves with present techniques from the small number of trajectories it is possible to calculate using full integration procedures. It is difficult to see how this situation is to be remedied.

It should be noted in passing that all the normal momentum acs (σ_z) quoted in Refs. 2-5 and 22 are in error. For example, denoting the values of σ_z quoted in Ref. 22 by σ_z', the definition used there is

$$\sigma_z' = 1 - \overline{\cos\theta}\ \sec\theta_o \qquad (3.12)$$

whereas the correct definition is

$$\sigma_z = 1 - \overline{V \cos\theta}\ \sec\theta_o \qquad (3.13)$$

This error is discussed and corrected in Ref. 23. Note further that Oman uses a σ_z different from the author's α_n; the relation between them is, comparing (3.5) and (3.13),

$$\sigma_z = 2 - \alpha_n \qquad (3.14)$$

3.2 Forces exerted on a target by a directed gas beam- A problem which is closely related to that of the acs is that of the forces exerted on a target by a directed beam of gas atoms; this problem is of considerable interest, particularly in view of the work of Mair[24] and Abuaf and Marsden[25]. These forces are determined by (a) the experimental geometry and (b) the momentum acs. Two possible experimental situations are the following:

(i) the cross-sectional area of that part of the incident beam which later strikes the target is independent of θ_o. [This situation is impossible for very grazing incidence, but is that relevant to the work of Ref. 25];

(ii) the incident beam surrounds the target always.

We denote the normal and tangential forces on the target by F_n and F_t and we define normalized forces $\mathcal{F}_n$ and $\mathcal{F}_t$ respectively:

$$\mathcal{F}_n(\theta_o) = F_n(\theta_o)/F_n(\pi) \qquad (3.15)$$

and

$$\mathcal{F}_t(\theta_o) = F_t(\theta_o)/F_n(\pi) \qquad (3.16)$$

in which π stands for 180°. Thus $\mathcal{F}_n(\theta_o)$ is the same as the normalized force of Ref. 25. For case (i) above it follows that

$$\mathcal{F}_n(\theta_o) = \left[\frac{2 - \alpha_n(\theta_o)}{2 - \alpha_n(\pi)}\right](-\cos\theta_o) \qquad (3.17)$$

and

$$\mathcal{F}_t(\theta_o) = \left[\frac{\alpha_t(\theta_o)}{2 - \alpha_n(\pi)}\right]\sin\theta_o \qquad (3.18)$$

It is here that the advantages of Oman's notation (3.14) would be felt. For case (ii) above, these forces have to be multiplied by an extra factor $(-\cos\theta_o)$; in view of the work of Ref. 25, however, we confine outselves here to case (i).

As examples of the results obtained from the model, $\mathcal{F}_n(\theta_o)$ and $\mathcal{F}_t(\theta_o)$ are shown as the dashed curves in Figs. 8.1-8.8 as functions of θ_o for the four combinations of μ = 0.1 and 0.9, R = 0.9 and 1.3, S = square and ϕ_o = 0; the calculations are

done from (3.17) and (3.18) using the corresponding results for $\alpha_n(\theta_o)$ and $\alpha_t(\theta_o)$. Also shown in these figures are the results for $\mathcal{F}$, denoted by $\mathcal{F}'$ and shown as the dotted curves, which are obtained from (3.17) and (3.18) and the correlation equations (3.7) and (3.8). These correlation equations may conveniently be written

$$\alpha_n(\theta_o) \approx \left[\frac{1 - \cos\theta_o' \sec\theta_o}{1 + \cos\theta_o'}\right] \alpha_n(\pi) \tag{3.19}$$

and

$$\alpha_t(\theta_o) \approx - \cos\theta_o \, \alpha_t(\pi) \tag{3.20}$$

in which θ_o' is the value of θ_o giving $\alpha_n(\theta_o) = 0$, and θ_o', $\alpha_n(\pi)$ and $\alpha_t(\pi)$ are found in each particular case from the corresponding $\alpha(\theta_o)$ curves. Combining (3.18)-(3.20) we have

$$\mathcal{F}_n'(\theta_o) = \frac{[2(1+\cos\theta_o') - \alpha_n(\pi)](-\cos\theta_o) - \alpha_n(\pi)\cos\theta_o'}{[2 - \alpha_n(\pi)](1 + \cos\theta_o')} \tag{3.21}$$

and

$$\mathcal{F}_t'(\theta_o) = \frac{\alpha_t(\pi)(-\sin 2\theta_o)}{[2 - \alpha_n(\pi)]} \tag{3.22}$$

The results for the few simplified pictures discussed above (cosine and specular reflection; $\alpha_e = 0$ and 1) are shown in these figures also (the solid curves); they are obtained by combining (3.11) with (3.17) and (3.18) and, in the notation used in (3.11), may be written

$$\mathcal{F}_{nco} = 0.6(- \cos\theta_o) + 0.4 \tag{3.23a}$$

$$\mathcal{F}_{tco} = 0.6 \sin\theta_o \tag{3.23b}$$

$$\mathcal{F}_{ncl} = \mathcal{F}_{nso} = \mathcal{F}_{nsl} = - \cos\theta_o \tag{3.23c}$$

$$\mathcal{F}_{tcl} = \mathcal{F}_{tsl} = \sin\theta_o \tag{3.23d}$$

and

$$\mathcal{F}_{tso} = 0 \tag{3.23e}$$

The simple equations (3.23) hold because the solid surface is at 0°K in our model (see Section 3.3 below). We may note the similarity of Figs. 8.1 - 8.4 with the corresponding figures of Ref. 25.

It is clear from Figs. 8.1 - 8.8 that none of the above simplified pictures (3.23) is adequate for a description of the forces on targets resulting from this model; this is particularly true of $\mathcal{F}_t(\theta_o)$. This conclusion echoes our similar, and directly

related, conclusion concerning the acs (3.11). The correlation formula (3.19) yields curves (3.21) of $\mathcal{F}'_n(\theta_o)$ which describe $\mathcal{F}_n(\theta_o)$ quite well; the agreement between $\mathcal{F}'_t(\theta_o)$ and $\mathcal{F}_t(\theta_o)$ is not as good. This is because the formula (3.19) for α_n is better than that (3.20) for α_t, particularly when $\alpha_t(\theta_o)$ has the maximum for $\theta_o < 180°$ which is discussed above.

3.3 Solid surface at non-zero temperature- For cases in which the surface may not be considered as being at 0°K (all published experimental data to date except, perhaps, those of Devienne et al.[9]), some of the above simplifications may not be made. For example, it is not permissible to set $2v_o = 2E_o = M = 2$ as is done above in (1.4) and (2.1). Also, the formula (3.1) may not in general be simplified to that (3.2). In fact, in three dimensions we obtain

$$\alpha_e = \frac{\overline{v_o^2} - \overline{v^2}}{\overline{v_o^2} - 4kT_s/M} \tag{3.24}$$

$$\alpha_t = 1 - \overline{v\cos(\phi-\phi_o)\sin\theta}/\overline{v_o}\sin\theta_o \tag{3.25}$$

and

$$\alpha_n = \frac{\overline{v_o}\cos\theta_o + \overline{v\cos\theta}}{\overline{v_o}\cos\theta_o + (\pi kT_s/2M)^{\frac{1}{2}}} \tag{3.26}$$

where k is the Boltzmann constant, and where a possible spread in incident speed, v_o, but not in incident direction, θ_o, is considered. The formula (3.25) is of the same form as (3.2) because, in thermal equilibrium, $\overline{v\cos(\phi-\phi_o)\sin\theta} = 0$. The formulae (3.17) and (3.18) for $\mathcal{F}_n$ and $\mathcal{F}_t$ become respectively

$$\mathcal{F}_n(\theta_o) = \frac{[2-\alpha_n(\theta_o)](-\cos\theta_o) + (\pi kT_s/2M)^{\frac{1}{2}}\,\alpha_n(\theta_o)/\overline{v_o}}{2 - \alpha_n(\pi) + (\pi kT_s/2M)^{\frac{1}{2}}\,\alpha_n(\pi)/\overline{v_o}} \tag{3.27}$$

and

$$\mathcal{F}_t(\theta_o) = \frac{\alpha_t(\theta_o)\sin\theta_o}{2 - \alpha_n(\pi) + (\pi kT_s/2M)^{\frac{1}{2}}\,\alpha_n(\pi)/\overline{v_o}} \tag{3.28}$$

and the correlation formulae (3.19) and (3.20) may again be used, this time to obtain the hot-surface analogues of (3.21) and (3.22). However, our correlation formulae may not be valid for $T_s > 0$.

Hot-surface analogues of (3.11) and (3.23) are of interest, as these, rather than those for $T_s = 0$, must be used for nearly all existing experimental data, for example those of Marsden et al.[25]. These formulae cannot be obtained without a more

detailed knowledge of the reflected velocity distribution densities but, if we make the assumption that, in each case, all the reflected atoms have the same speed, we may obtain formulae for the various α's which replace (3.11). We define τ by

$$\tau = (2kT_s/E_o)^{\frac{1}{2}} \tag{3.29}$$

and then these formulae may be written as follows.

$$\alpha_{ecl} = \alpha_{esl} = \alpha_{tcl} = \alpha_{tco} = 1 \tag{3.30a}$$

$$\alpha_{eco} = \alpha_{eso} = \alpha_{tso} = \alpha_{nso} = 0 \tag{3.30b}$$

$$\alpha_{tsl} = 1 - \tau \tag{3.30c}$$

$$\alpha_{ncl} = \frac{1 + (2\tau/3)\ \sec\theta_o}{1 + (\pi/8)^{\frac{1}{2}}\tau\sec\theta_o} \tag{3.30d}$$

$$\alpha_{nsl} = \frac{1 - \tau}{1 + (\pi/8)^{\frac{1}{2}}\tau\sec\theta_o} \tag{3.30e}$$

$$\alpha_{nco} = \frac{1 + (2/3)\ \sec\theta_o}{1 + (\pi/8)^{\frac{1}{2}}\tau\sec\theta_o} \tag{3.30f}$$

The analogues of (3.23) are now found by using (3.29) and (3.30) in (3.17) and (3.18).

REFERENCES

As many references are to the same Symposia, the following notation is used for brevity.

"Symposium 4" stands for "Proceedings of the Fourth International Symposium on Rarefied Gas Dynamics", held at Toronto (1964). In Rarefied Gas Dynamics, Fourth Symposium, Vol. II, Academic Press (1966).

"Symposium 5" stands for "Proceedings of the Fifth International Symposium on Rarefied Gas Dynamics", held at Oxford (1966). In Rarefied Gas Dynamics, Fifth Symposium, Vol. I, Academic Press (1967).

1. F.O. Goodman, Symposium 5; p. 35.

2. R.A. Oman et al., A.I.A.A. Journal, 2, 1722 (1964).

3. R.A. Oman, A. Bogan and C.H. Li, Symposium 4, p. 396; also in Grumman Research Department Report RE-181J (1964).

4. R.A. Oman, Grumman Research Department Report RE-222 (1965).

5. R.A. Oman, Symposium 5, p. 83.

6. F.O. Goodman, unpublished material.

7. F.O. Goodman and H.Y. Wachman, M.I.T. Fluid Dynamics Research Laboratory Report No. 66-1 (1966). Also in J. Chem. Phys, Vol. 46, No. 6, March 1967, p. 2376.

8. W.F. Meggers, Key to Periodic Chart of the Atoms, W.M. Welch Scientific Company, Chicago (1956).

9. F.M. Devienne, J.C. Roustan and R. Clapier, Symposium 5, p. 269.

10. J.N. Smith, Jr., J. Chem. Phys, 40, 2520 (1964).

11. J.N. Smith, Jr., and H. Saltsburg, J. Chem. Phys, 40, 3585, (1964).

12. J.N. Smith, Jr. and H. Saltsburg, Symposium 4, p. 491.

13. H. Saltsburg, J.N. Smith, and R.L. Palmer, Symposium 5, p. 223.

14. J.J. Hinchen and W.M. Foley, Symposium 4, p. 505.

15. J.J. Hinchen and W.M. Foley, United Aircraft Research Laboratories Report D910245-7 (1965).

16. J.J. Hinchen and E.F. Shepherd, Symposium 5, p. 239.

17. R.M. Logan and R.E. Stickney, J. Chem. Phys, 44, 195 (1966).

18. R.M. Logan, J.C. Keck and R.E. Stickney, Symposium 5, p. 49.

19. F.O. Goodman, J. Phys. Chem. Solids, 26, 85 (1965).

20. A.J. Howsmon, Symposium 4, p. 417.

21. A.J. Howsmon, Symposium 5, p. 67.

22. R.A. Oman, Grumman Research Department Report RM-237 (1964).

23. R.A. Oman, V.S. Calia and C.H. Weiser, Grumman Research Department Report RE-272 (1966).

24. W.N. Mair, Symposium 5, p. 187.

25. N. Abuaf and D.G.H. Marsden, Symposium 5, p. 199.

26. F.O. Goodman, Symposium 4, p. 366.

27. L.A. Girifalco and V.G. Weizer, Phys. Rev., 114, 687 (1959).

28. C. Kittel, in Introduction to Solid State Physics, Second Edition, Wiley (1963), p. 40.

System	μ	R
He-W	0.0218	1.0
Ar-W	0.217	1.1
Xe-W	0.714	1.2
He-Ni	0.0682	1.2
Ar-Ni	0.680	1.4

Table Values of μ and R chosen for the five systems (see Section 2.1 and the Appendix).

APPENDIX

Estimation of R from (2.4)

There are no published direct data on appropriate values of λ for gas-solid systems; instead, indirect methods of estimating λ must be used. We use the estimated values of the Morse parameters, a, for the gas-W systems in Ref. 26 in conjunction with the following empirical formula[6] relating a and λ:

$$a\lambda \simeq 5.08 \qquad \text{(A1)}$$

[The Morse potential is defined by

$$W(u) = D[\exp\{-2a(u - u_m)\} - 2\exp\{-a(u - u_m)\}] \qquad \text{(A2)}$$

where W(u) is the interaction potential of the two atoms when their separation is u; D, a and u_m are the three Morse potential parameters]. Further, we assume that the gas-Ni parameters are the same as the gas-W ones; this is a reasonable assumption as the Morse a for Ni-Ni is about the same[27] as that for W-W.

The values of ℓ needed for insertion into (2.4) are taken to be the lattice spacing for W and the nearest neighbour distance for Ni (See Ref. 28).

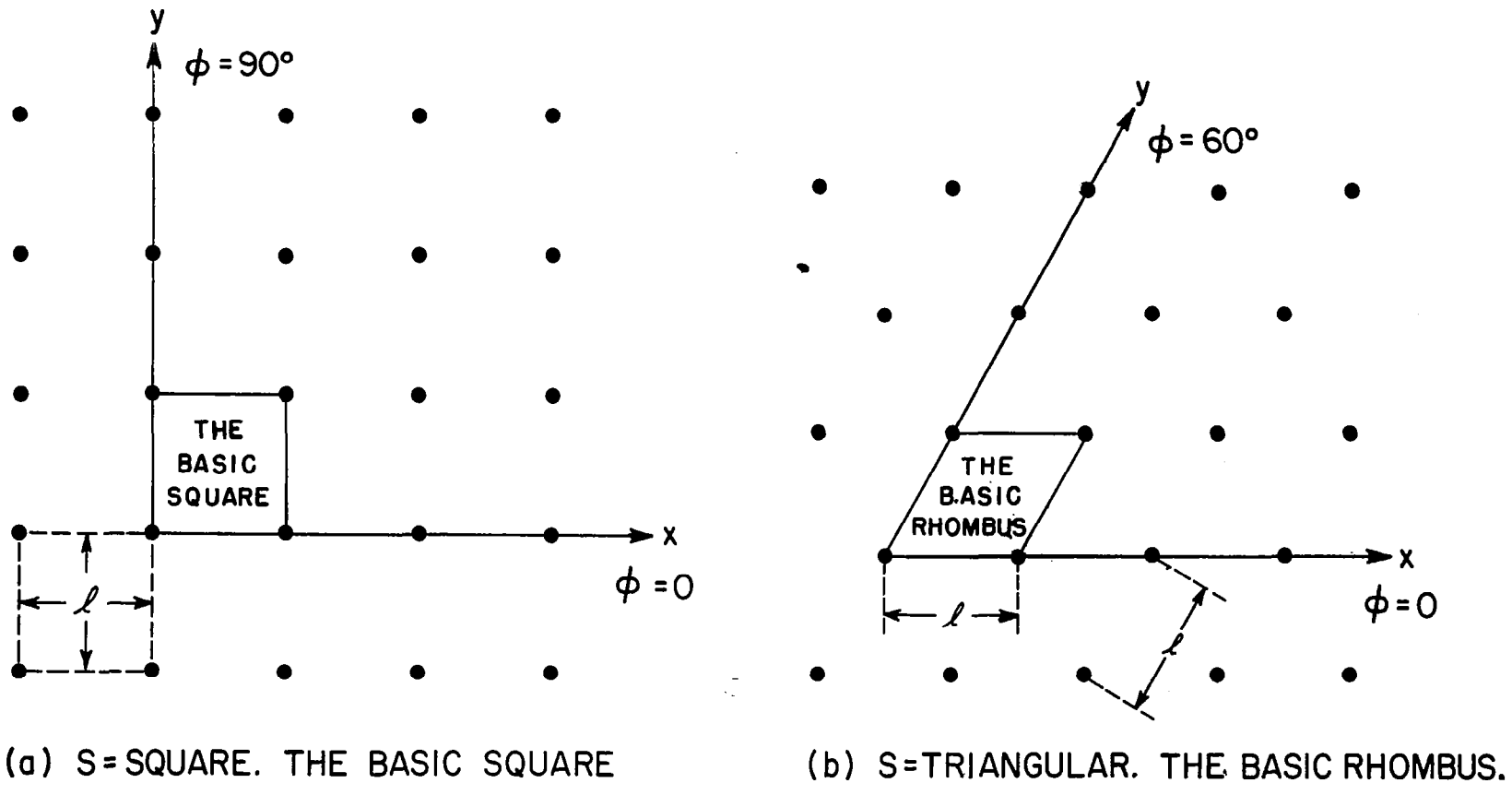

(a) S = SQUARE. THE BASIC SQUARE

(b) S = TRIANGULAR. THE BASIC RHOMBUS.

Fig. 1.1 (a and b). The two surface arrays, S, used in this paper and their respective basic surface elements (square and rhombus) over which the aiming points are uniformly distributed in an n × n array.

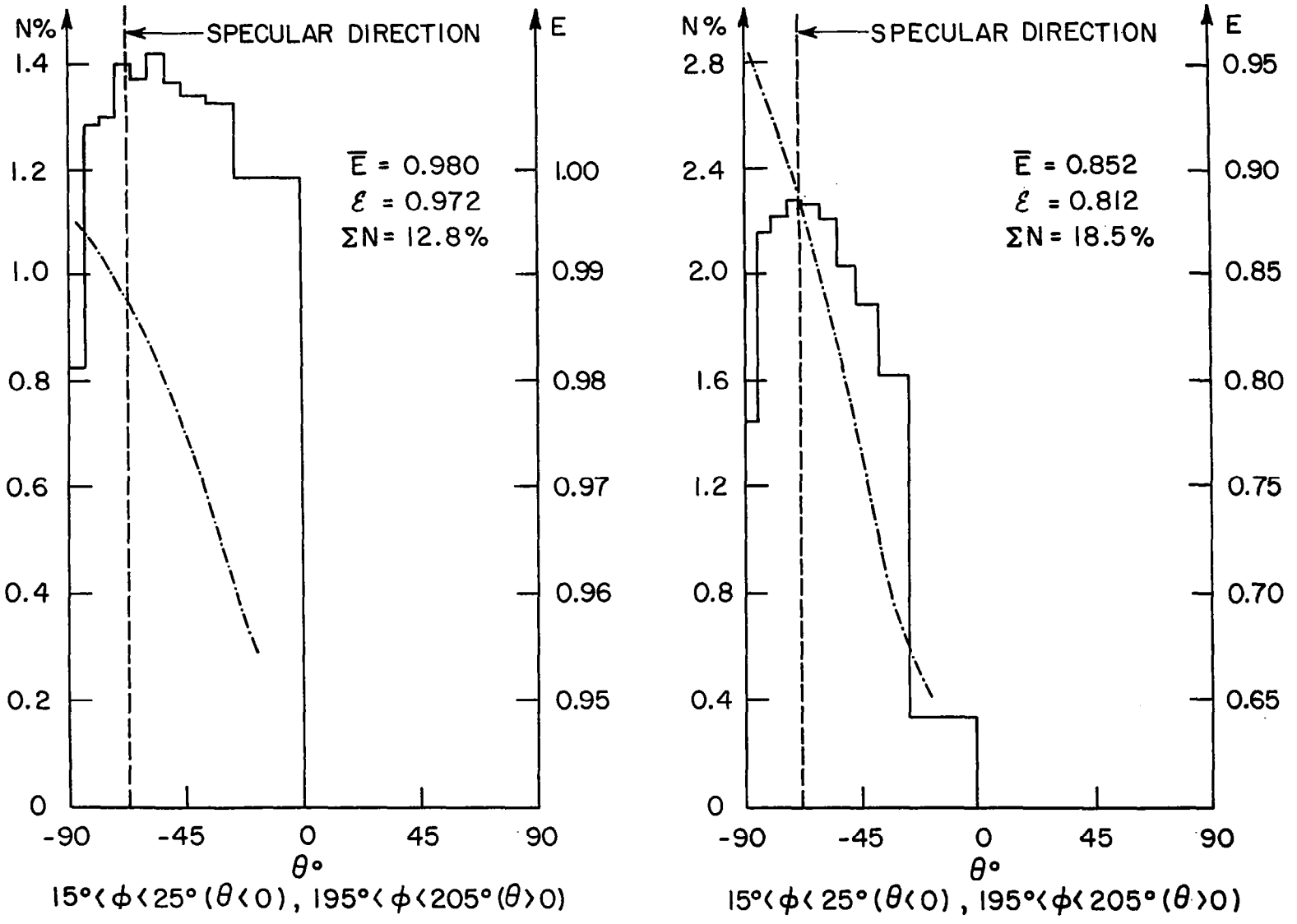

Fig. 2.1 $N(\theta)$ and $E(\theta)$ for $\mu = 0.0218$, $R = 1.0$, $\theta_o = 112.5°$, $\phi_o = 20°$, $n = 150$ *(left)* and for $\mu = 0.217$, $R = 1.1$, $\theta_o = 112.5°$, $\phi_o = 20°$, $n = 150$ *(right)*

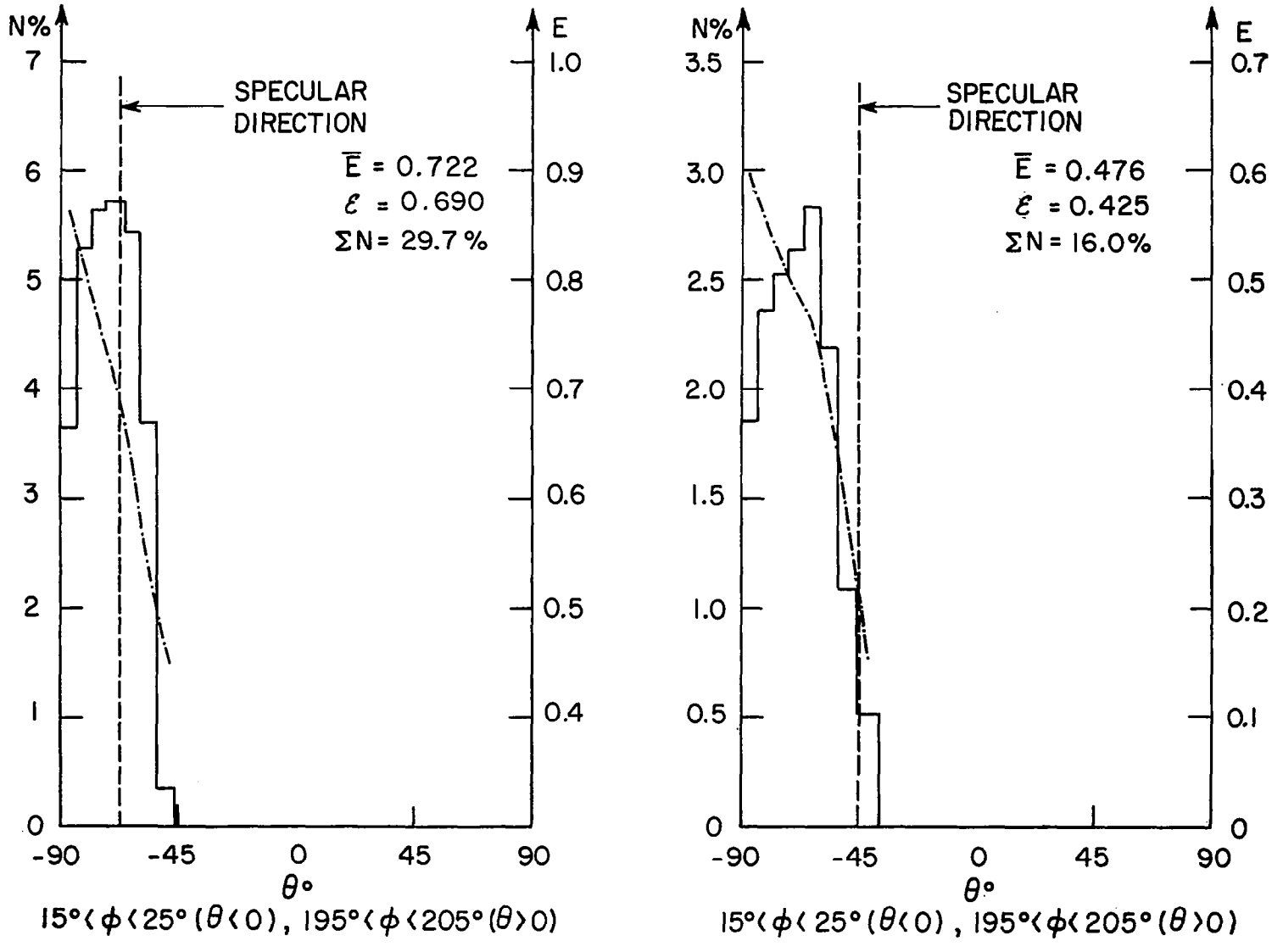

Fig. 2.2 N(θ) and E(θ) for μ = 0.714, R = 1.2, θ_o = 112.5°, ϕ_o = 20°, n = 150 *(left)* and for μ = 0.714, R = 1.2, θ_o = 135°, ϕ_o = 20°, n = 150 *(right)*

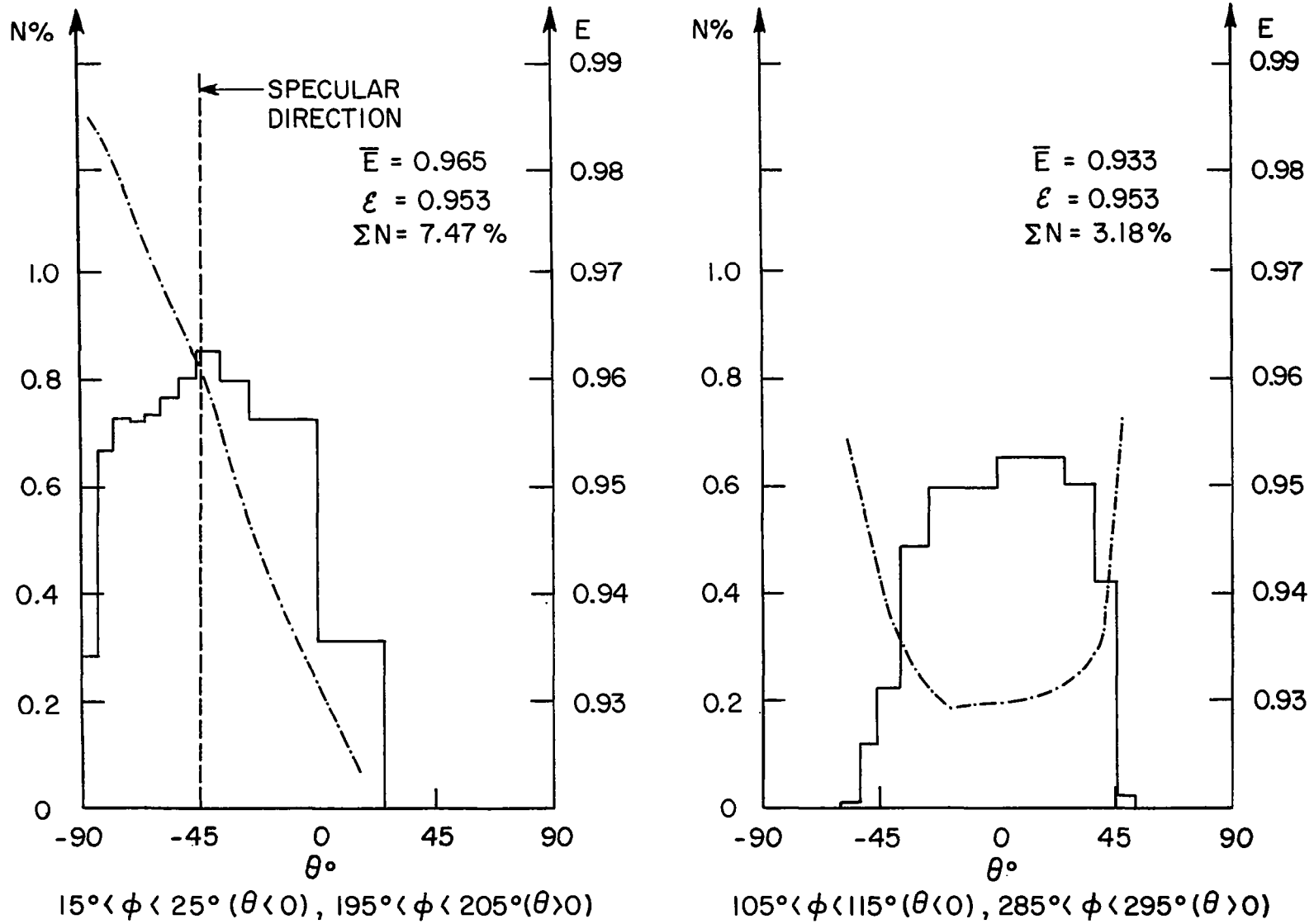

Fig. 2.3 N(θ) and E(θ) for μ = 0.0218, R = 1.0, θ_o = 135°, ϕ_o = 20°, n = 150

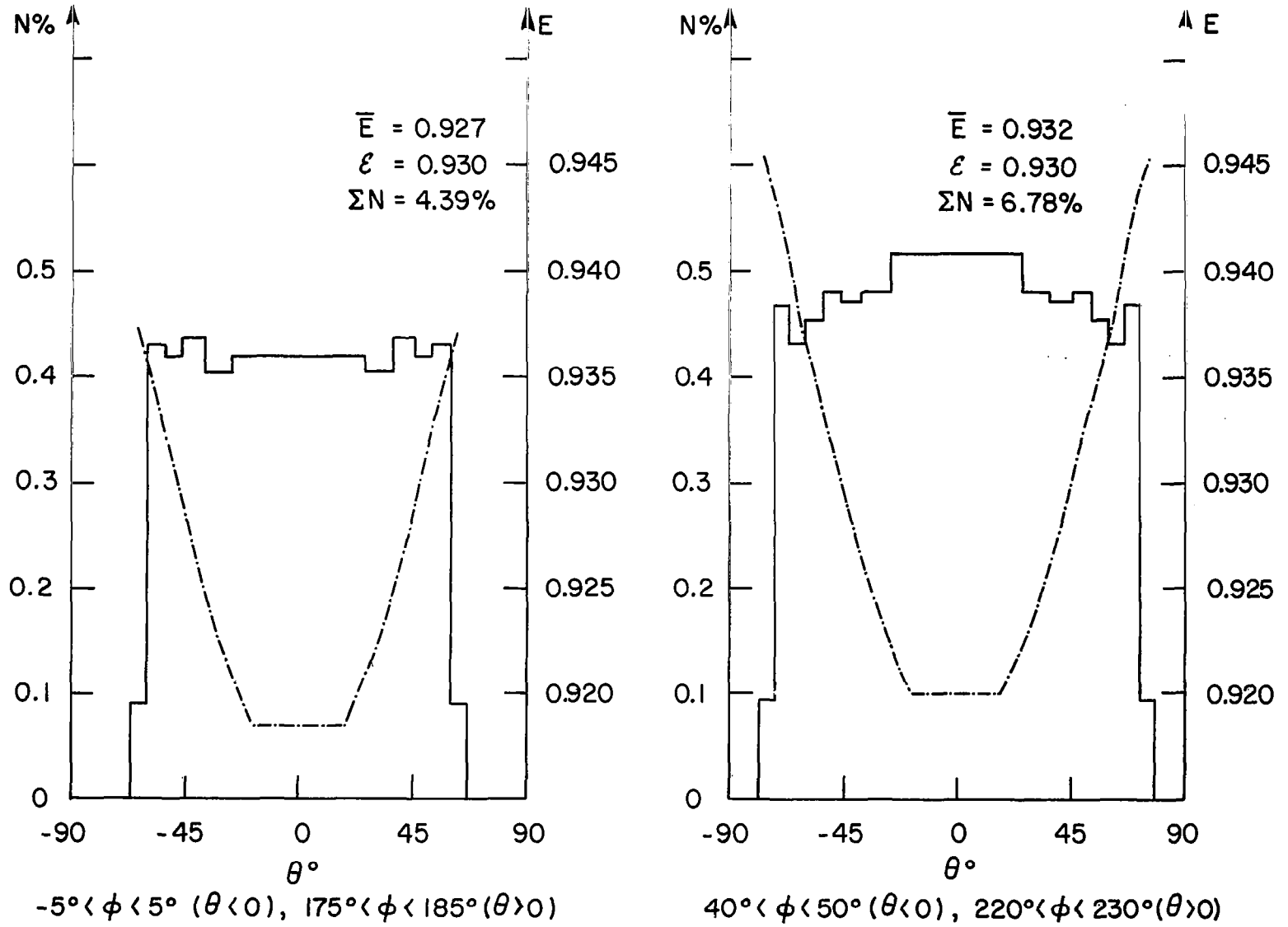

Fig. 2.4 $N(\theta)$ and $E(\theta)$ for $\mu = 0.0218$, $R = 1.0$, $\theta_o = 180°$, $n = 150$

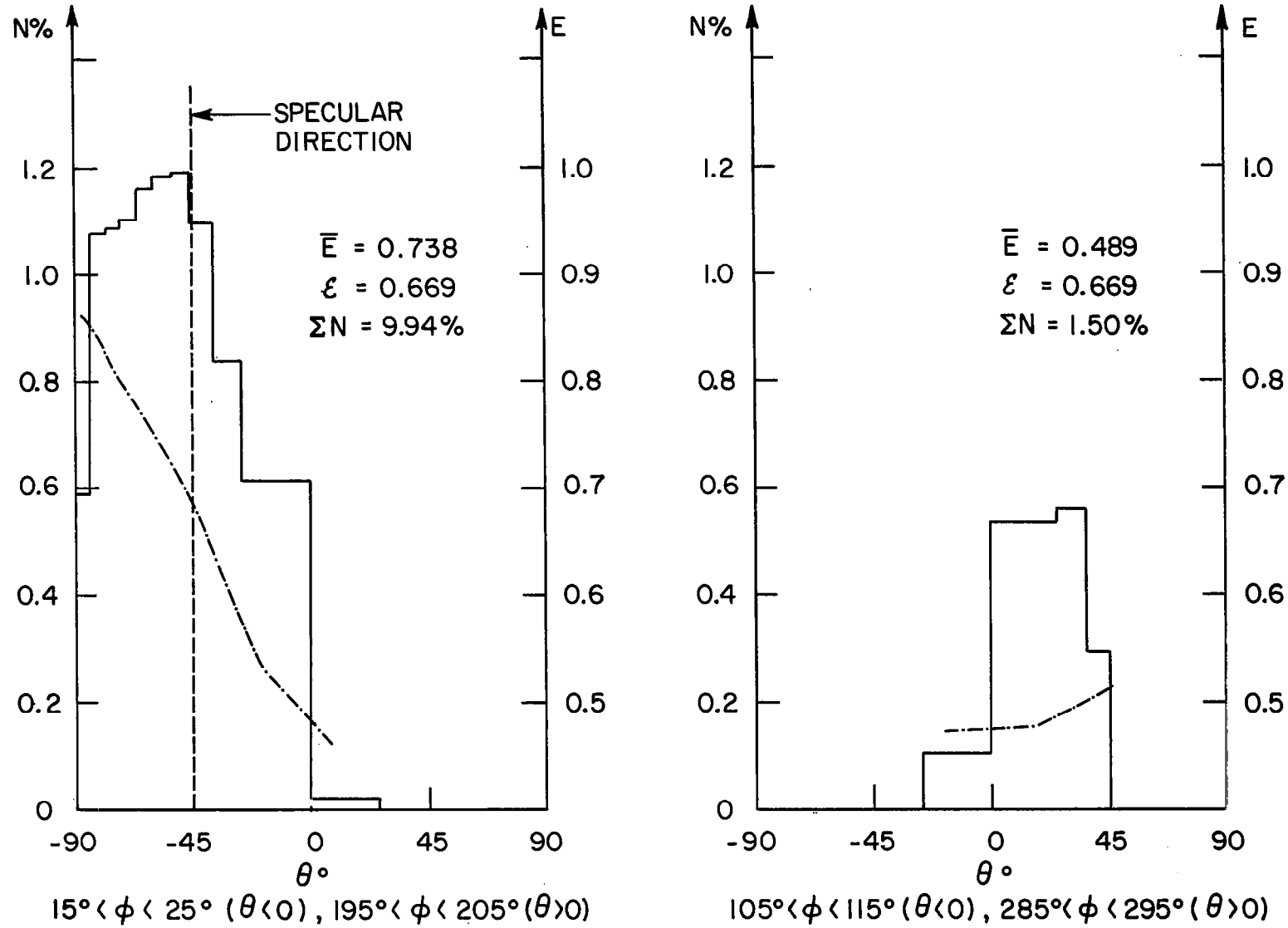

Fig. 2.5 N(θ) and E(θ) for μ = 0.217, R = 1.1, θ_o = 135°, ϕ_o = 20°, n = 150

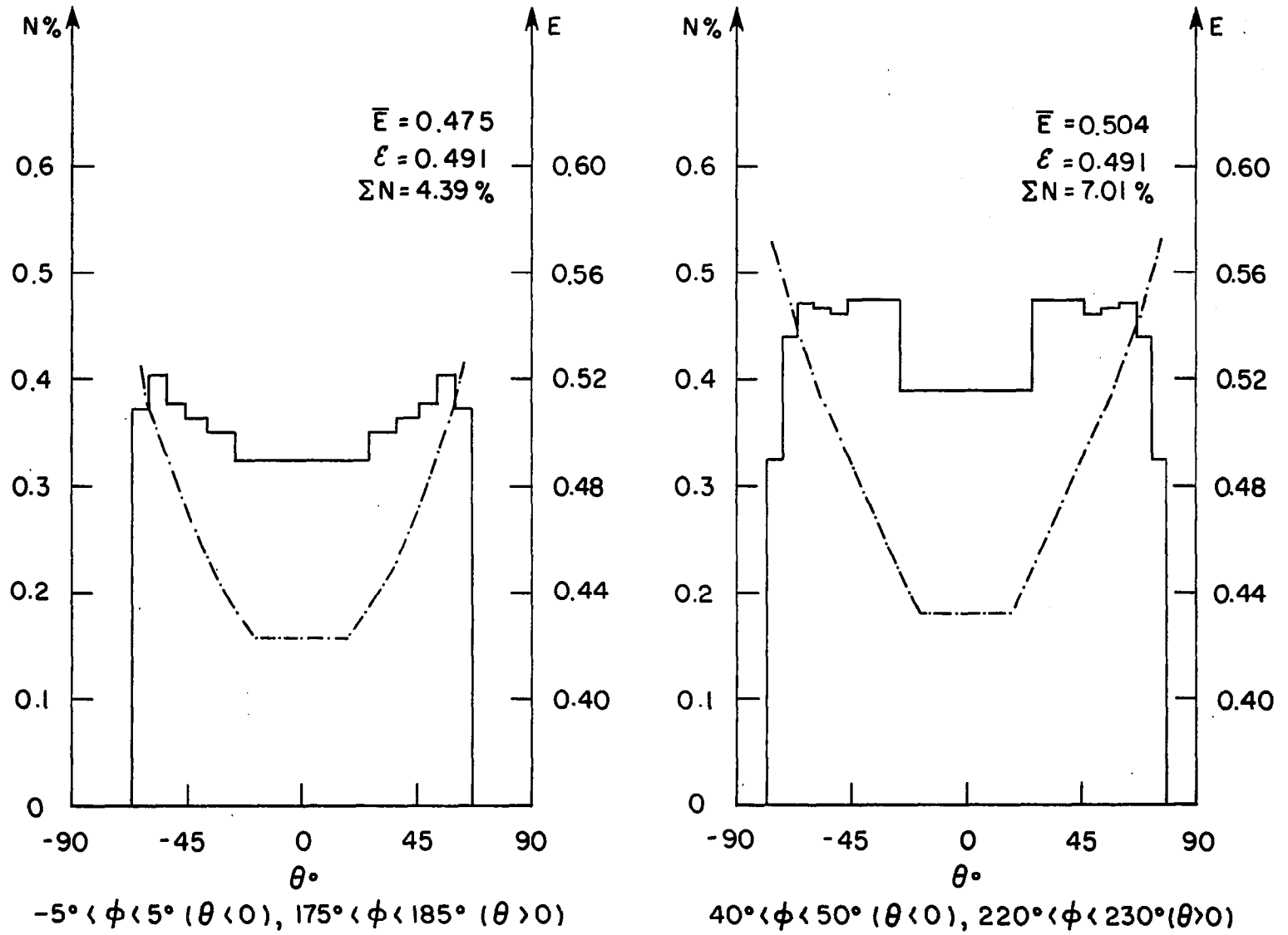

Fig. 2.6 N(θ) and E(θ) for μ = 0.217, R = 1.1, θ_0 = 180°, n = 150

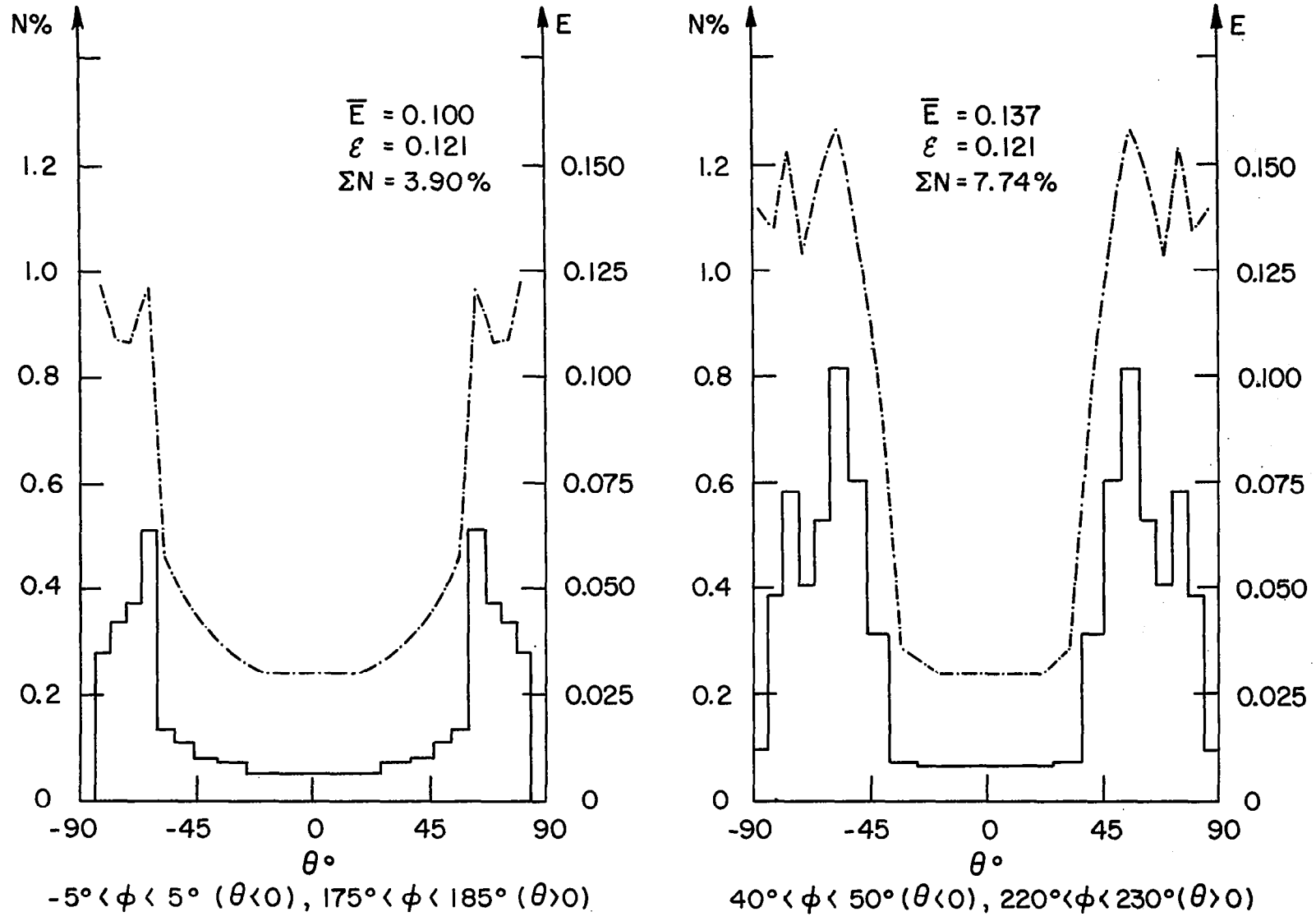

Fig. 2.7 N(θ) and E(θ) for μ = 0.714, R = 1.2, θ_o = 180°, n = 150

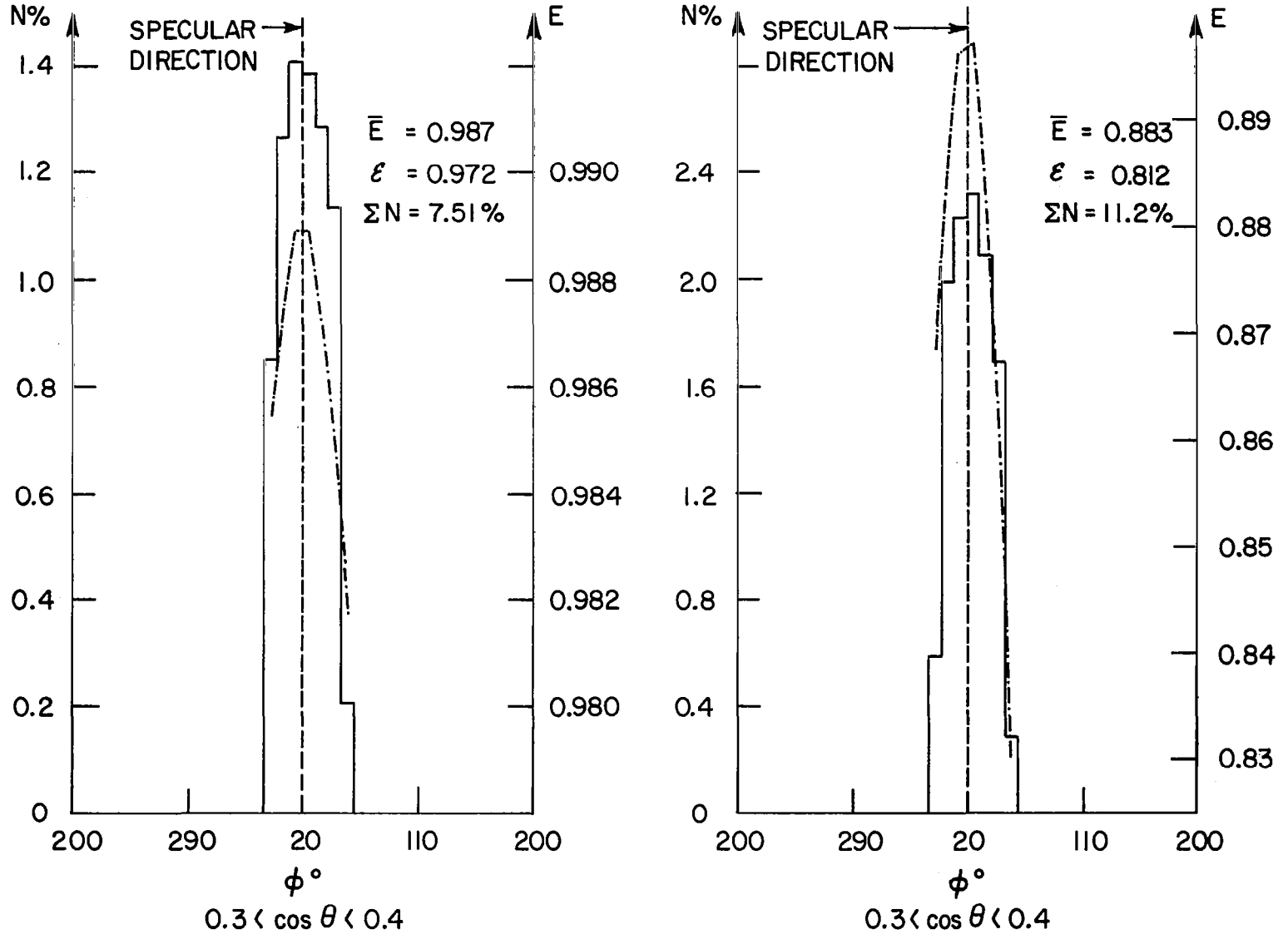

Fig. 3.1 $N(\phi)$ and $E(\phi)$ for $\mu = 0.0218$, $R = 1.0$, $\theta_o = 112.5°$, $\phi_o = 20°$, $n = 150$ *(left)* and for $\mu = 0.217$, $R = 1.1$, $\theta_o = 112.5°$, $\phi_o = 20°$, $n = 150$ *(right)*

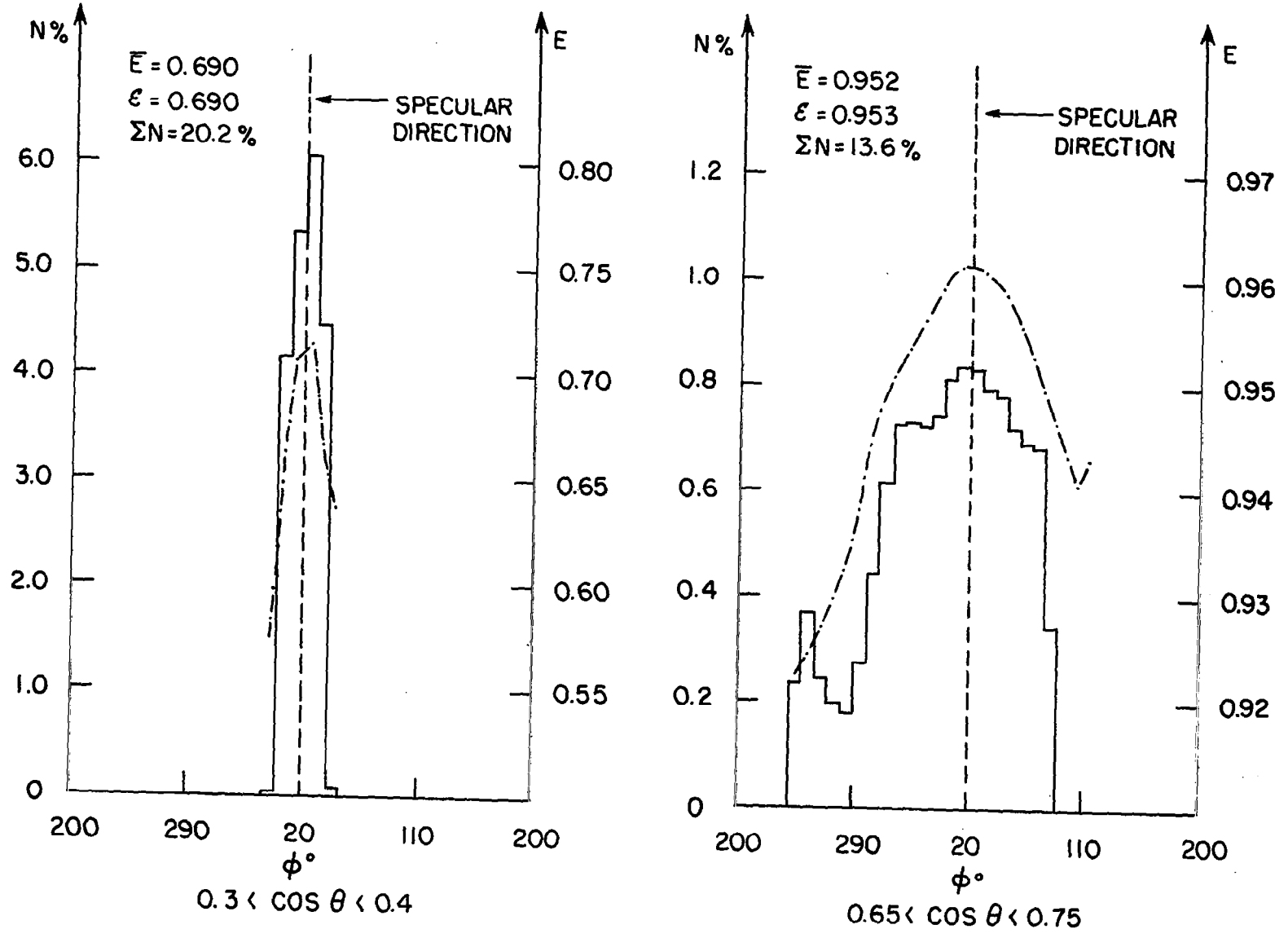

Fig. 3.2 $N(\phi)$ and $E(\phi)$ for $\mu = 0.714$, $R = 1.2$, $\theta_o = 112.5°$, $\phi_o = 20°$, $n = 150$ *(left)* and for $\mu = 0.0218$, $R = 1.0$, $\theta_o = 135°$, $\phi_o = 20°$, $n = 150$ *(right)*

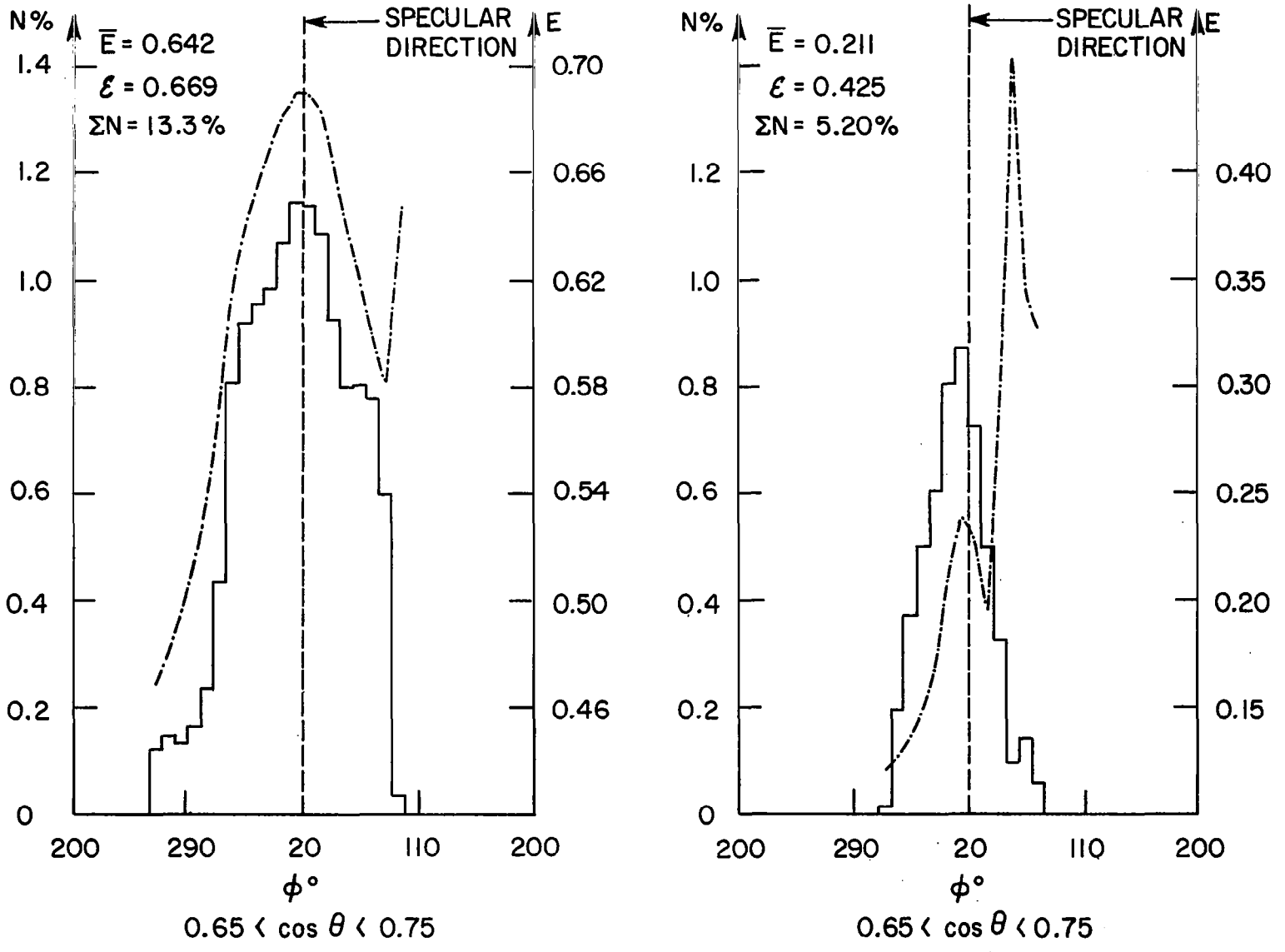

Fig. 3.3 $N(\phi)$ and $E(\phi)$ for $\mu = 0.217$, $R = 1.1$, $\theta_o = 135°$, $\phi_o = 20°$, $n = 150$ *(left)* and for $\mu = 0.714$, $R = 1.2$, $\theta_o = 135°$, $\phi_o = 20°$, $n = 150$ *(right)*

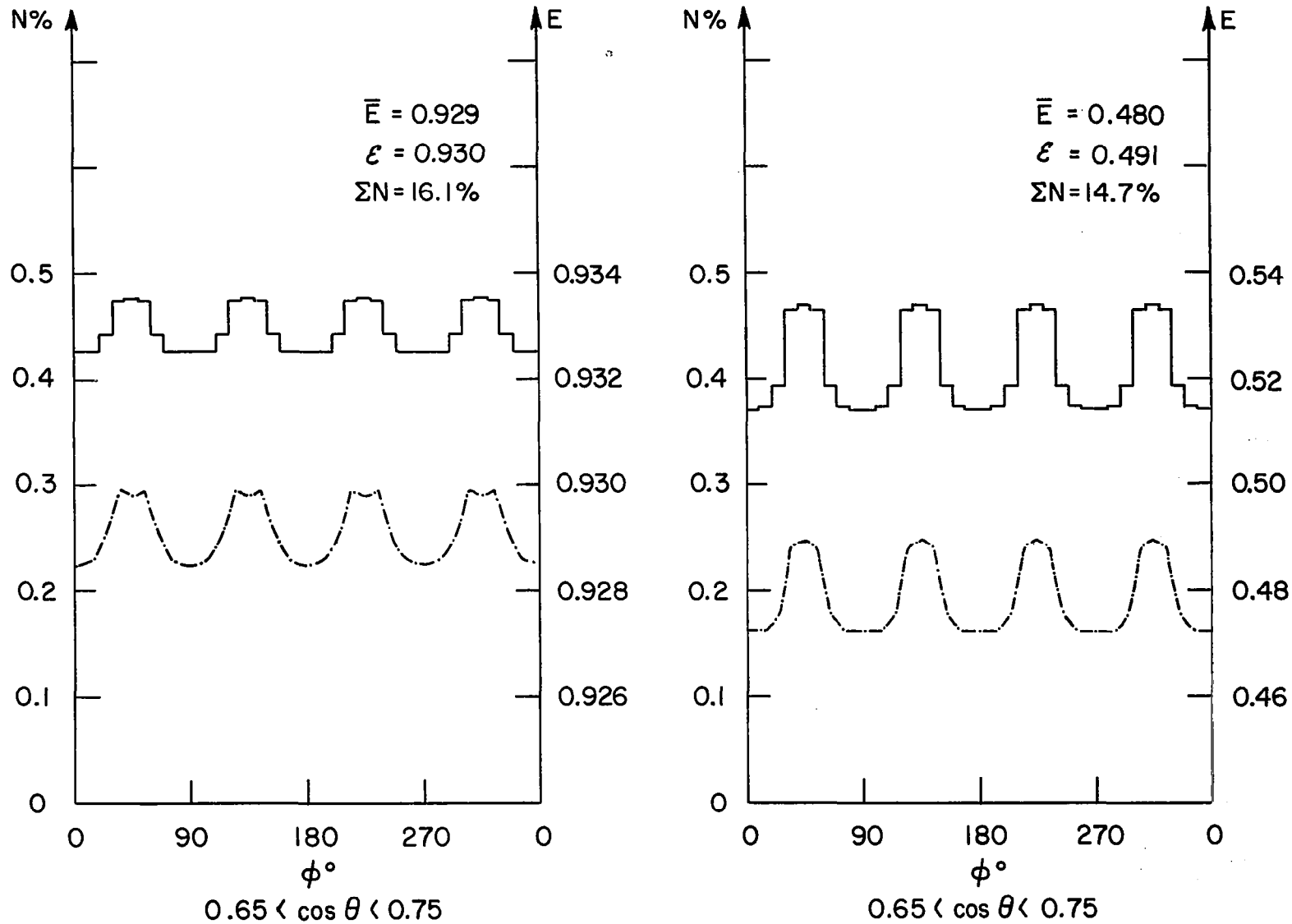

Fig. 3.4 $N(\phi)$ and $E(\phi)$ for $\mu = 0.0218$, $R = 1.0$, $\theta_o = 180°$, $n = 150$ *(left)* and for $\mu = 0.217$, $R = 1.1$, $\theta_o = 180°$, $n = 150$ *(right)*

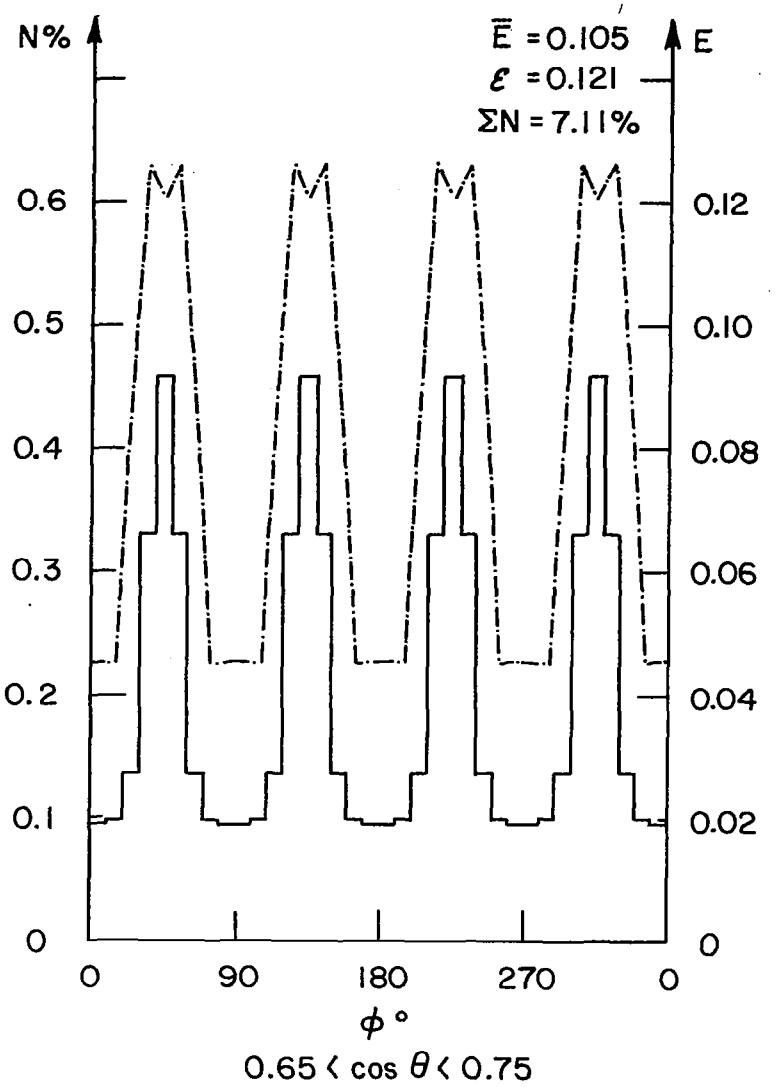

Fig. 3.5 $N(\phi)$ and $E(\phi)$ for $\mu = 0.714$, $R = 1.2$, $\theta_o = 180°$, $n \simeq 150$

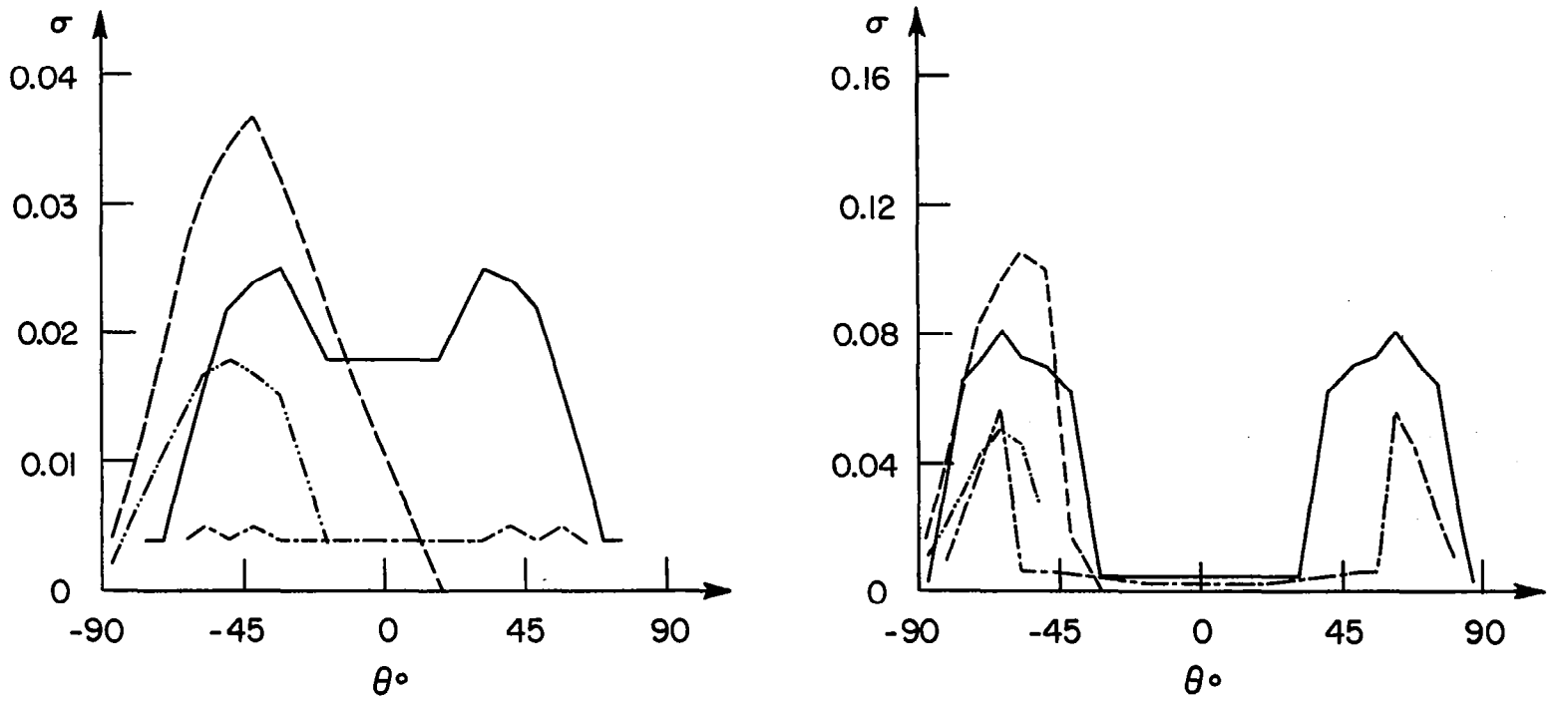

($\sigma' = 0.047$, $\sum = 0.051$) ——·——·—— $\phi = 20°$ and $200°$ for $\theta_0 = 112.5°$ ($\sigma' = 0.073$, $\sum = 0.077$)

($\sigma' = 0.059$, $\sum = 0.071$) – – – – – – $\phi = 20°$ and $200°$ for $\theta_0 = 135°$ ($\sigma' = 0.114$, $\sum = 0.121$)

($\sigma' = 0.034$, $\sum = 0.032$) ——— $\phi = 45°$ and $225°$ for $\theta_0 = 180°$ ($\sigma' = 0.078$, $\sum = 0.074$)

($\sigma' = 0.026$, $\sum = 0.032$) —·—·—·— $\phi = 0$ and $180°$ for $\theta_0 = 180°$ ($\sigma' = 0.065$, $\sum = 0.074$)

Fig. 4.1 $\sigma(\theta)$ for $\mu = 0.217$, R = 1.1, $\phi_0 = 20°$, n = 150 *(left)*
and for $\mu = 0.714$, R = 1.2, $\phi_0 = 20°$, n = 150 *(right)*

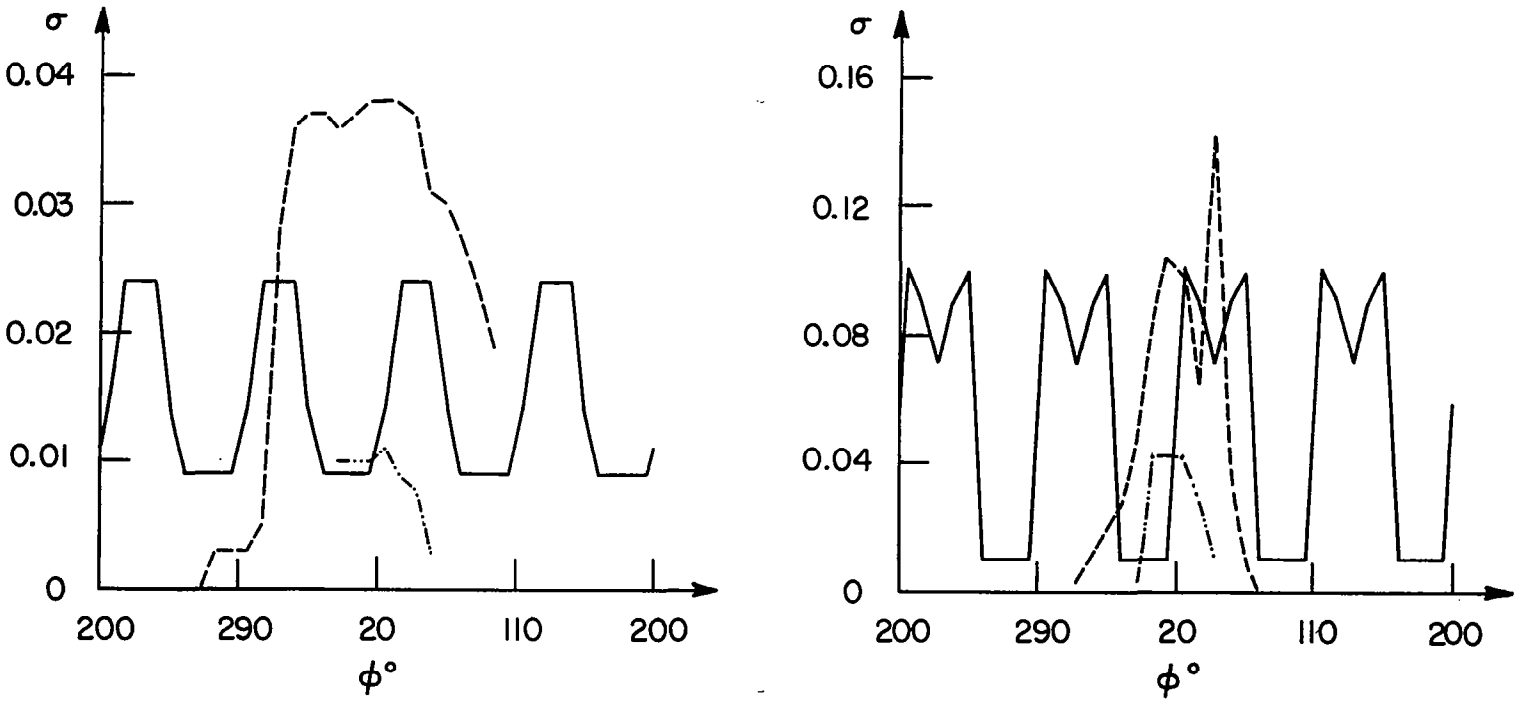

$(\sigma' = 0.013, \sum = 0.051)$ ——·——·—— $\cos\theta = 0.35$ for $\theta_0 = 112.5°$ $(\sigma' = 0.043, \sum = 0.077)$

$(\sigma' = 0.046, \sum = 0.071)$ — — — — — $\cos\theta = 0.70$ for $\theta_0 = 135°$ $(\sigma' = 0.100, \sum = 0.121)$

$(\sigma' = 0.019, \sum = 0.032)$ ———— $\cos\theta = 0.70$ for $\theta_0 = 180°$ $(\sigma' = 0.091, \sum = 0.074)$

Fig. 4.2 $\sigma(\phi)$ for $\mu = 0.217$, $R = 1.1$, $\phi_o = 20°$, $n = 150$ *(left)*
and for $\mu = 0.714$, $R = 1.2$, $\phi_o = 20°$, $n = 150$ *(right)*

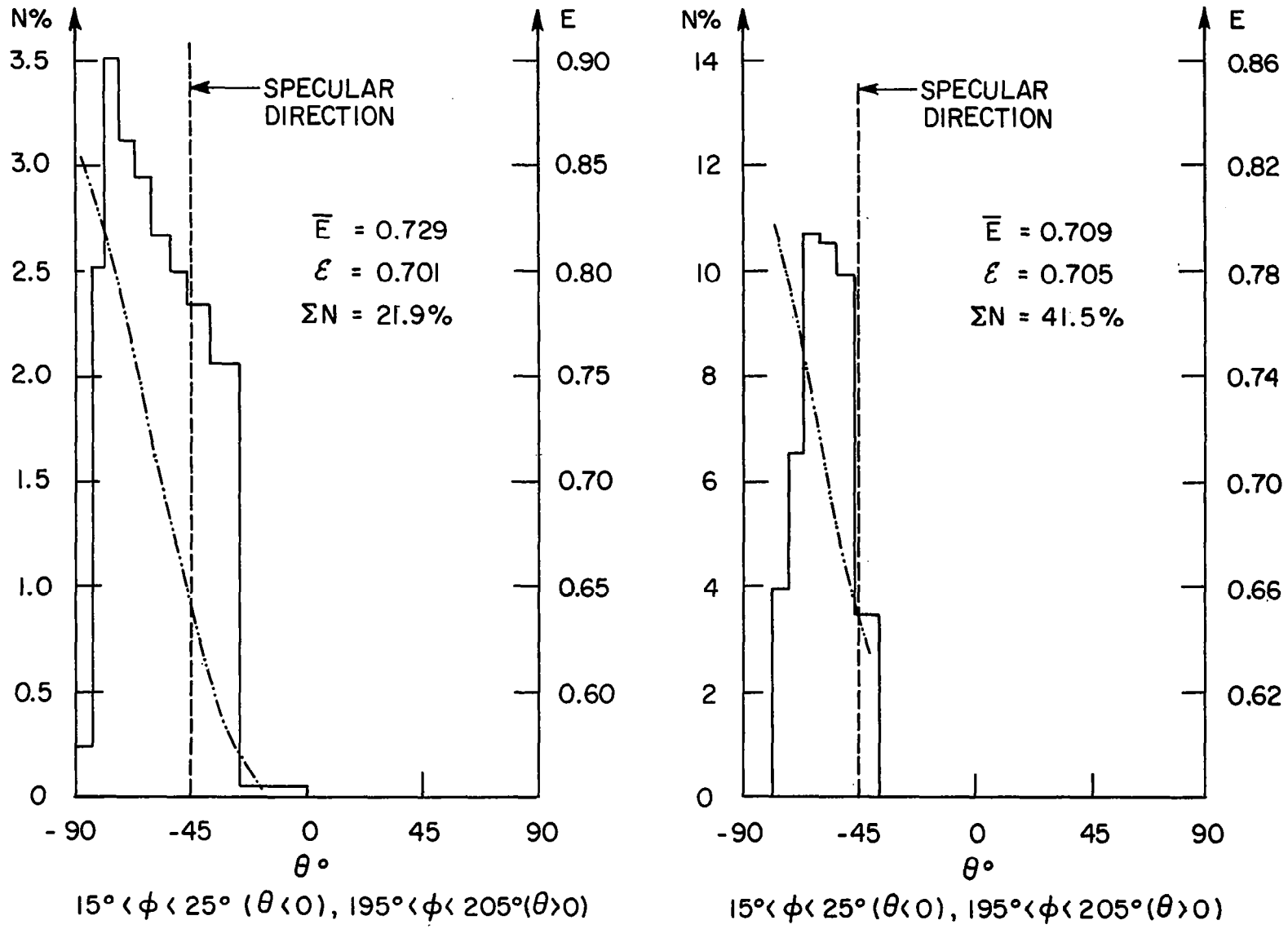

Fig. 5.1 N(θ) and E(θ) for μ = 0.217, R = 2, θ_o = 135°, ϕ_o = 20°, n = 150 *(left)* and for μ = 0.217, R = 4, θ_o = 135°, ϕ_o = 20°, n = 150 *(right)*

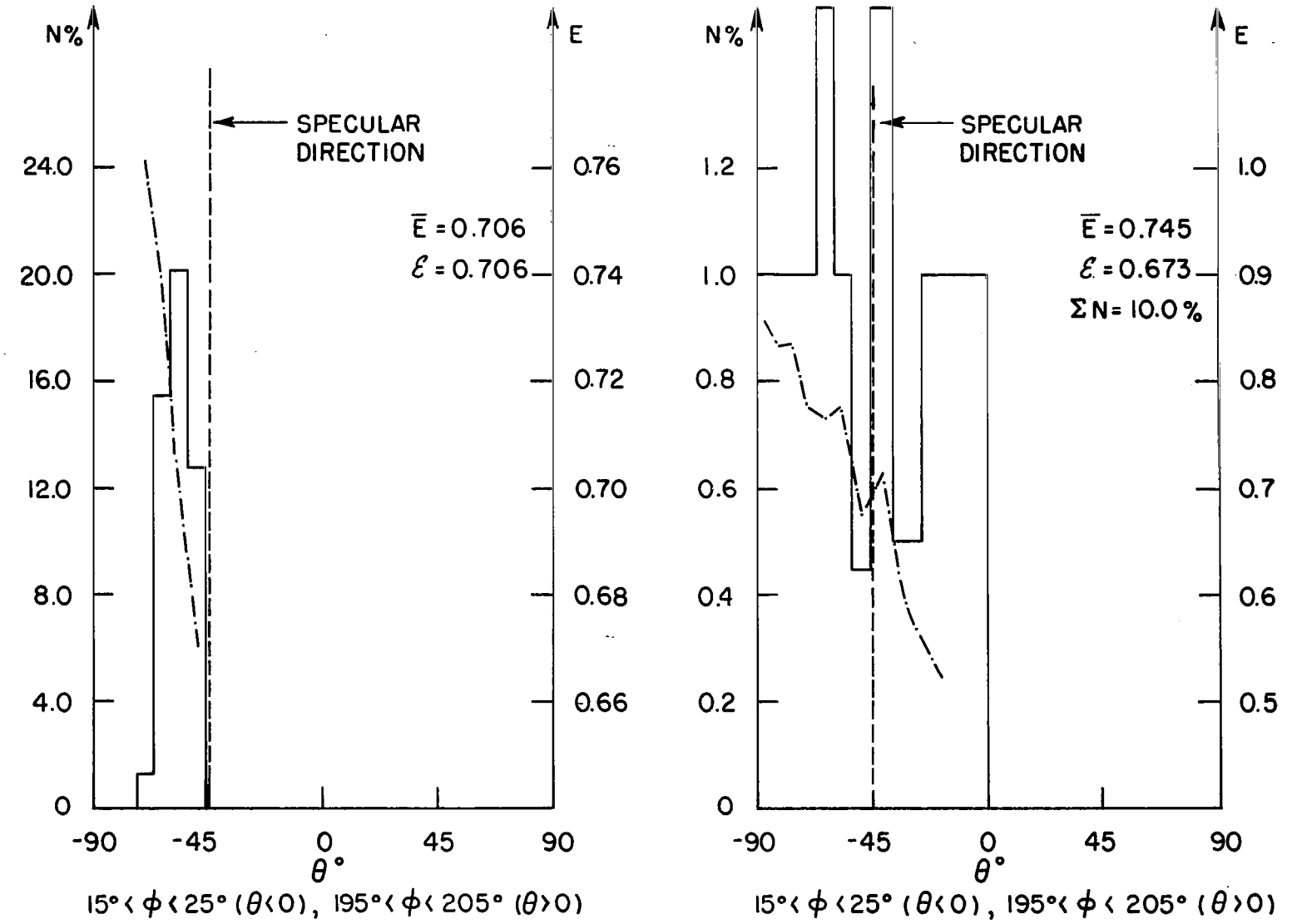

Fig. 5.2 N(θ) and E(θ) for μ = 0.217, R = 6, θ_o = 135°, ϕ_o = 20°, n = 150 *(left)* and for μ = 0.217, R = 1.1, θ_o = 135°, ϕ_o = 20°, n = 10 *(right)*

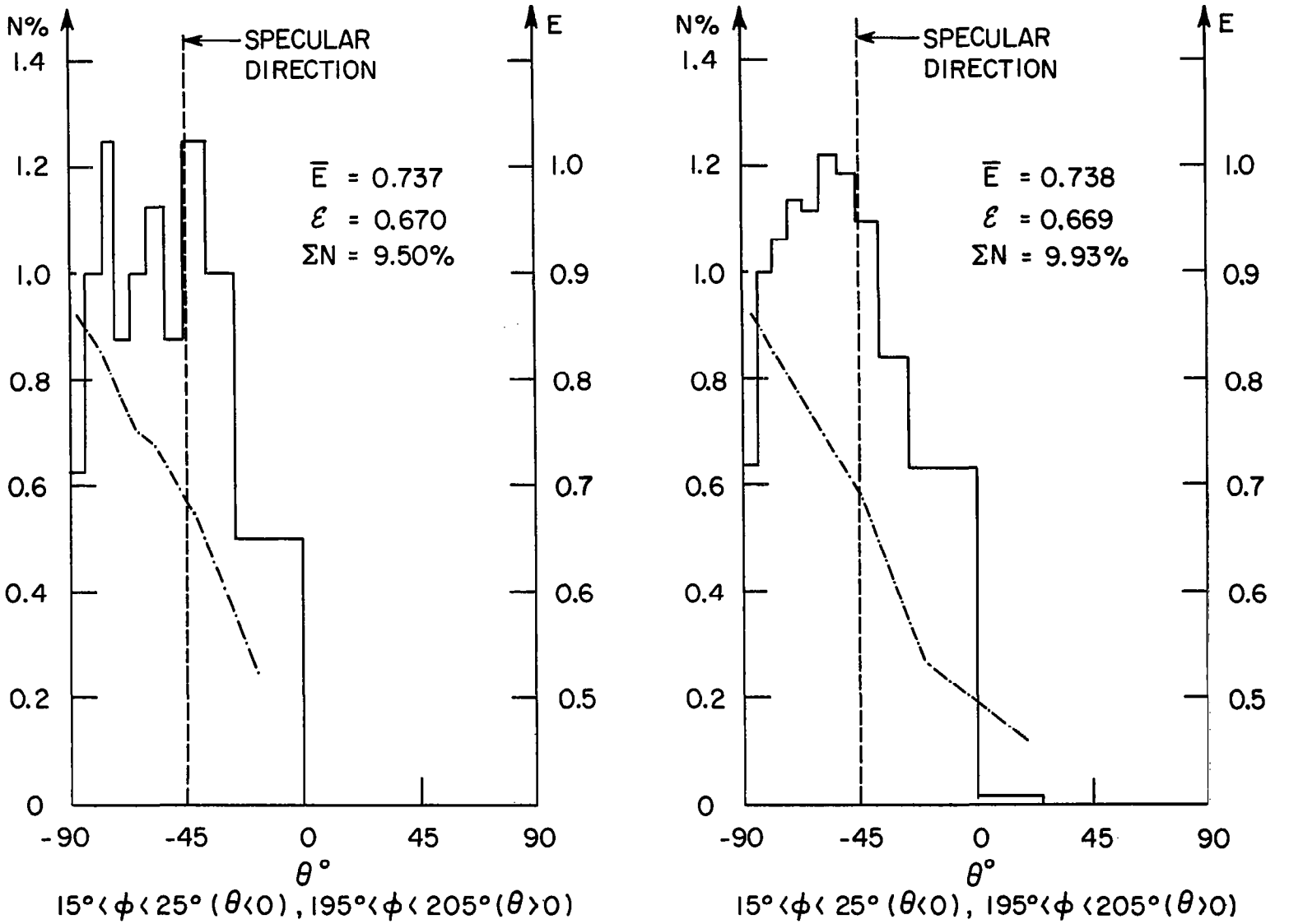

Fig. 5.3 N(θ) and E(θ) for μ = 0.217, R = 1.1, θ_o = 135°, ϕ_o = 20°, n = 20 *(left)* and for μ = 0.217, R = 1.1, θ_o = 135°, ϕ_o = 20°, n = 100 *(right)*

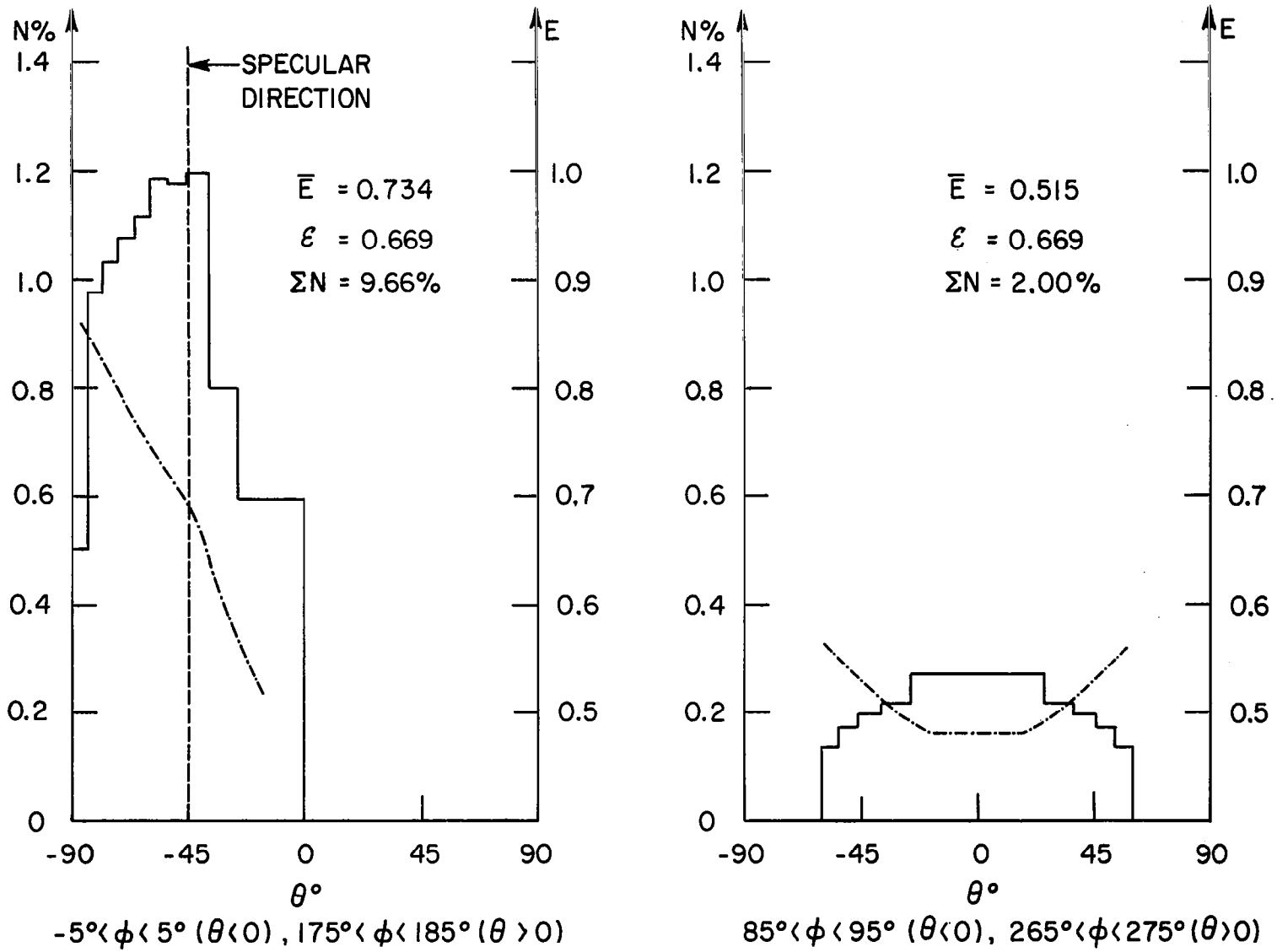

Fig. 5.4 N(θ) and E(θ) for μ = 0.217, R = 1.1, θ_o = 135°, ϕ_o = 0, n = 150

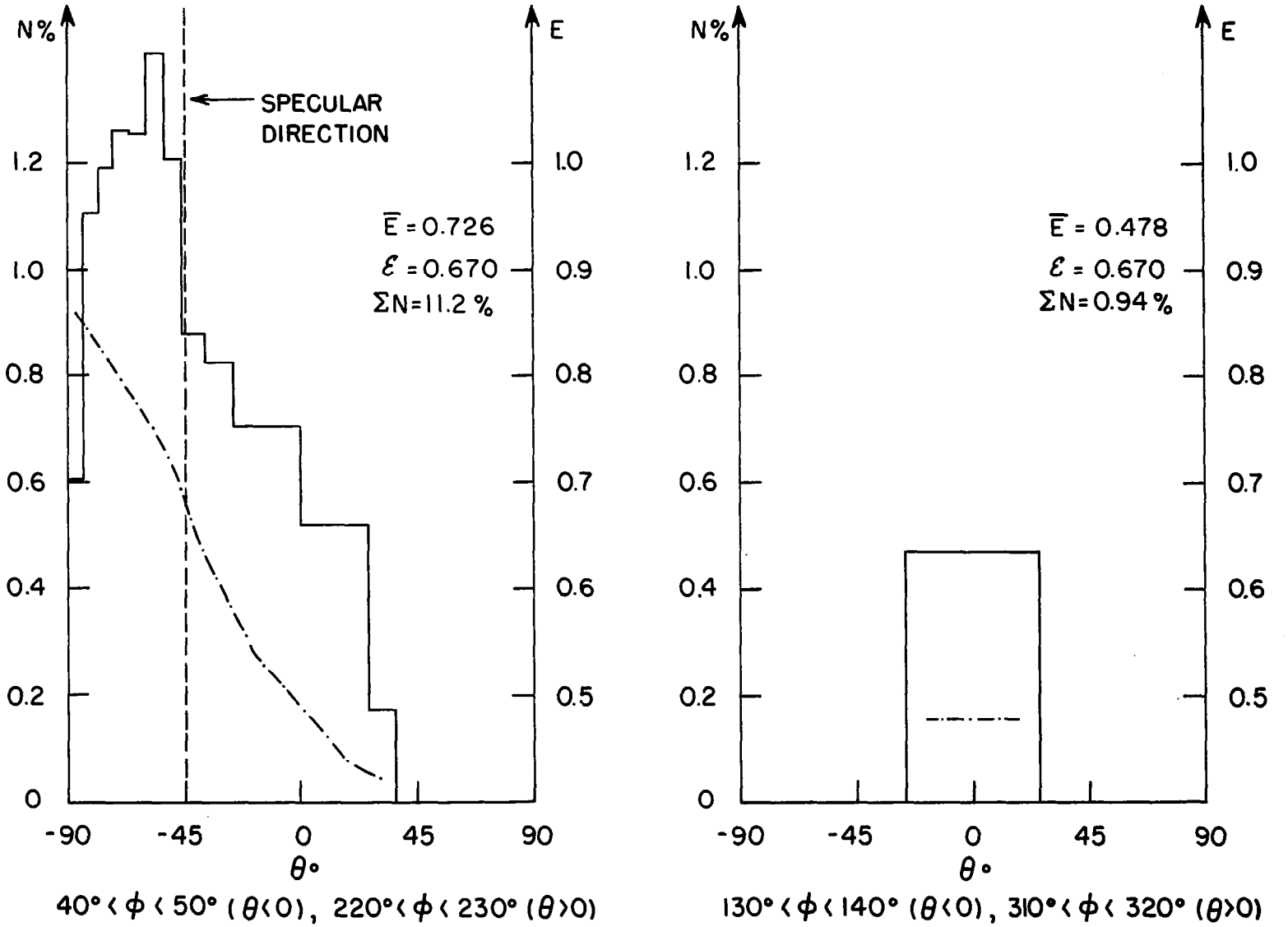

Fig. 5.5 N(θ) and E(θ) for μ = 0.217, R = 1.1, θ_o = 135°, ϕ_o = 45°, n = 150

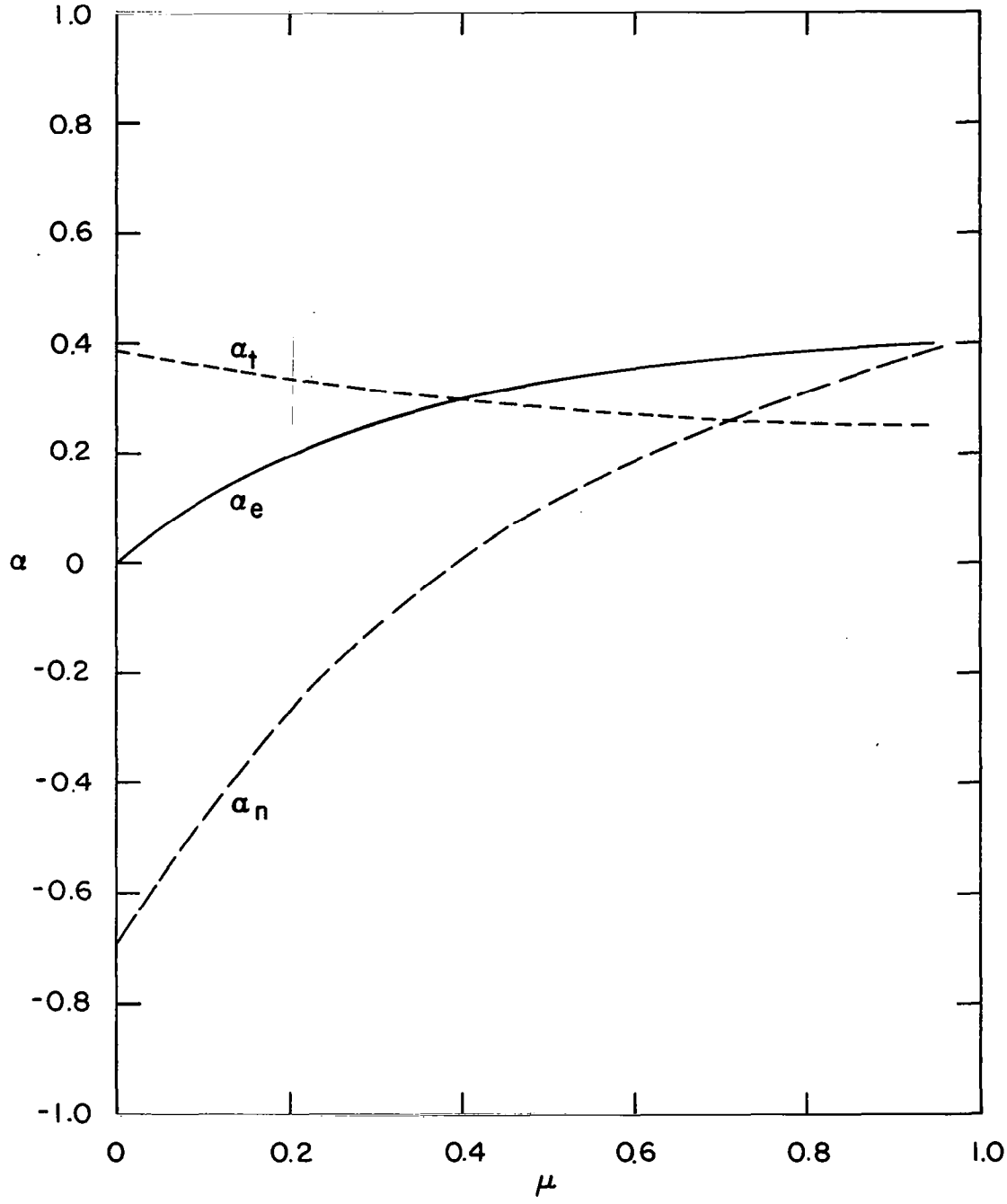

Fig. 6.1 $\alpha(\mu)$ for R = 0.9, S = square, $\theta_o = 112.5°$, $\phi_o = 0$

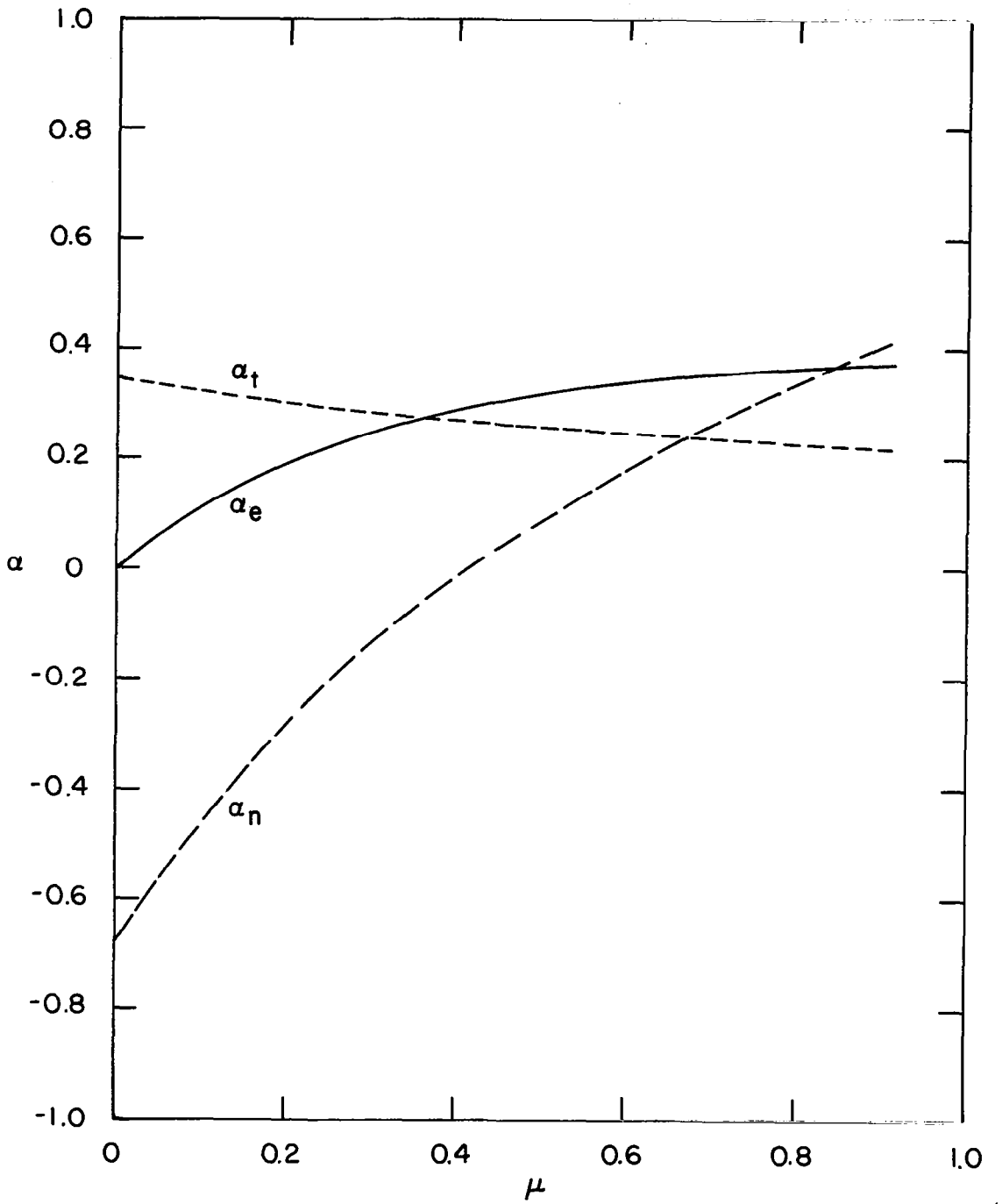

Fig. 6.1a $\alpha(\mu)$ for R = 0.9, S = triangular, $\theta_o = 112.5°$, $\phi_o = 0$

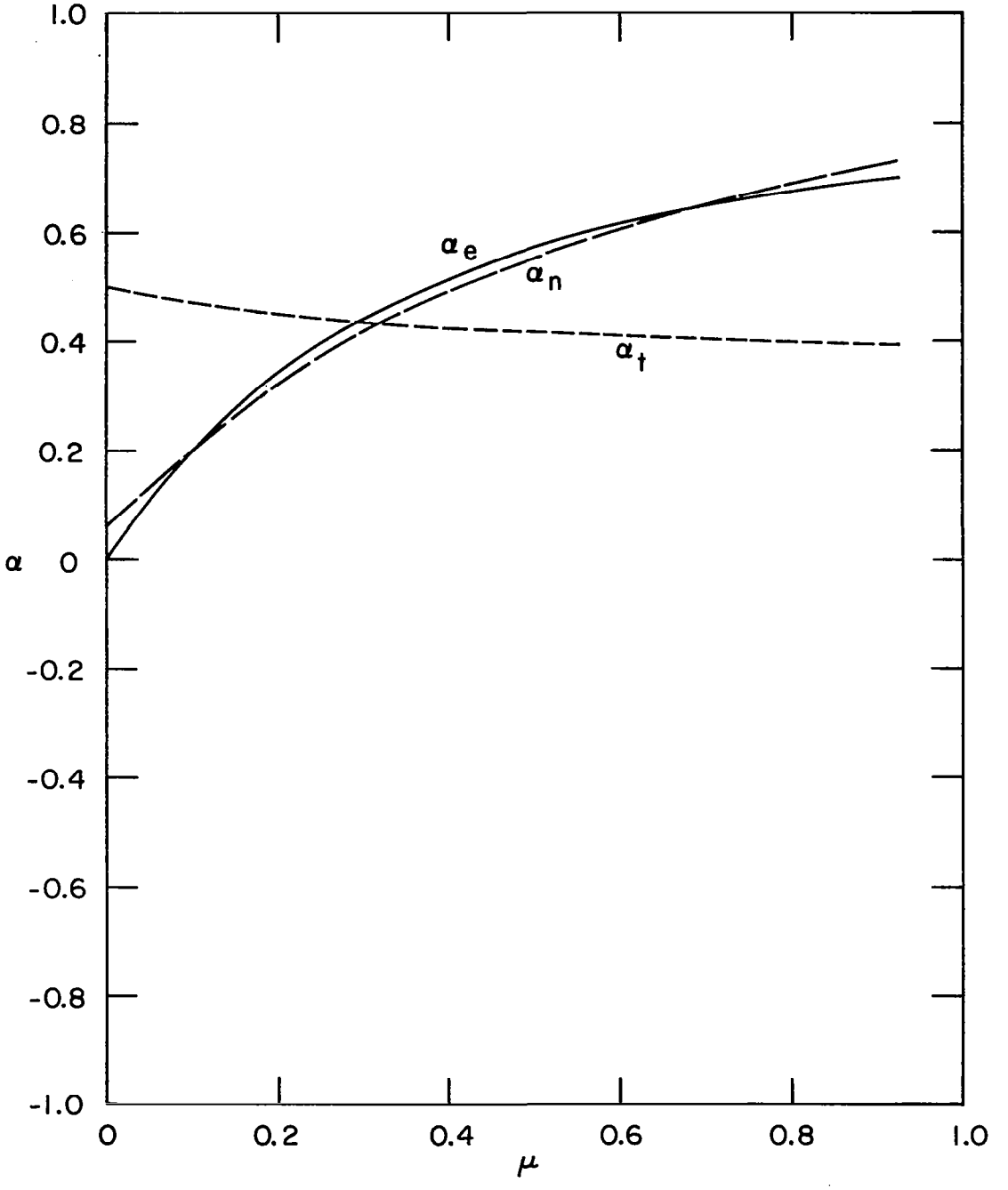

Fig. 6.2 $\alpha(\mu)$ for R = 0.9, S = square, $\theta_o = 135°$, $\phi_o = 0$

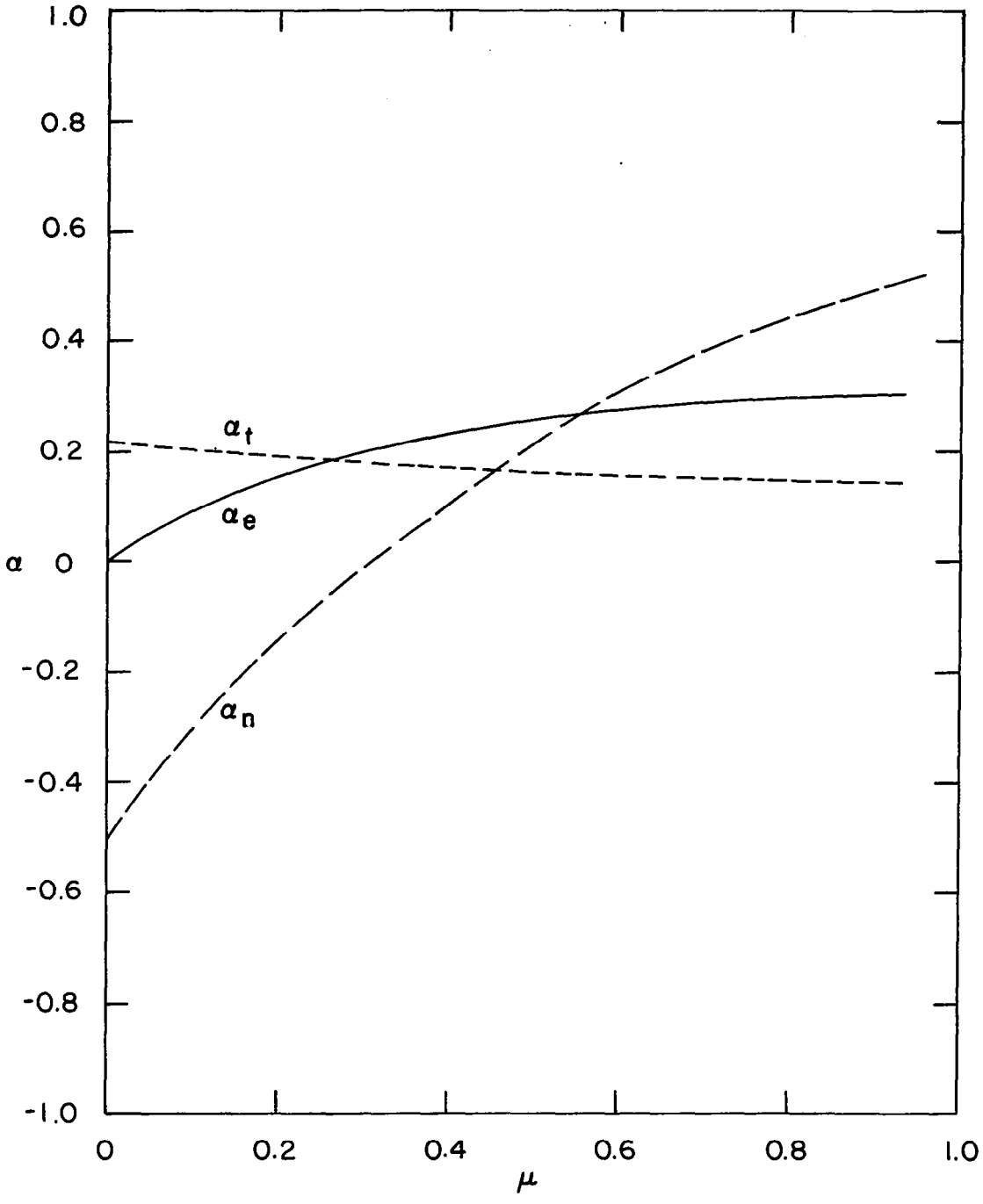

Fig. 6.3 $\alpha(\mu)$ for R = 1.3, S = square, θ_o = 112.5°, ϕ_o = 0

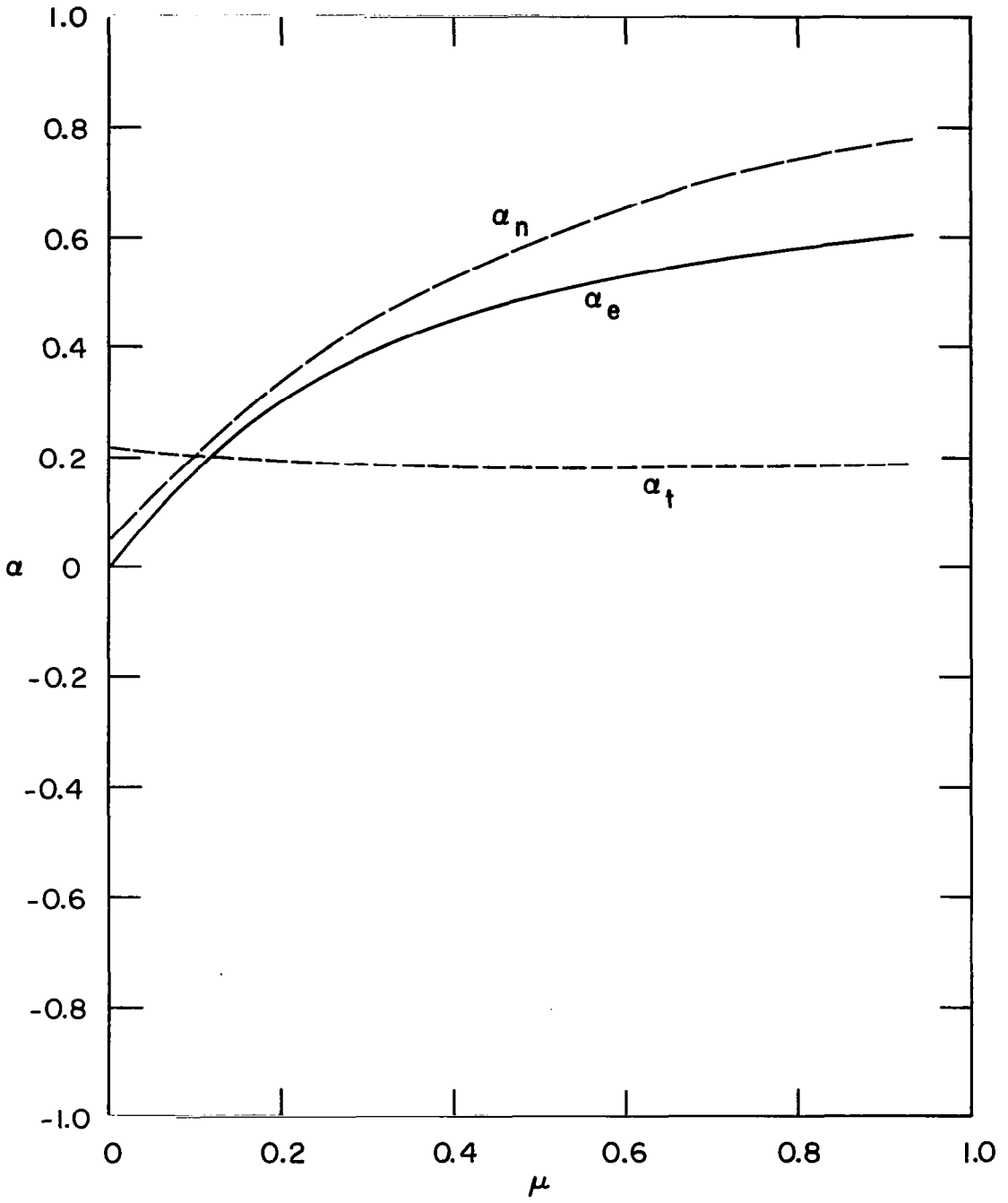

Fig. 6.4 $\alpha(\mu)$ for R = 1.3, S = square, $\theta_o = 135°$, $\phi_o = 0$.

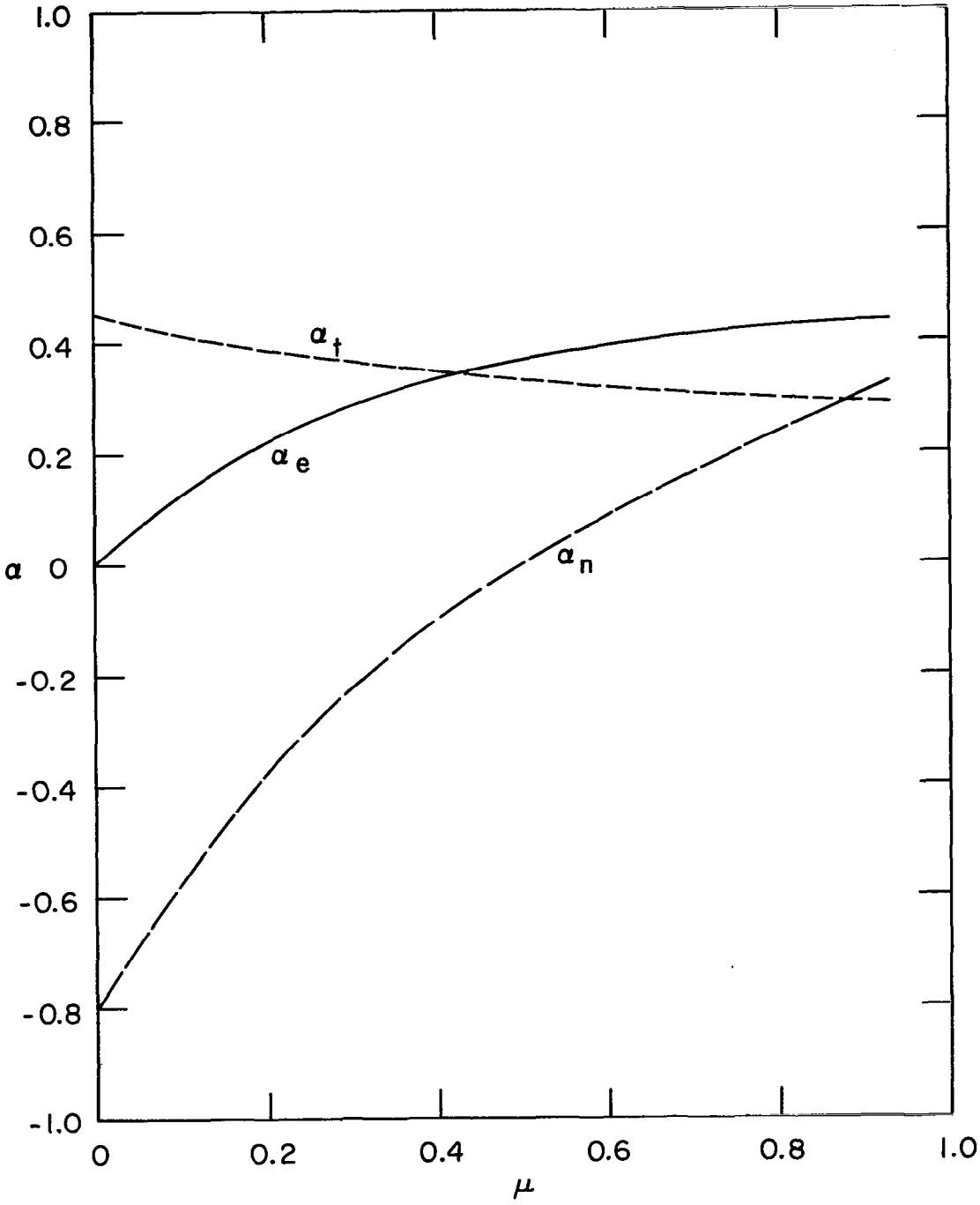

Fig. 6.5 $\alpha(\mu)$ for R = 0.9, S = square, θ_o = 112.5°, ϕ_o = 45°

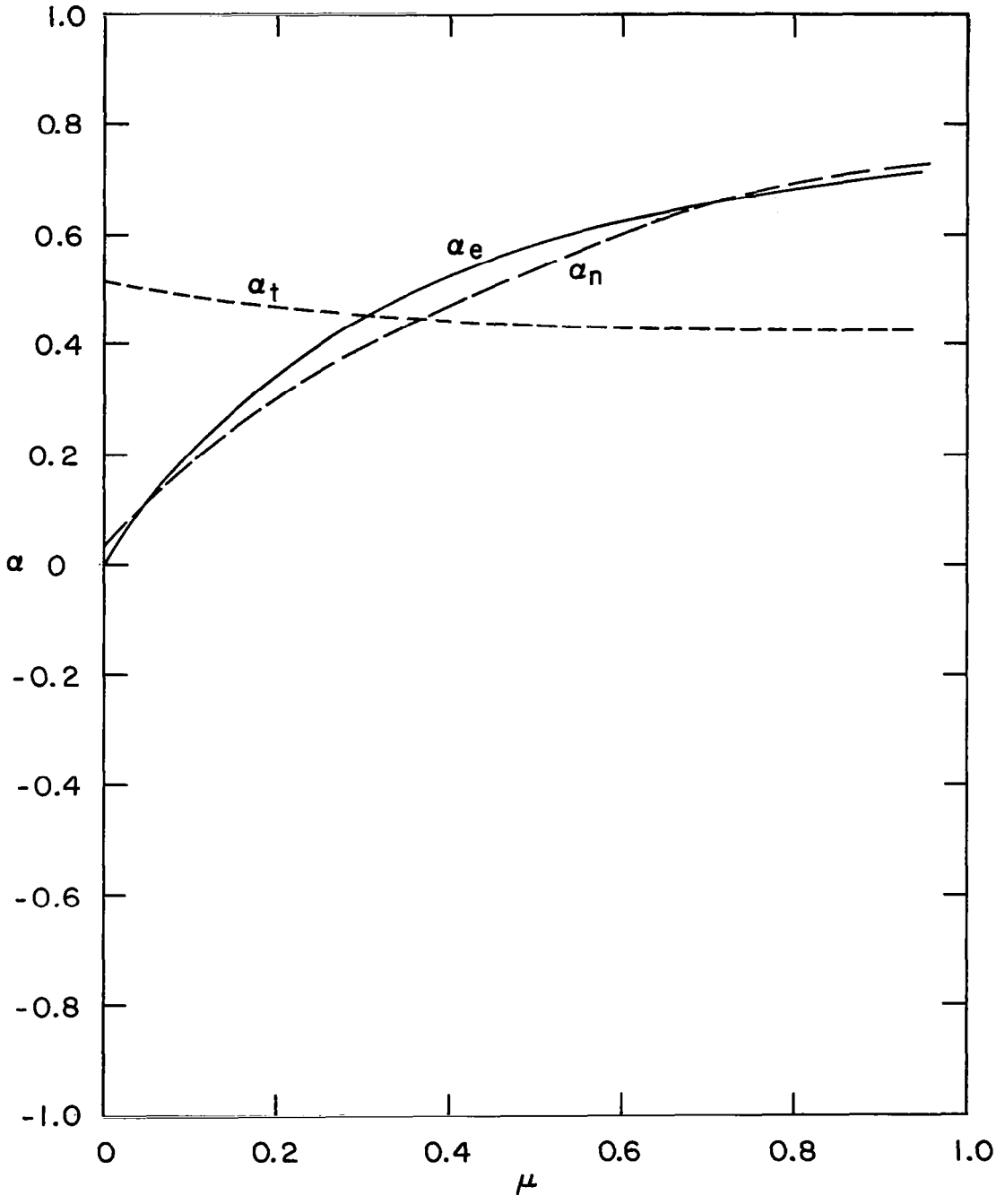

Fig. 6.6 $\alpha(\mu)$ for R = 0.9, S = square, $\theta_o = 135°$, $\phi_o = 45°$

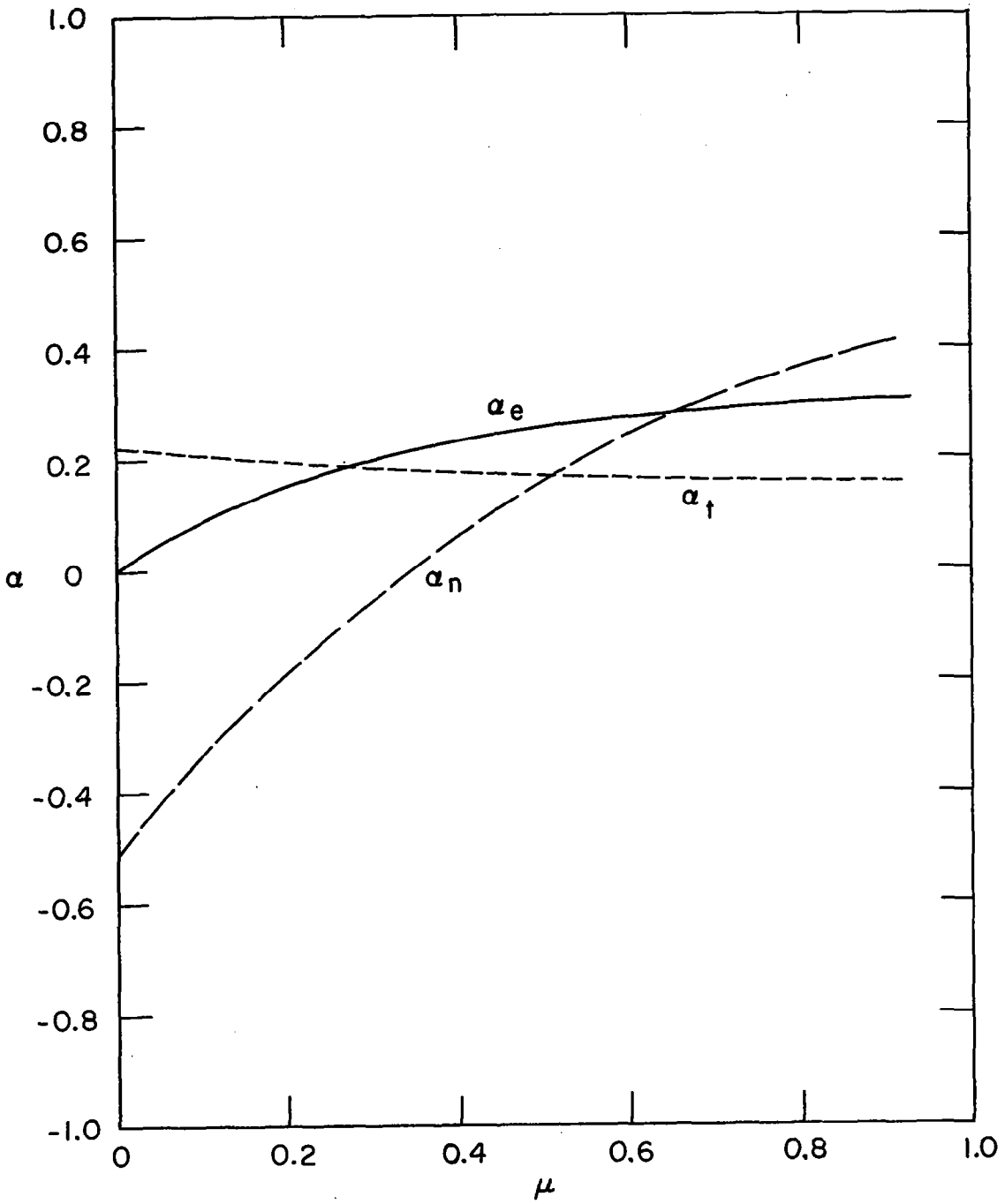

Fig. 6.7 $\alpha(\mu)$ for R = 1.3, S = square, θ_o = 112.5°, ϕ_o = 45°

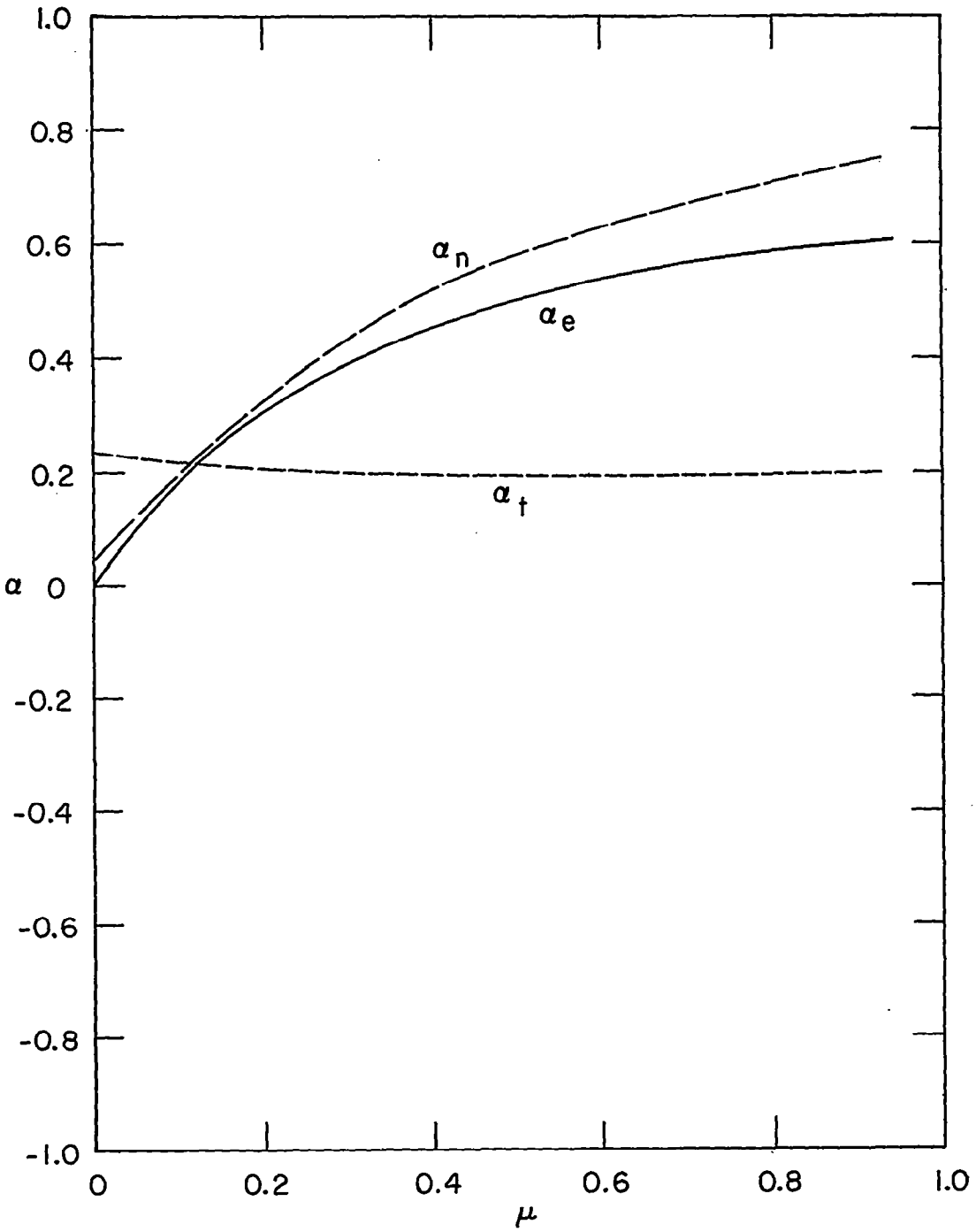

Fig. 6.8 $\alpha(\mu)$ for R = 1.3, S = square, $\theta_o = 135°$, $\phi_o = 45°$

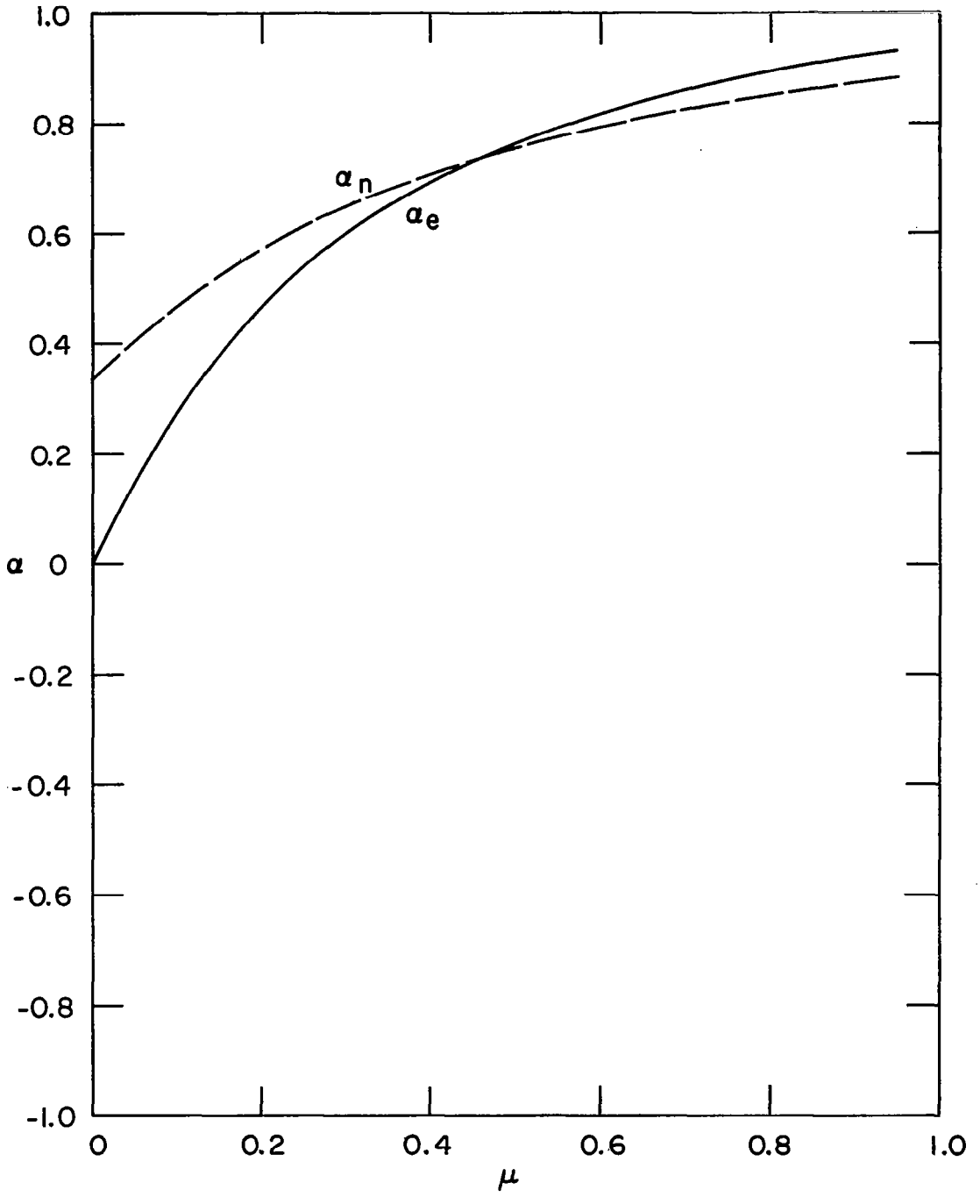

Fig. 6.9 $\alpha(\mu)$ for R = 0.9, S = square, θ_o = 180°

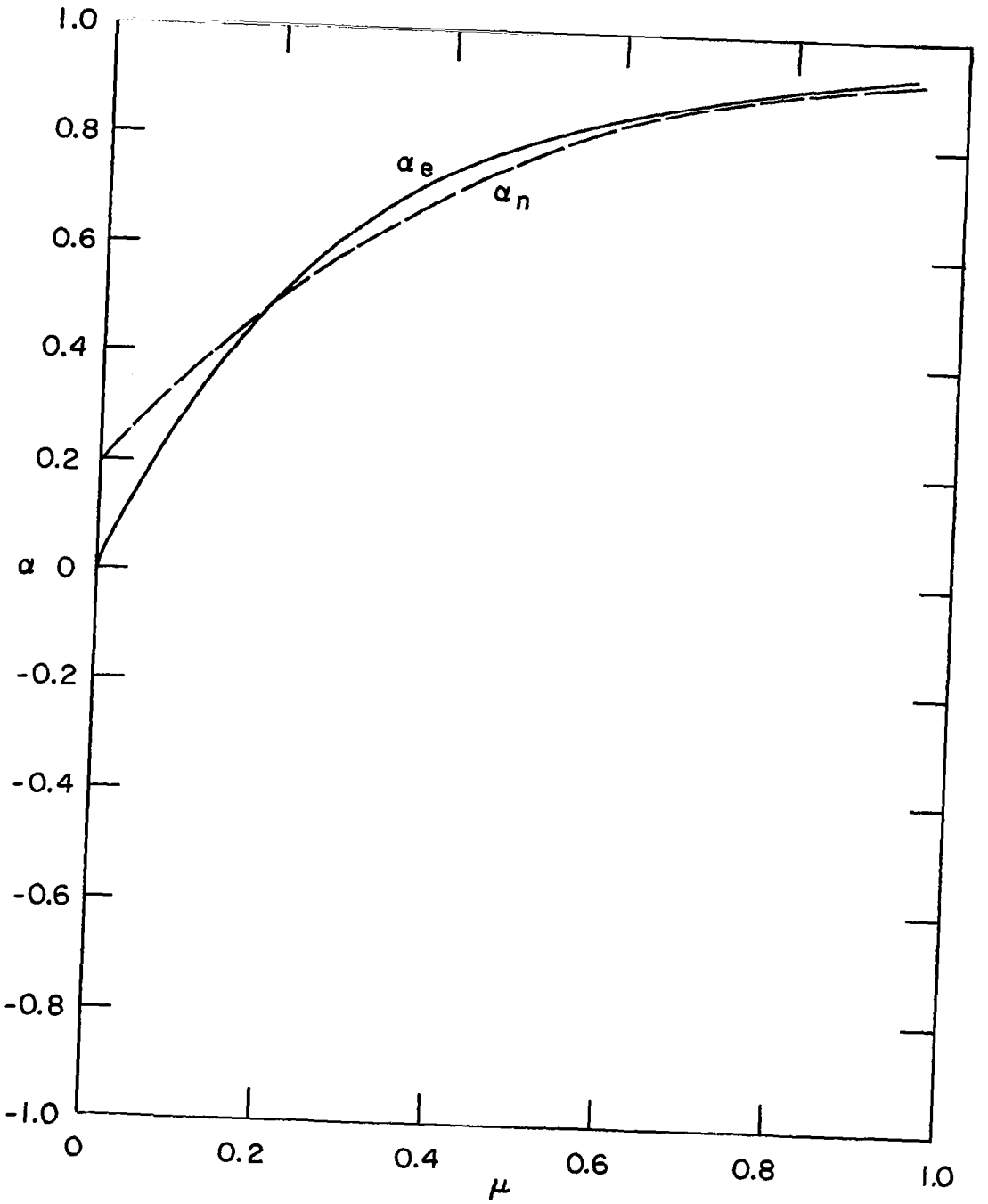

Fig. 6.10 $\alpha(\mu)$ for R = 1.3, S = square, $\theta_o = 180°$

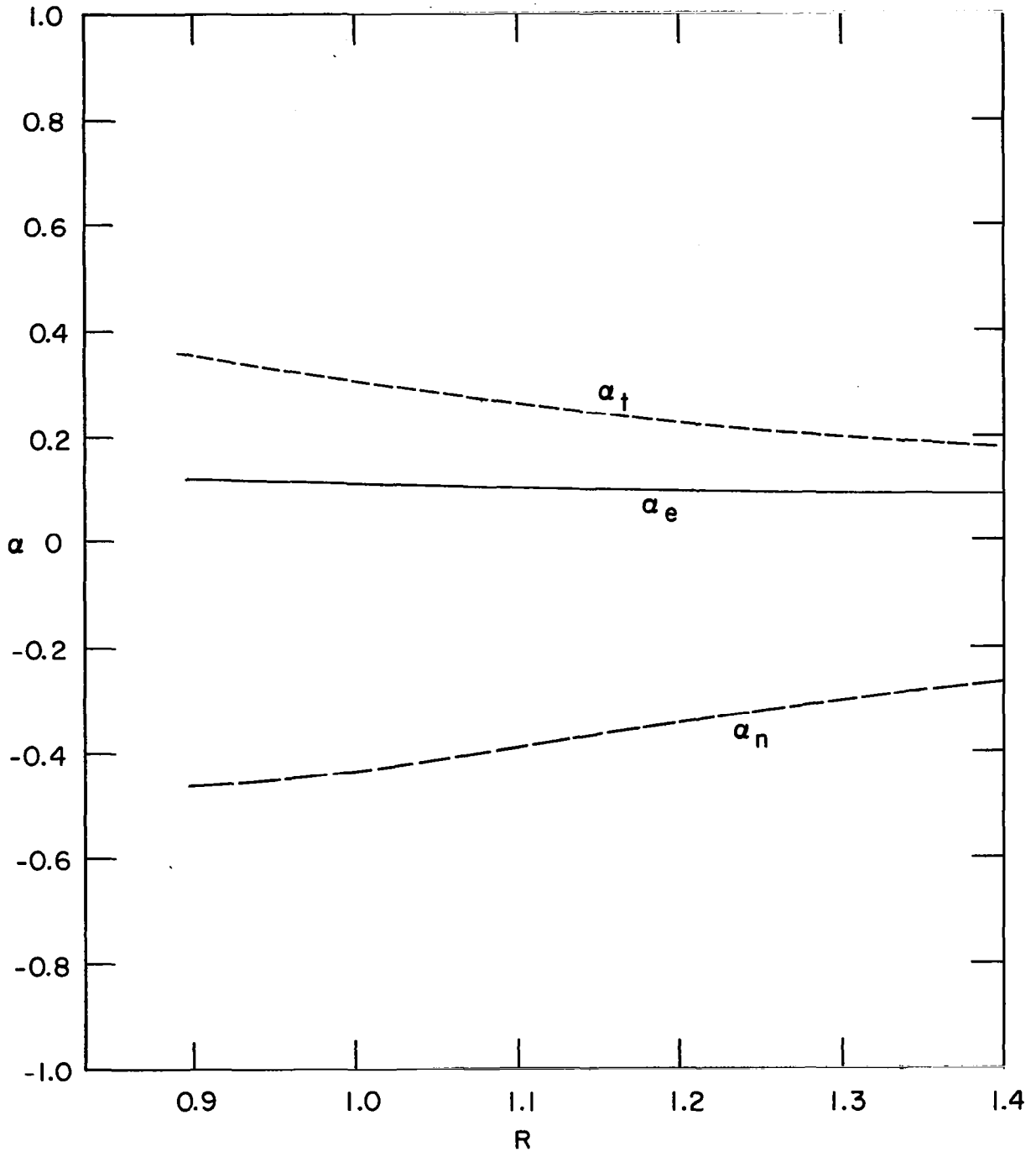

Fig. 6.11 $\alpha(R)$ for $\mu = 0.1$, S = square, $\theta_o = 112.5°$, $\phi_o = 0$

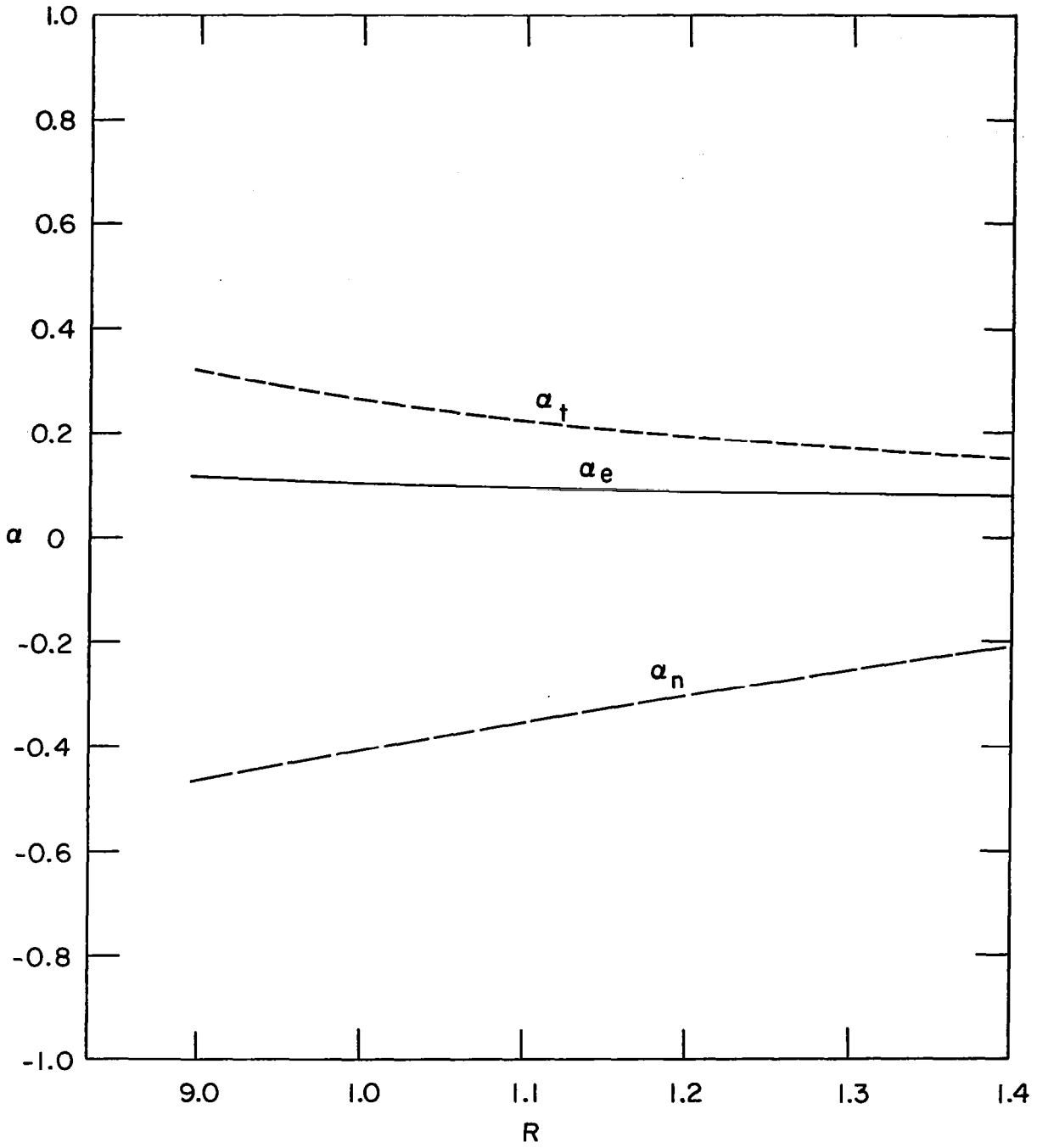

Fig. 6.11a $\alpha(R)$ for $\mu = 0.1$, S = triangular, $\theta_o = 112.5°$, $\phi_o = 0$

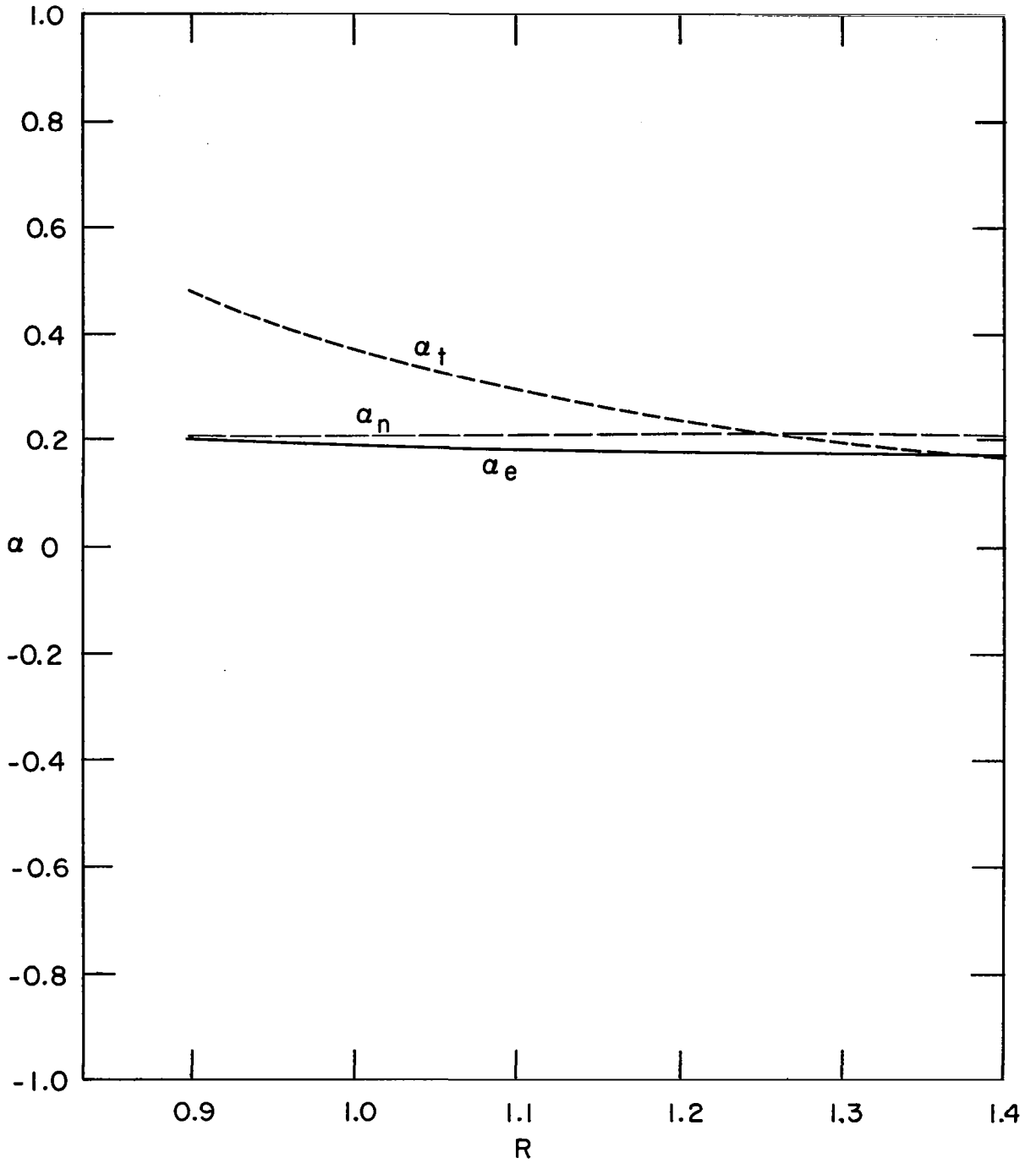

Fig. 6.12 $\alpha(R)$ for $\mu = 0.1$, S = square, $\theta_o = 135°$, $\phi_o = 0$

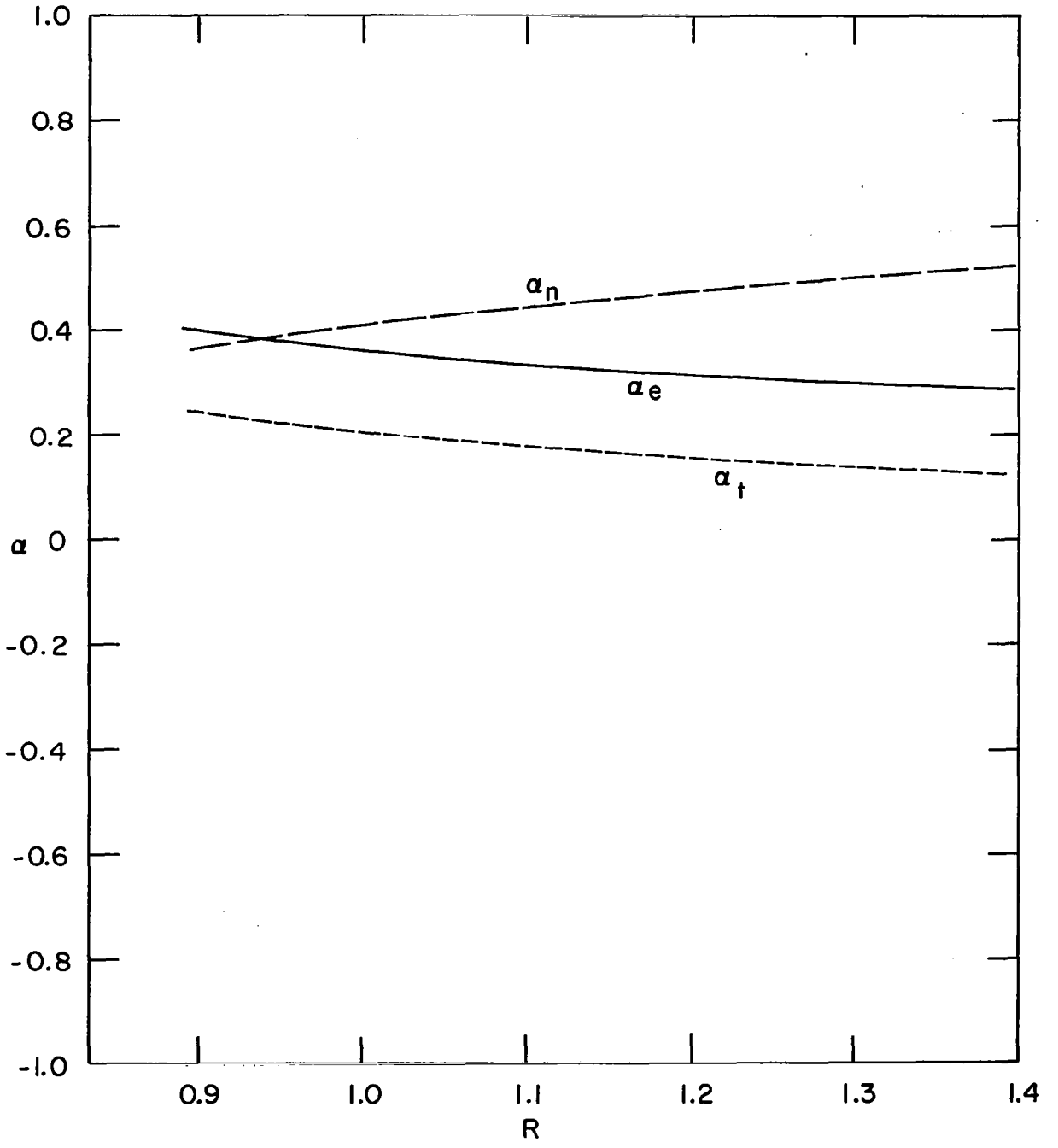

Fig. 6.13 $\alpha(R)$ for $\mu = 0.9$, S = square, $\theta_o = 112.5°$, $\phi_o = 0$

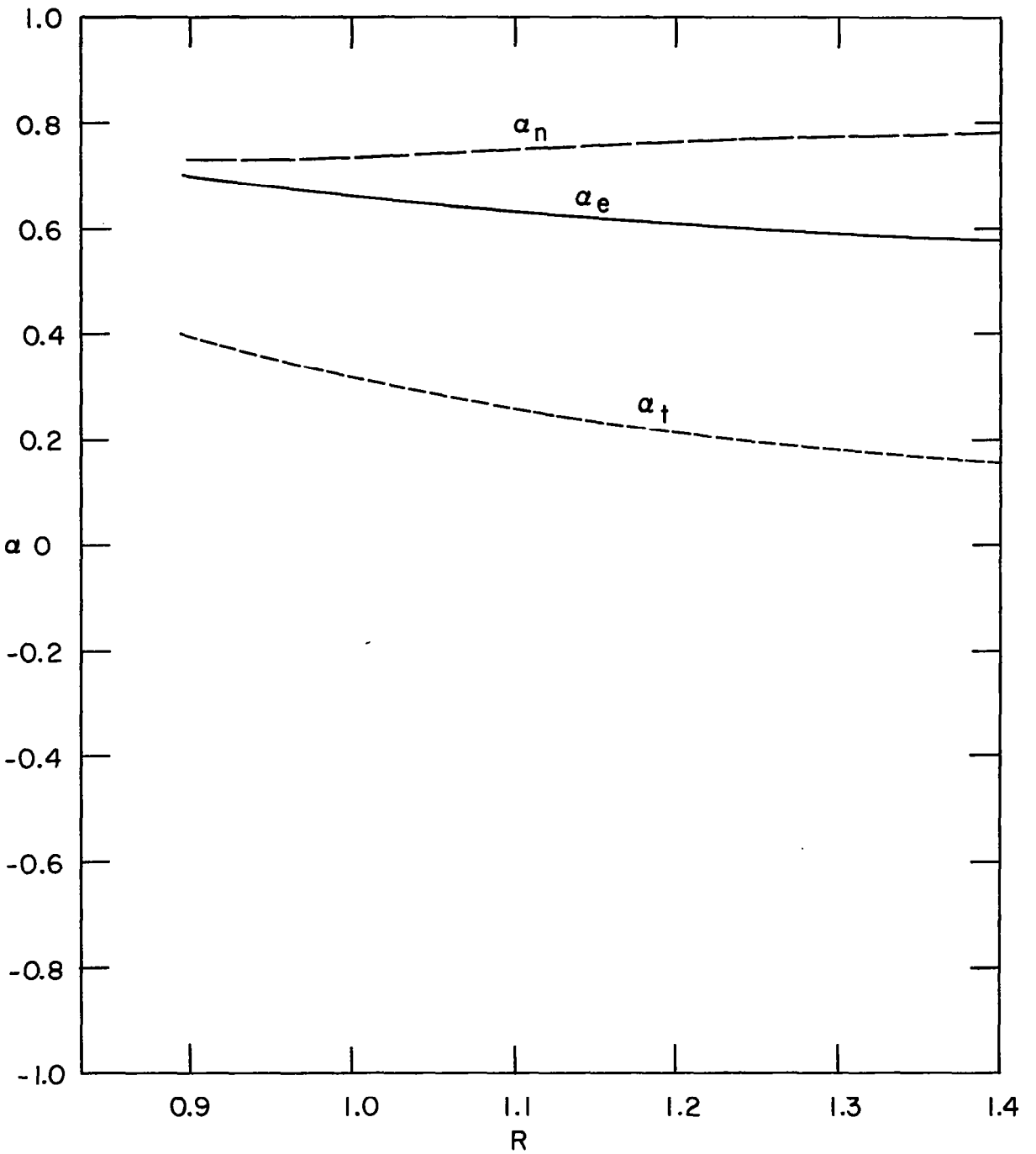

Fig. 6.14 $\alpha(R)$ for $\mu = 0.9$, S = square, $\theta_o = 135°$, $\phi_o = 0$

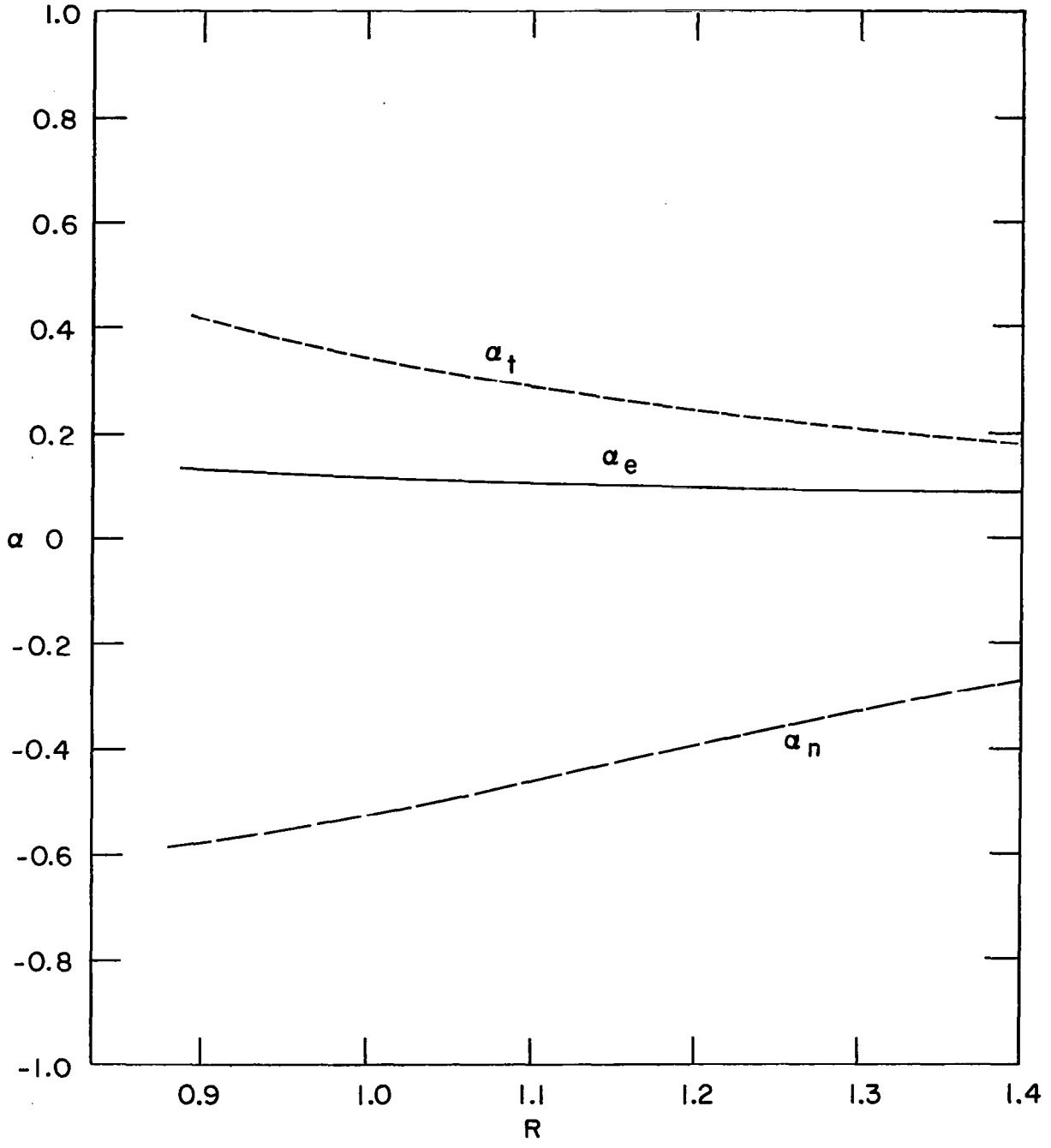

Fig. 6.15 $\alpha(R)$ for $\mu = 0.1$, S = square, $\theta_o = 112.5°$, $\phi_o = 45°$

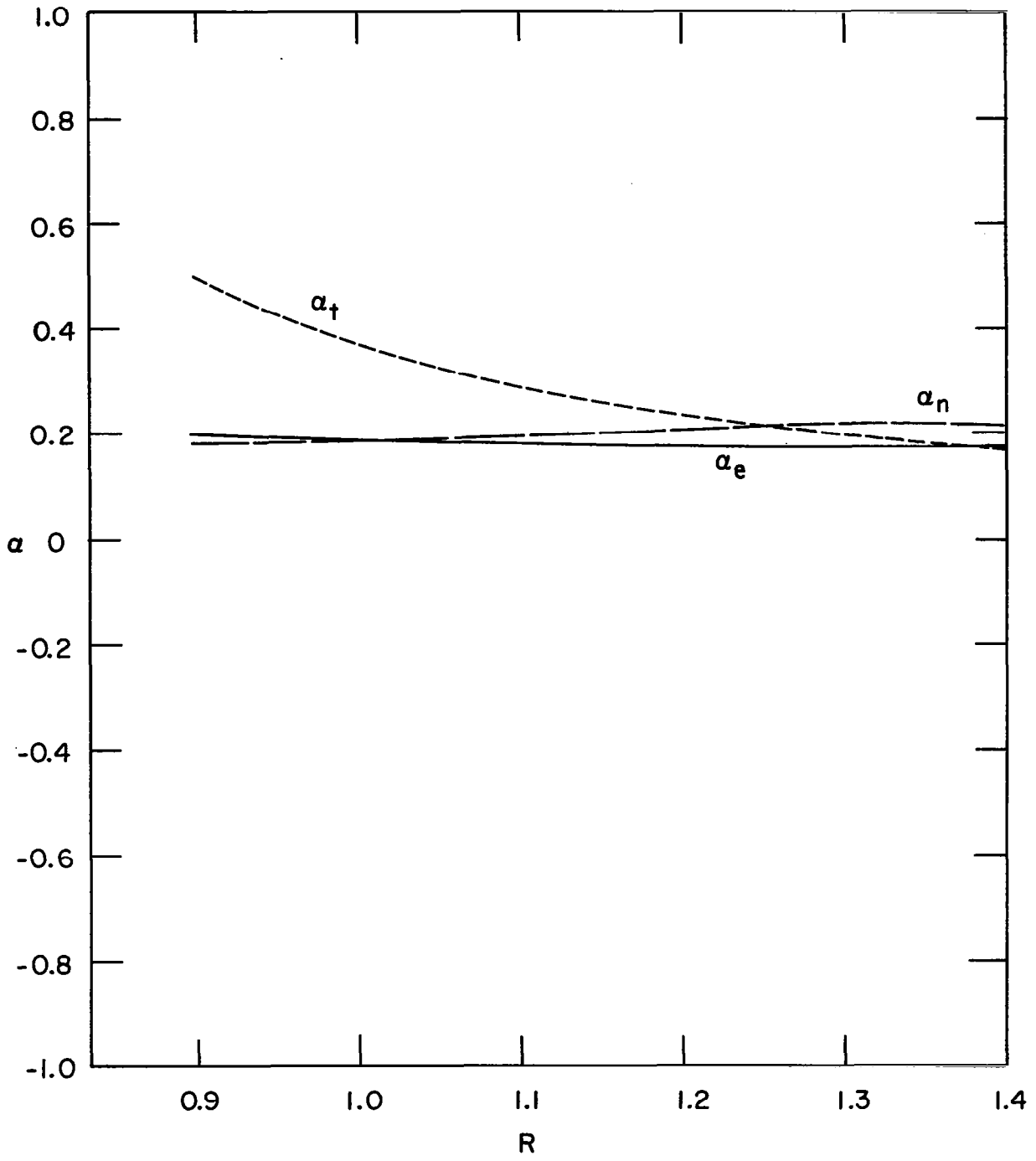

Fig. 6.16 $\alpha(R)$ for $\mu = 0.1$, S = square, $\theta_o = 135°$, $\phi_o = 45°$

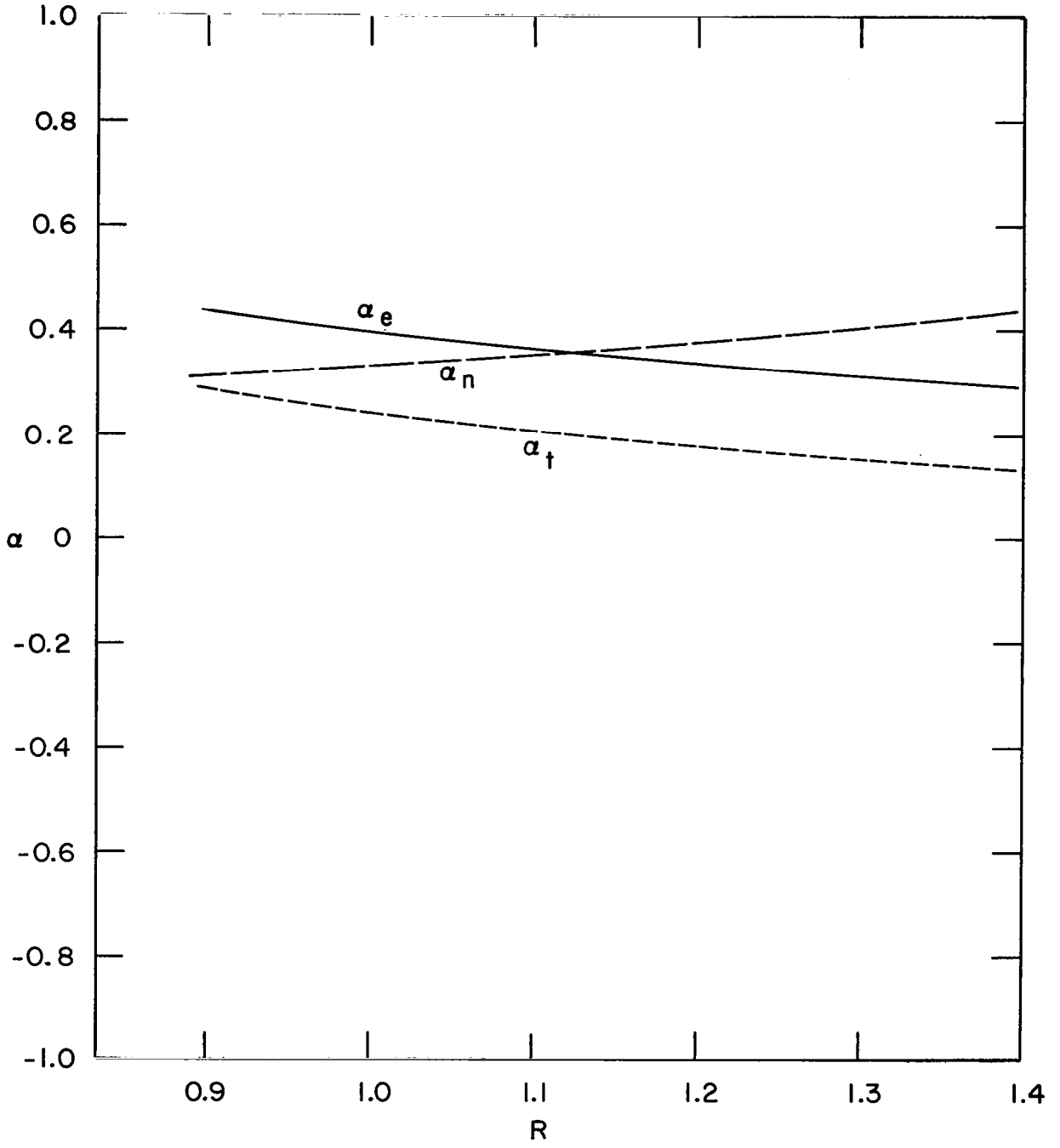

Fig. 6.17 $\alpha(R)$ for $\mu = 0.9$, S = square, $\theta_o = 112.5°$, $\phi_o = 45°$

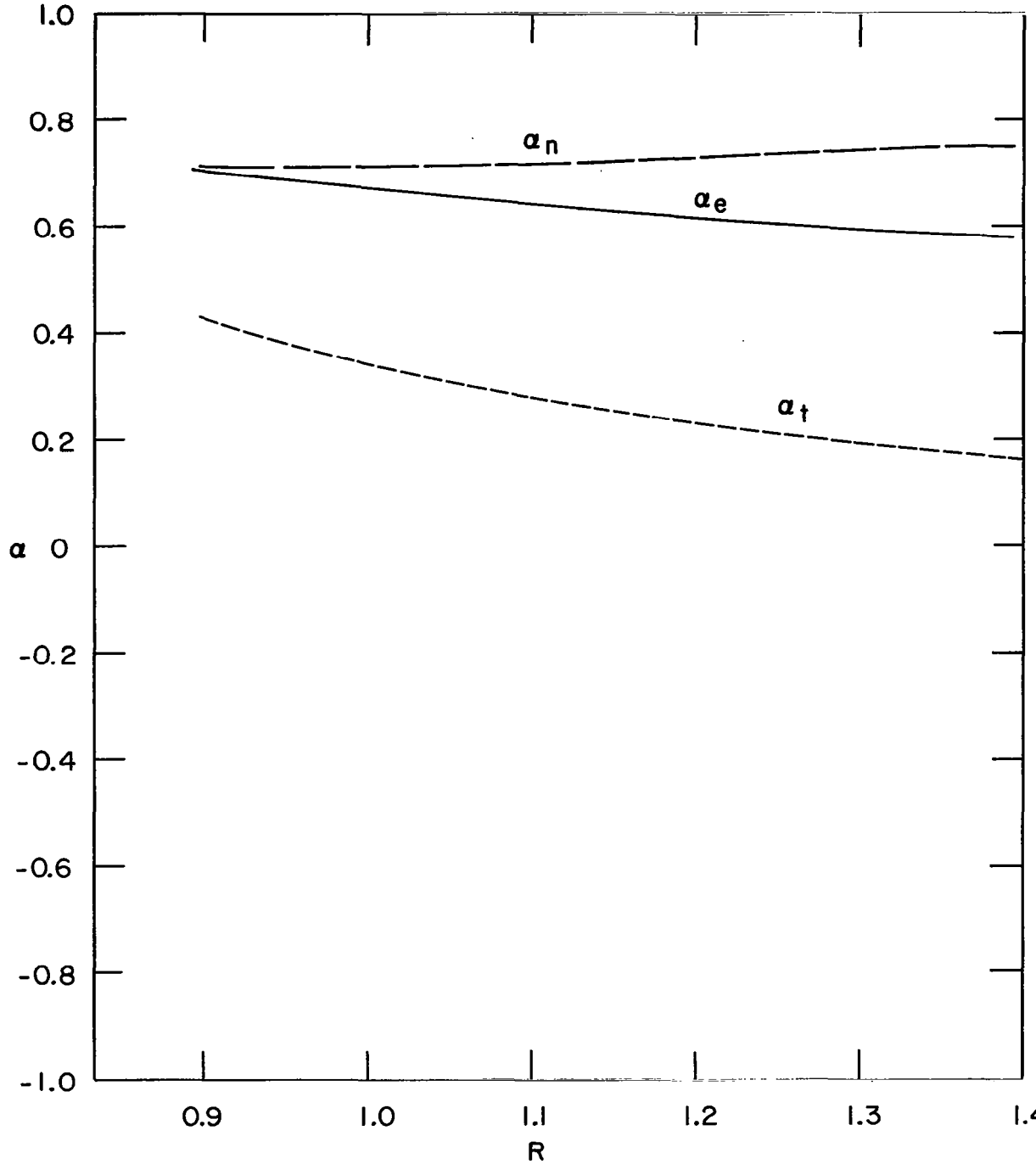

Fig. 6.18 $\alpha(R)$ for $\mu = 0.9$, S = square, $\theta_o = 135°$, $\phi_o = 45°$

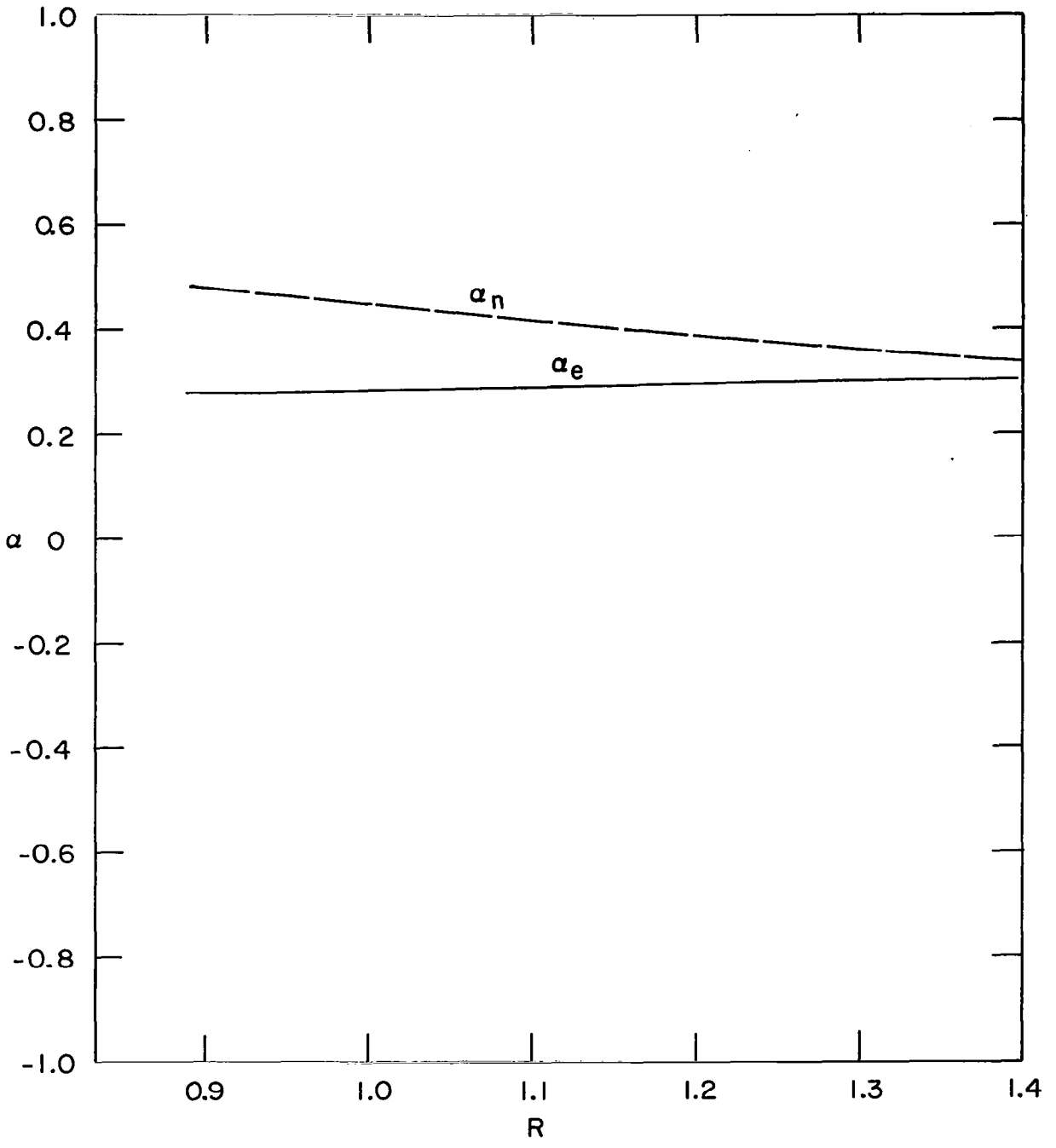

Fig. 6.19 $\alpha(R)$ for $\mu = 0.1$, S = square, $\theta_o = 180°$

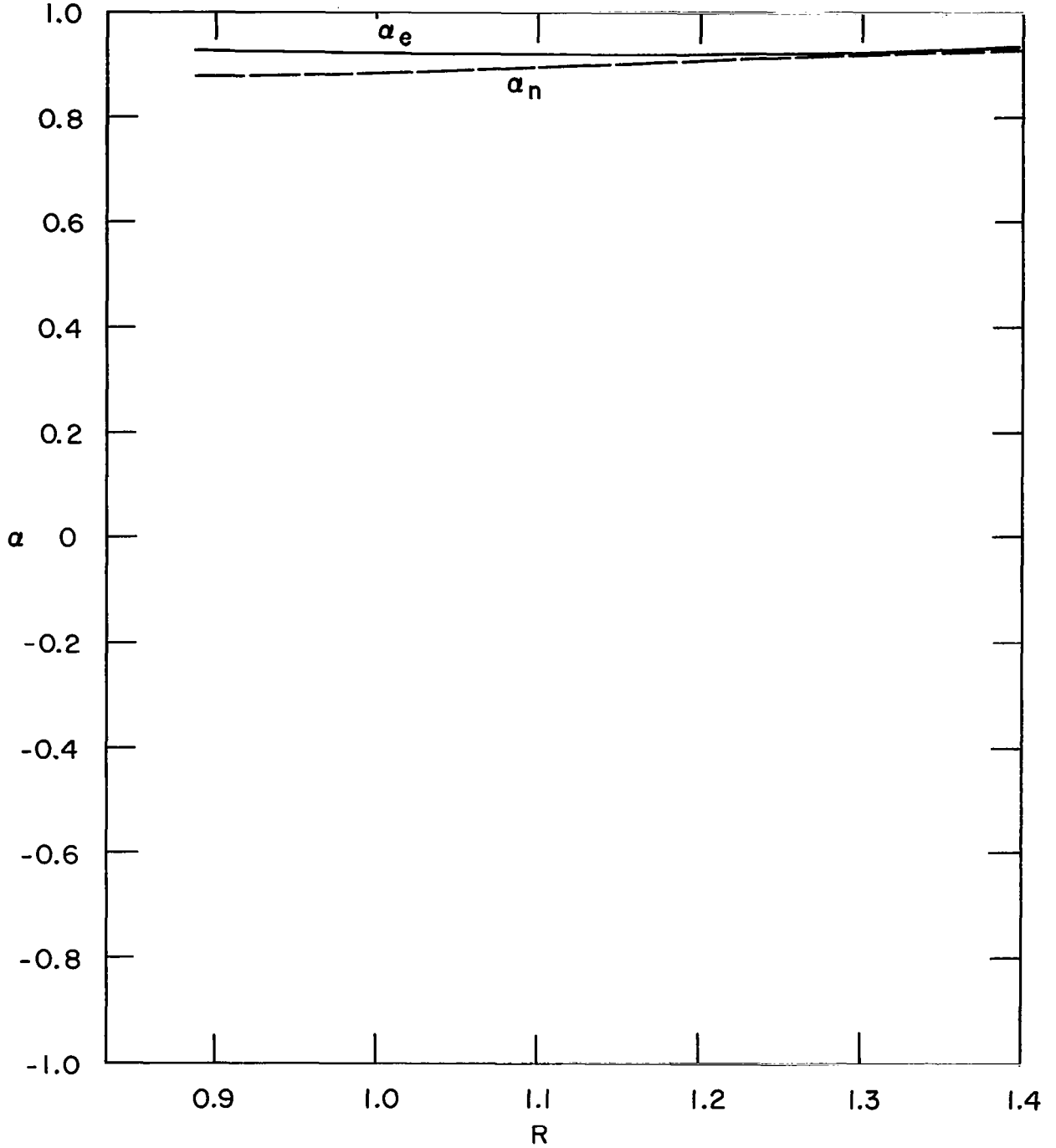

Fig. 6.20 $\alpha(R)$ for $\mu = 0.9$, S = square, $\theta_o = 180°$

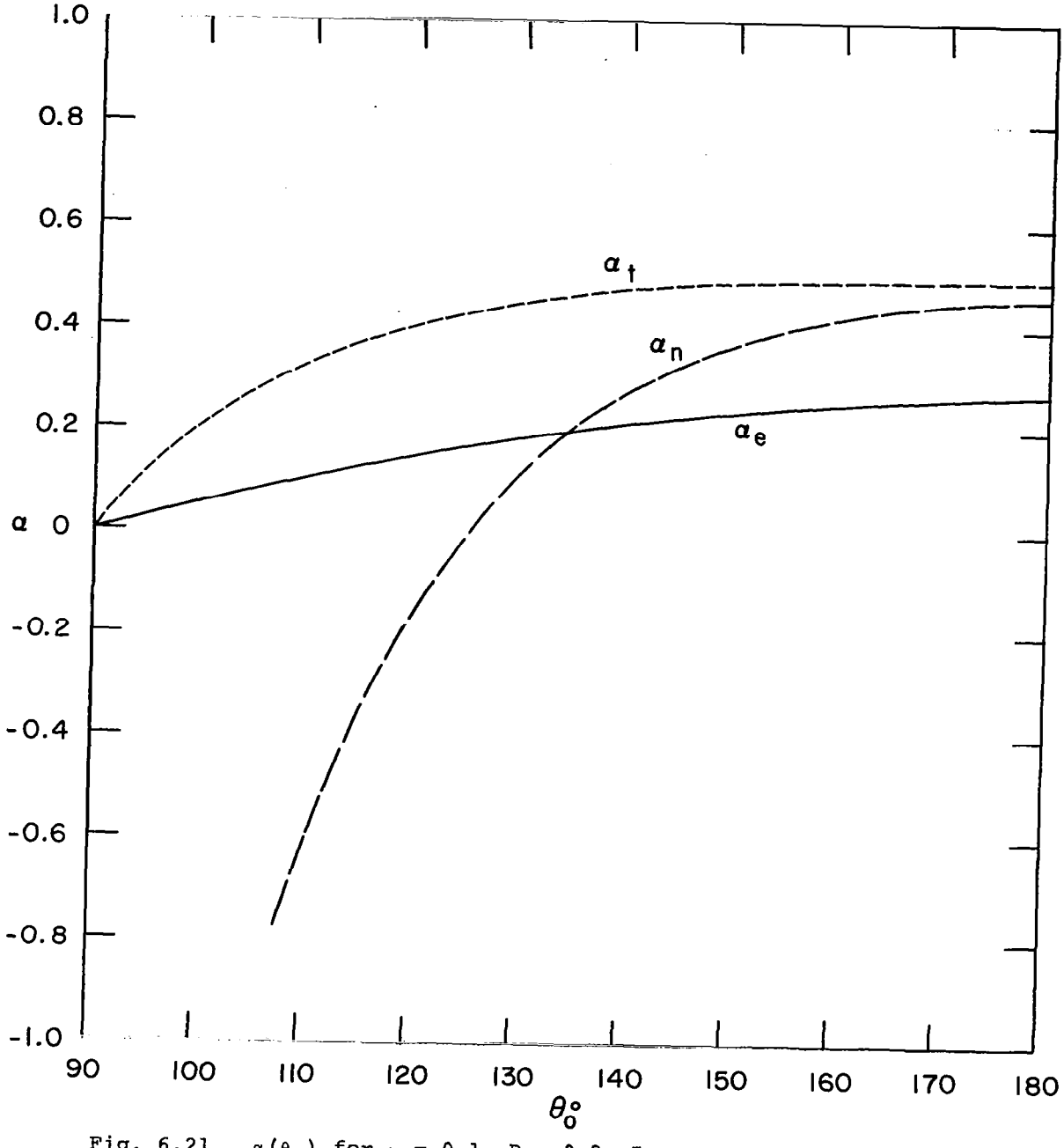

Fig. 6.21 $\alpha(\theta_o)$ for $\mu = 0.1$, R = 0.9, S = square, $\phi_o = 0$

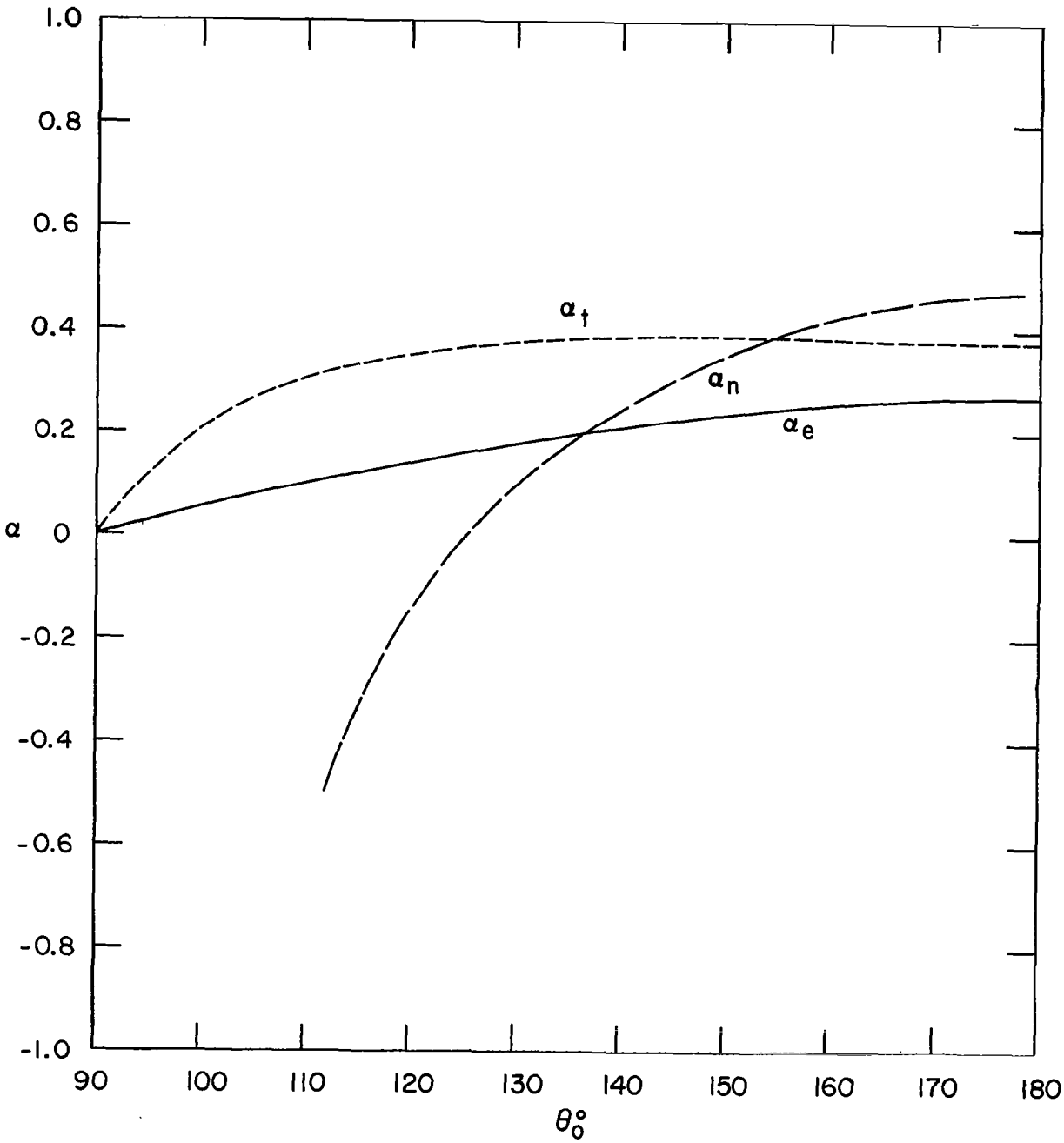

Fig. 6.21a $\alpha(\theta_o)$ for $\mu = 0.1$, $R = 0.9$, S = triangular, $\phi_o = 0$

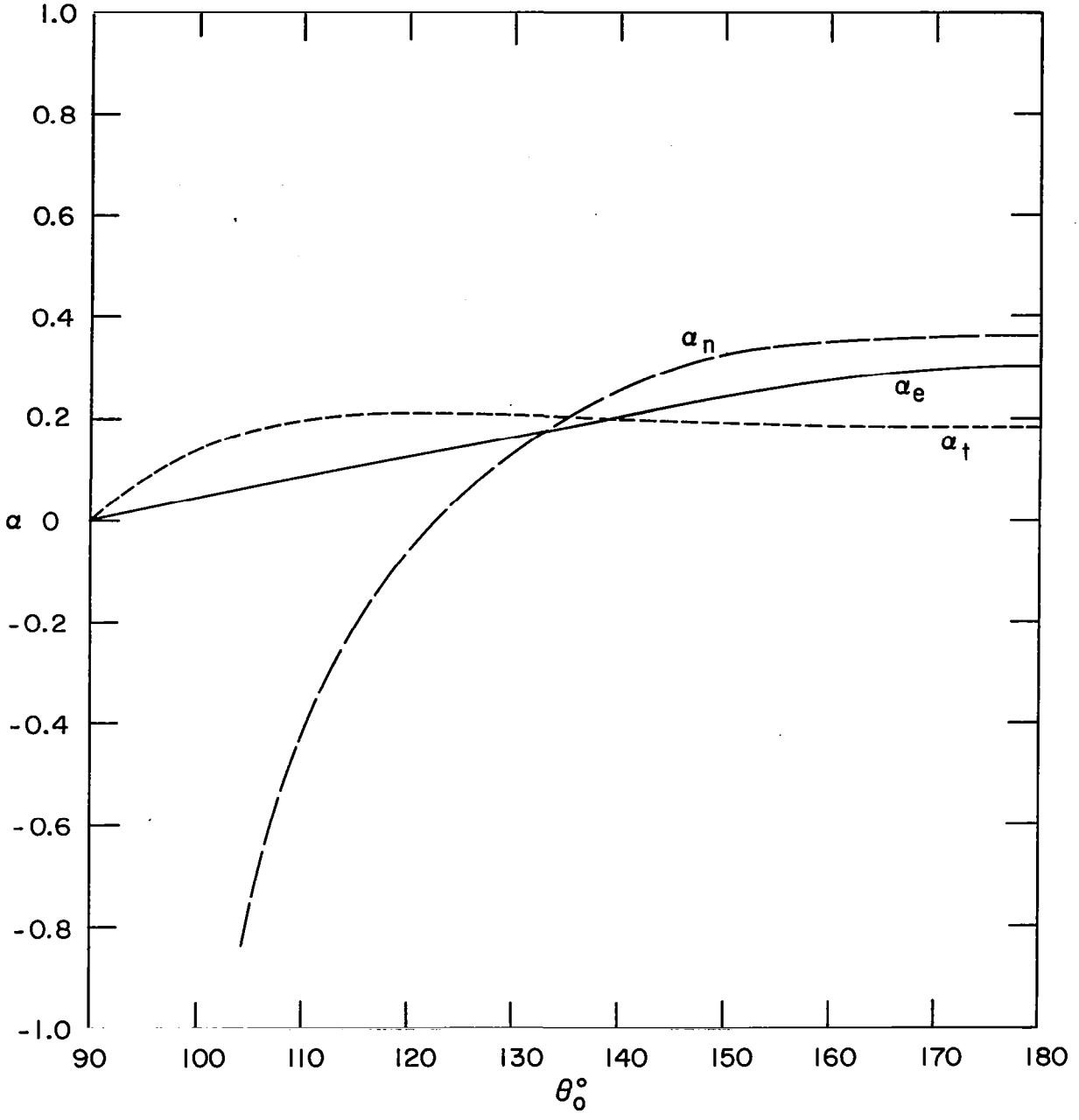

Fig. 6.22 $\alpha(\theta_o)$ for $\mu = 0.1$, $R = 1.3$, S = square, $\phi_o = 0$

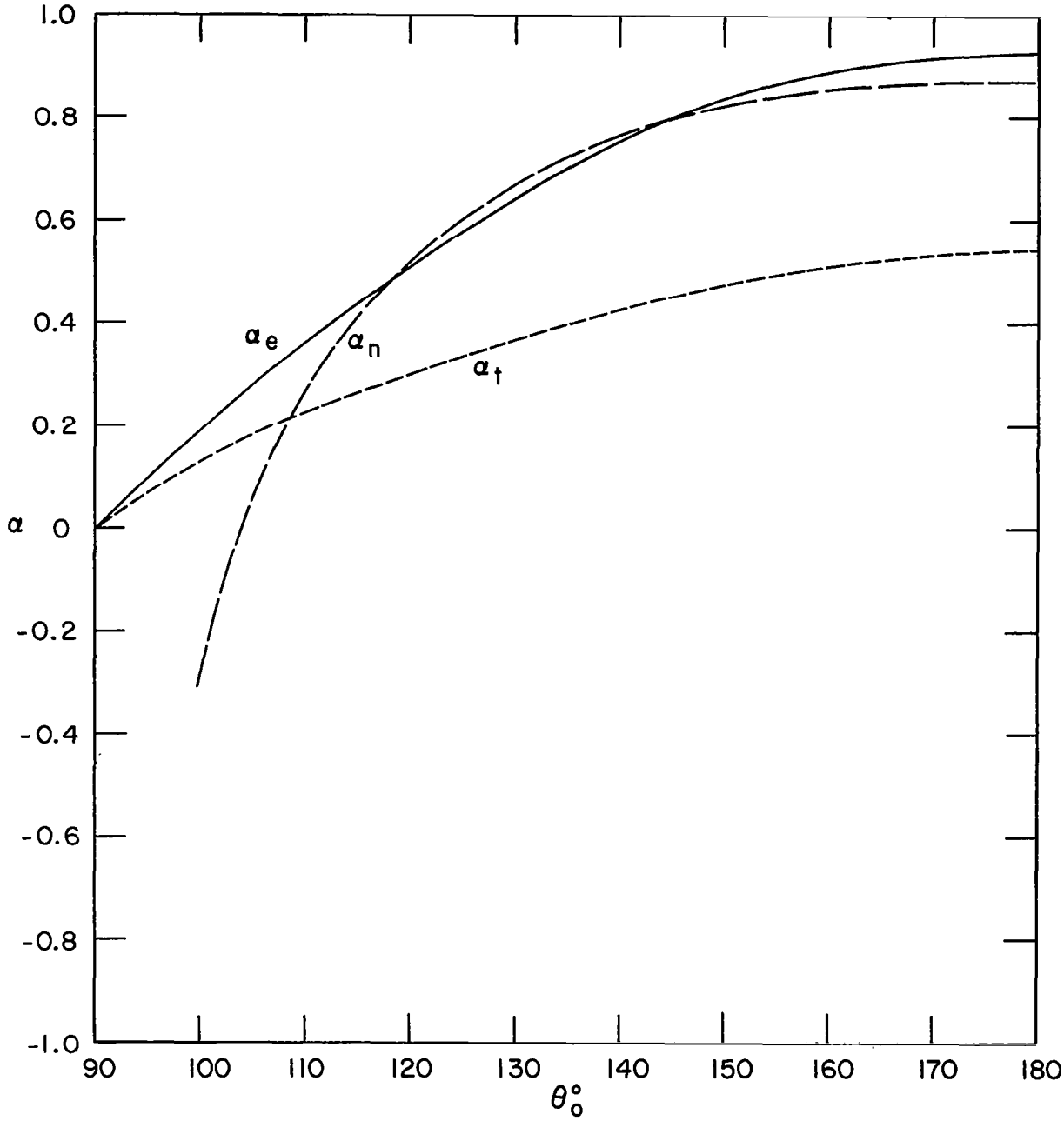

Fig. 6.23 $\alpha(\theta_o)$ for $\mu = 0.9$, R = 1.3, S = square, $\phi_o = 0$

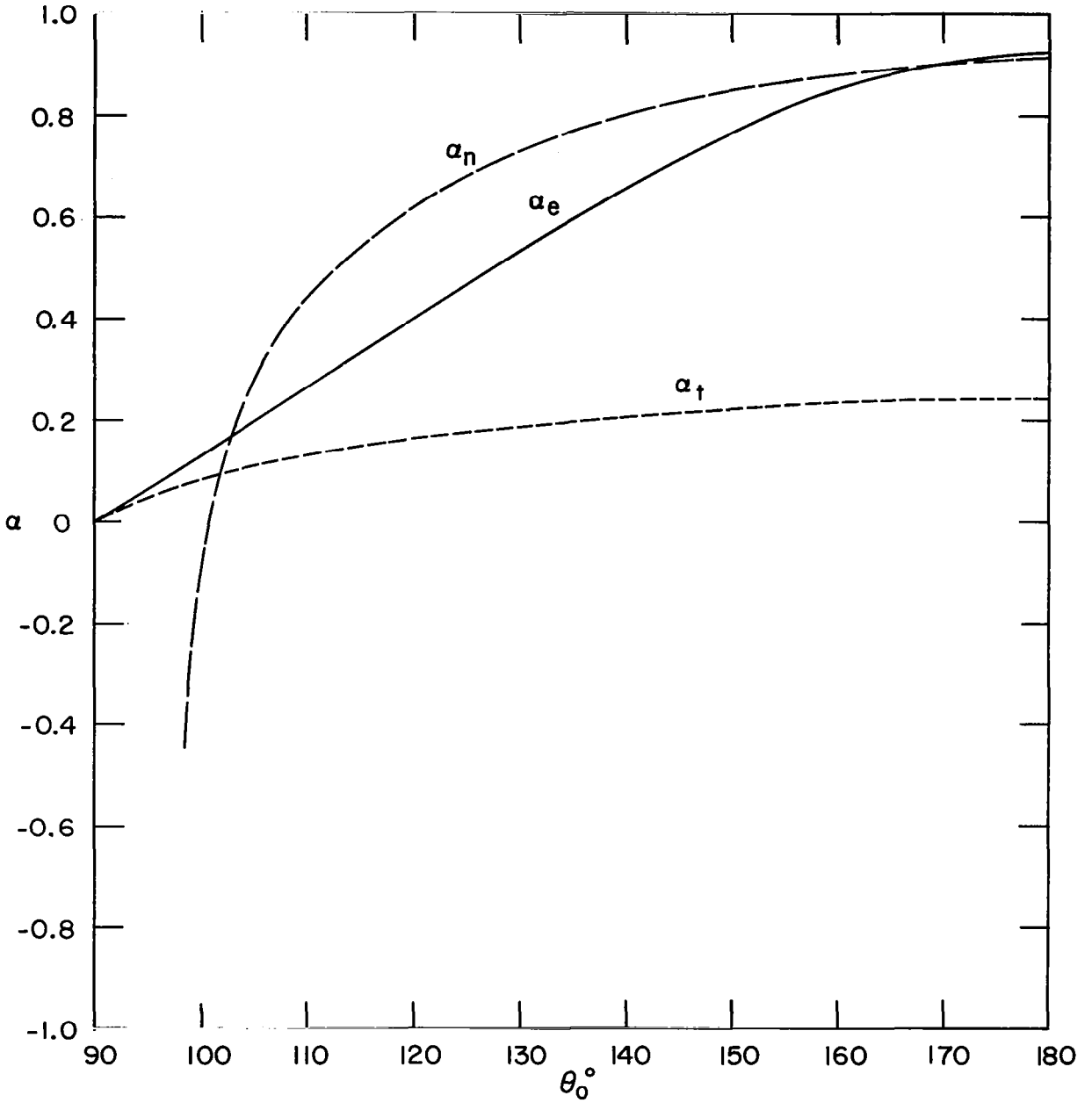

Fig. 6.24 $\alpha(\theta_0)$ for $\mu = 0.9$, $R = 1.3$, S = square, $\phi_0 = 0$

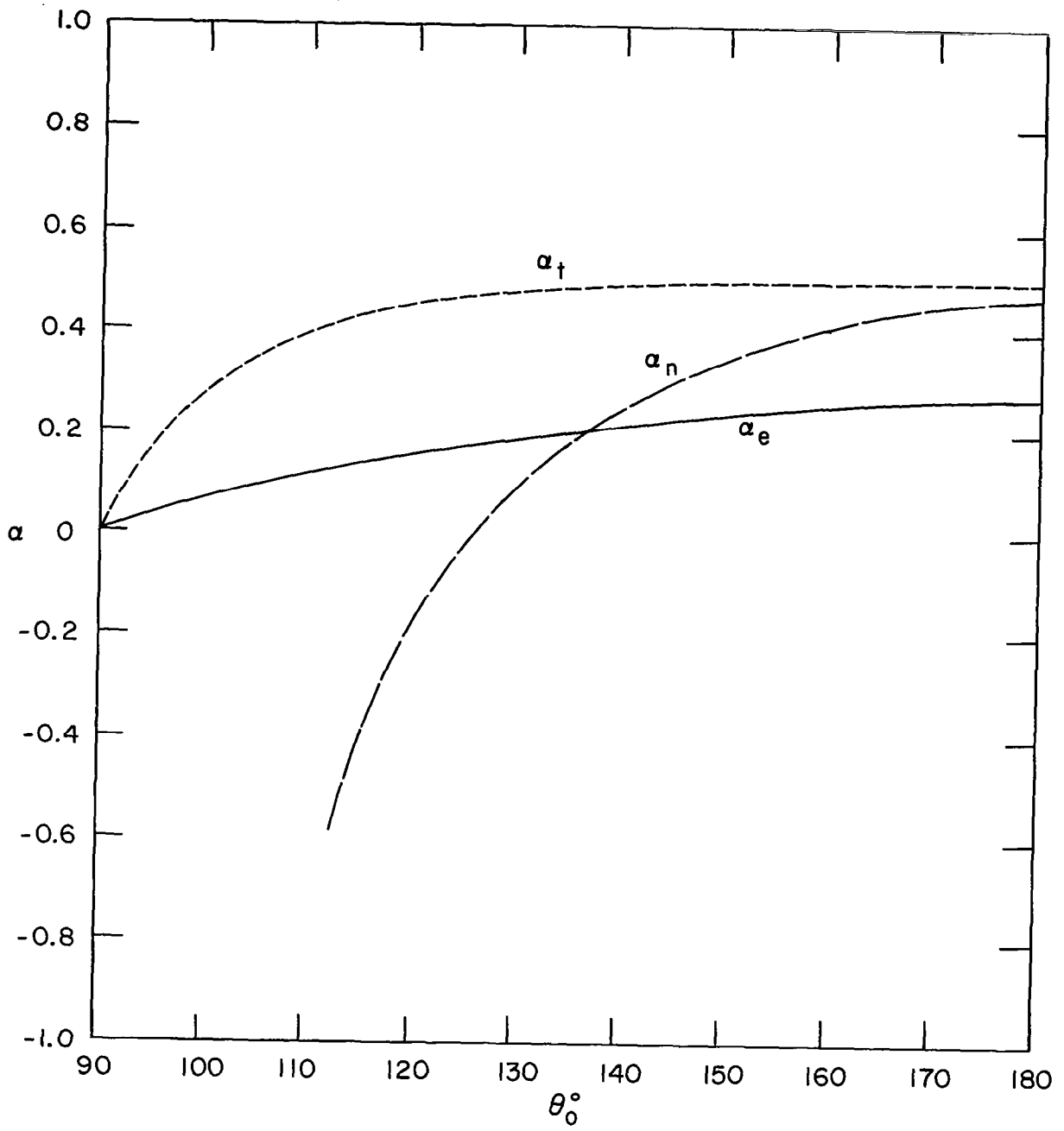

Fig. 6.25 $\alpha(\theta_o)$ for $\mu = 0.1$, R = 0.9, S = square, $\phi_o = 45°$

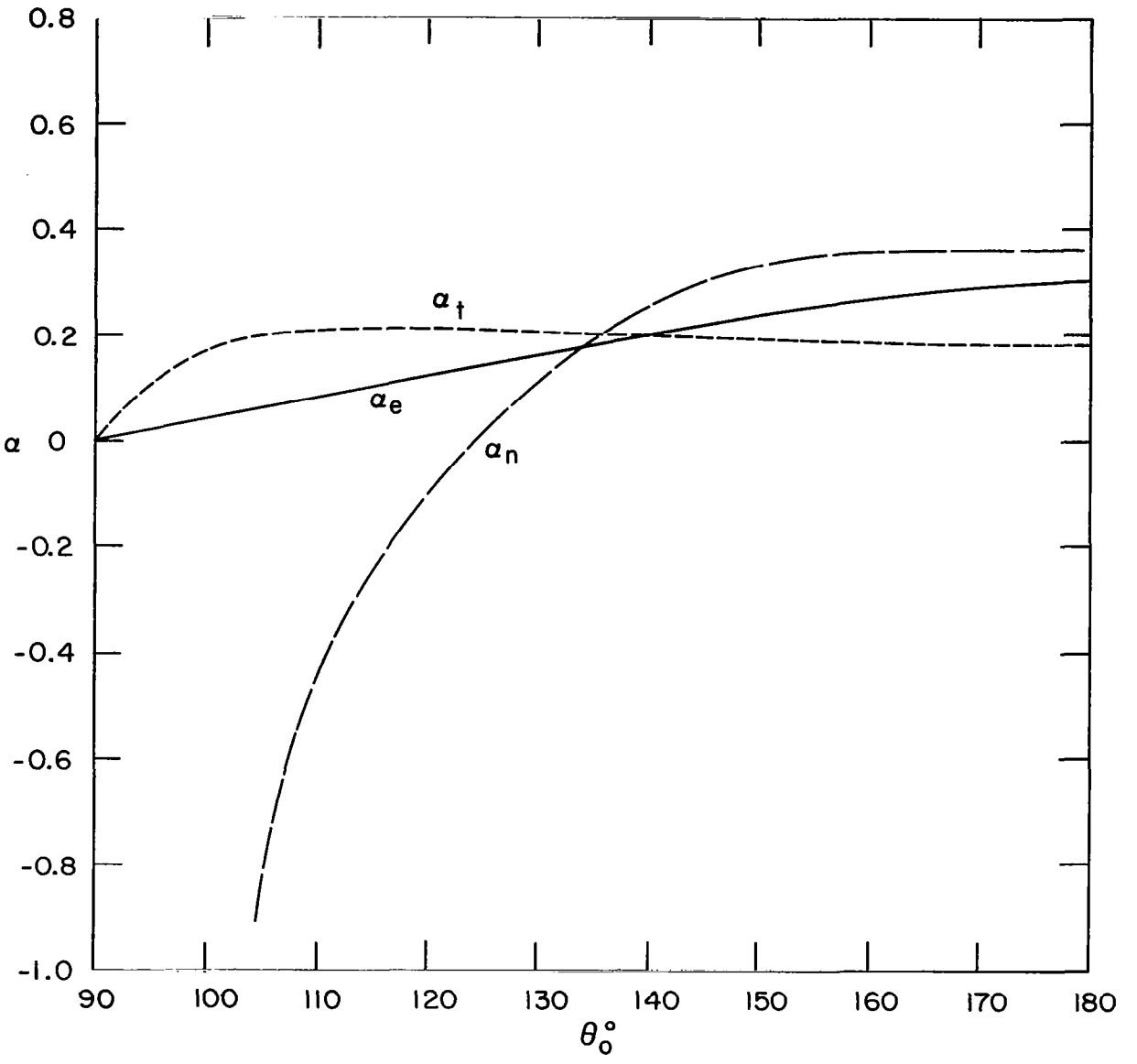

Fig. 6.26 $\alpha(\theta_o)$ for $\mu = 0.1$, R = 1.3, S = square, $\phi_o = 45°$

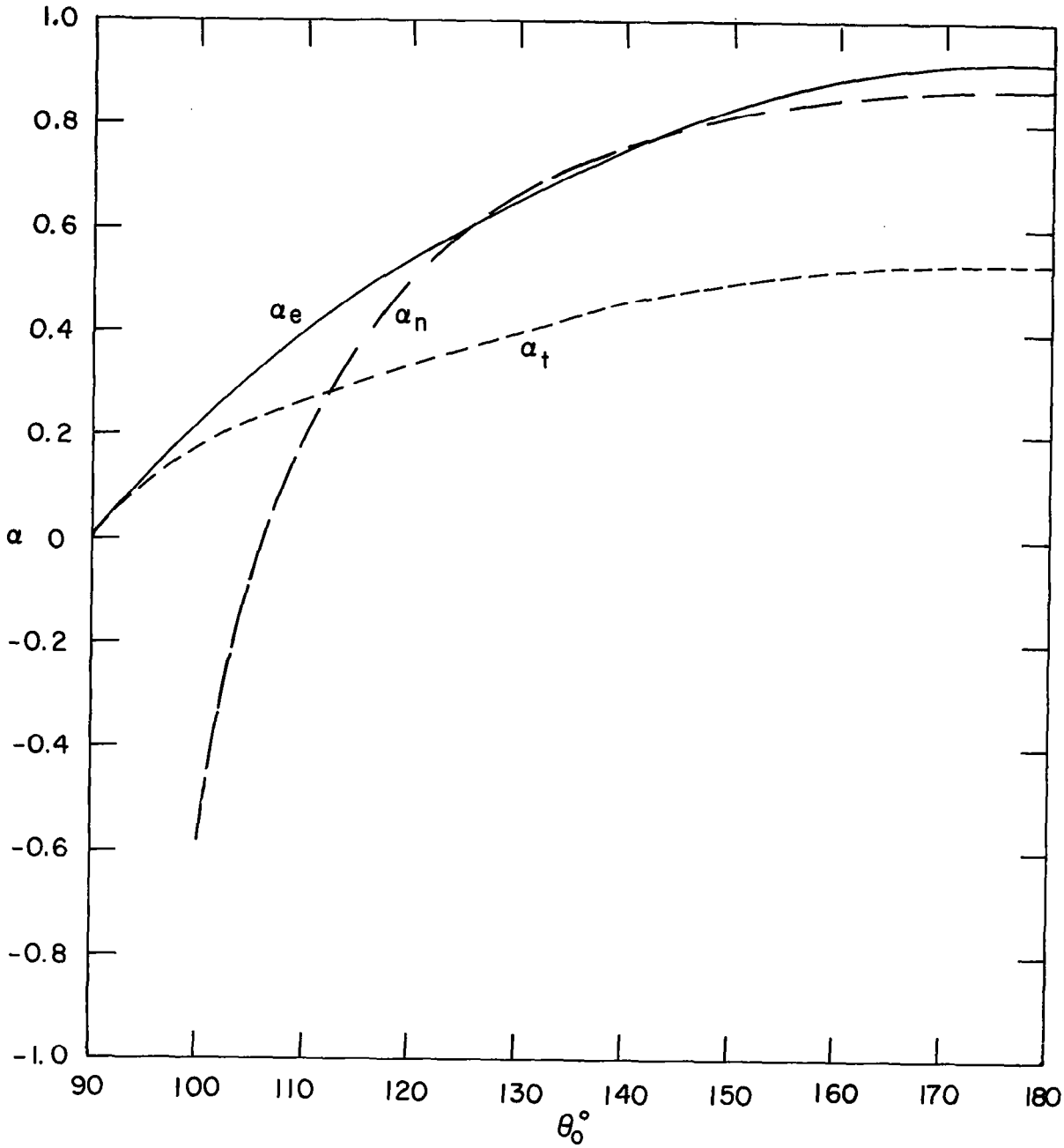

Fig. 6.27 $\alpha(\theta_o)$ for $\mu = 0.9$, R = 0.9, S = square, $\phi_o = 45°$

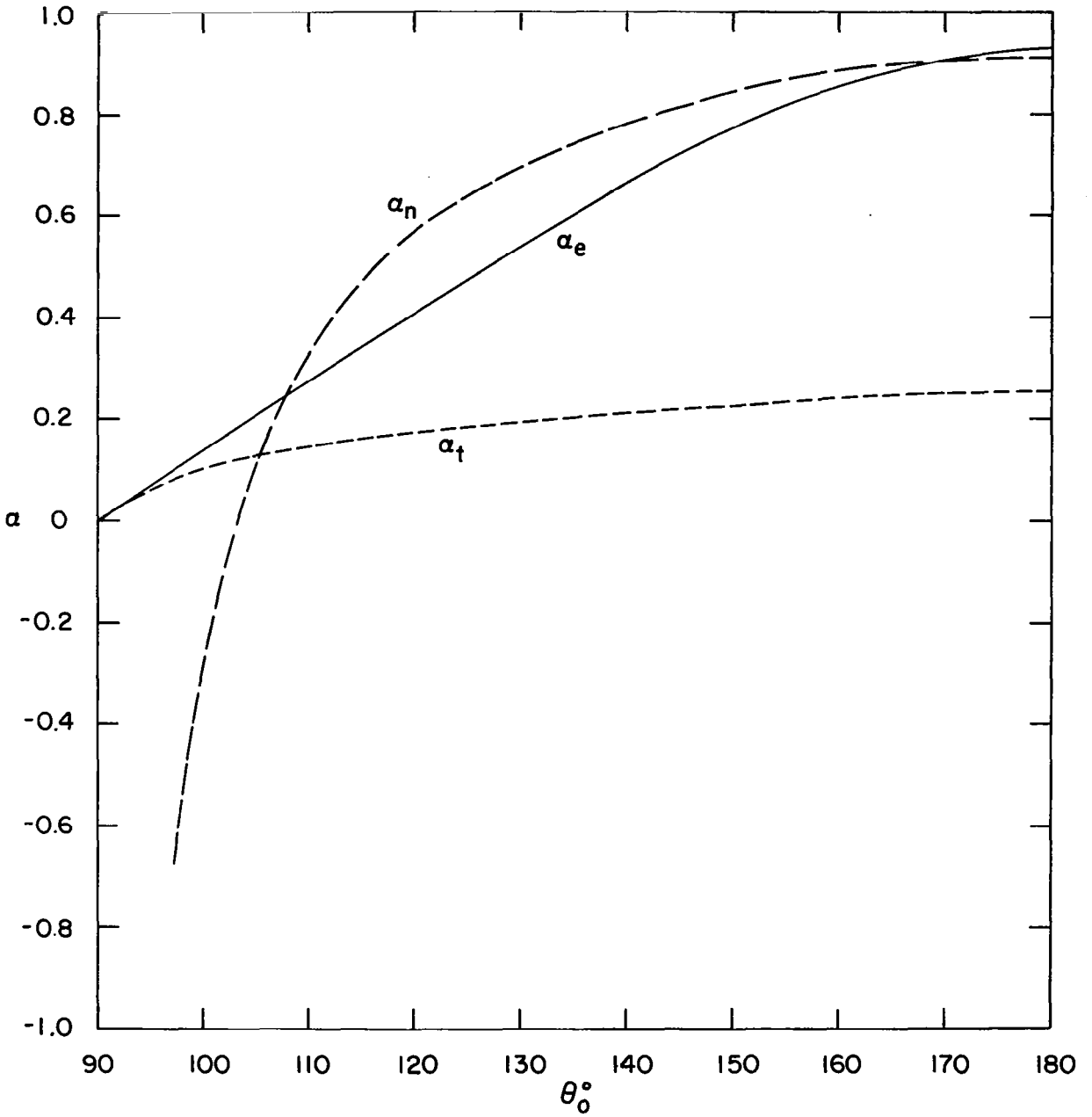

Fig. 6.28 $\alpha(\theta_o)$ for $\mu = 0.9$, R = 1.3, S = square, $\phi_o = 45°$

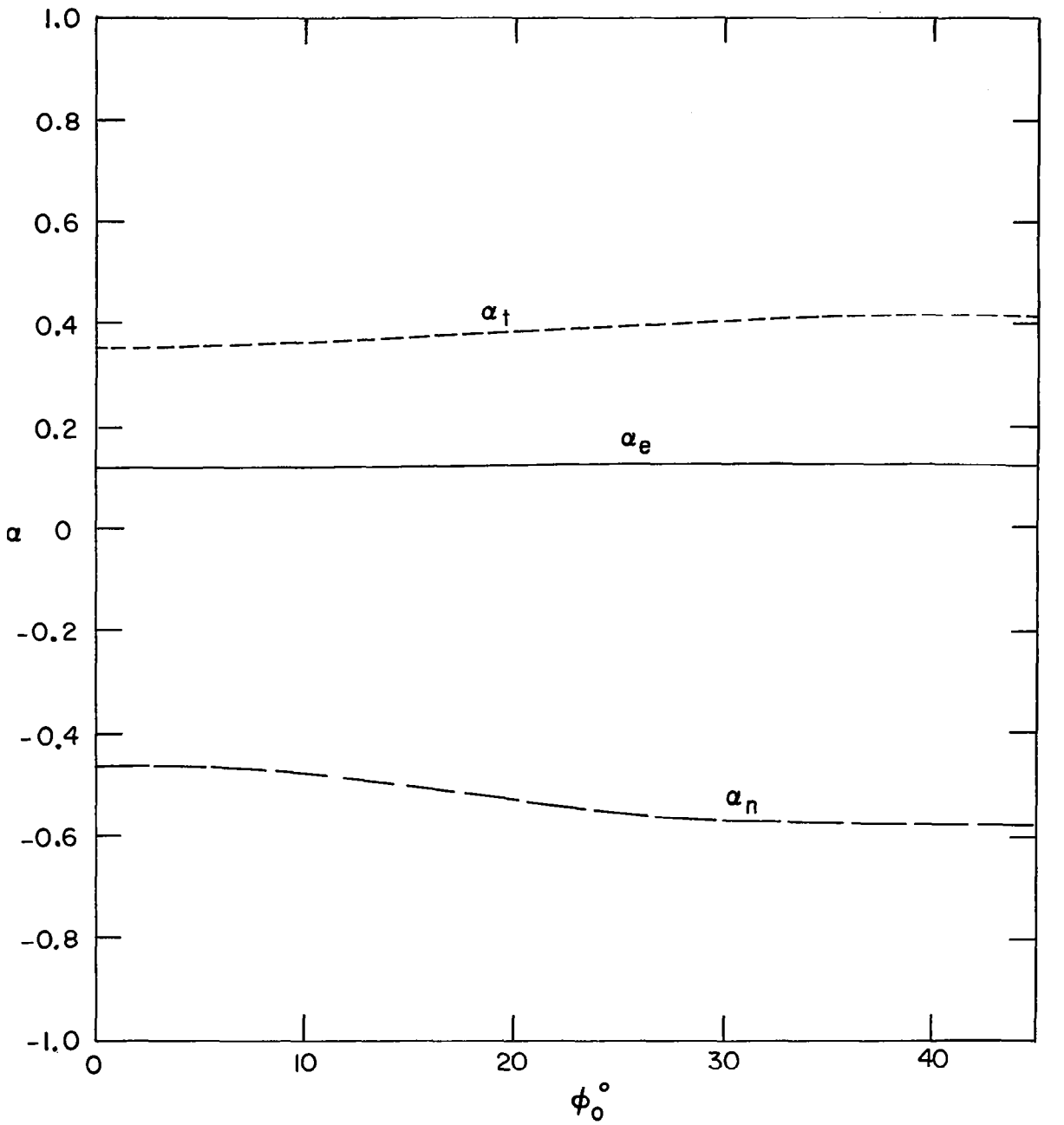

Fig. 6.29 $\alpha(\phi_o)$ for $\mu = 0.1$, $R = 0.9$, S = square, $\theta_o = 112.5°$

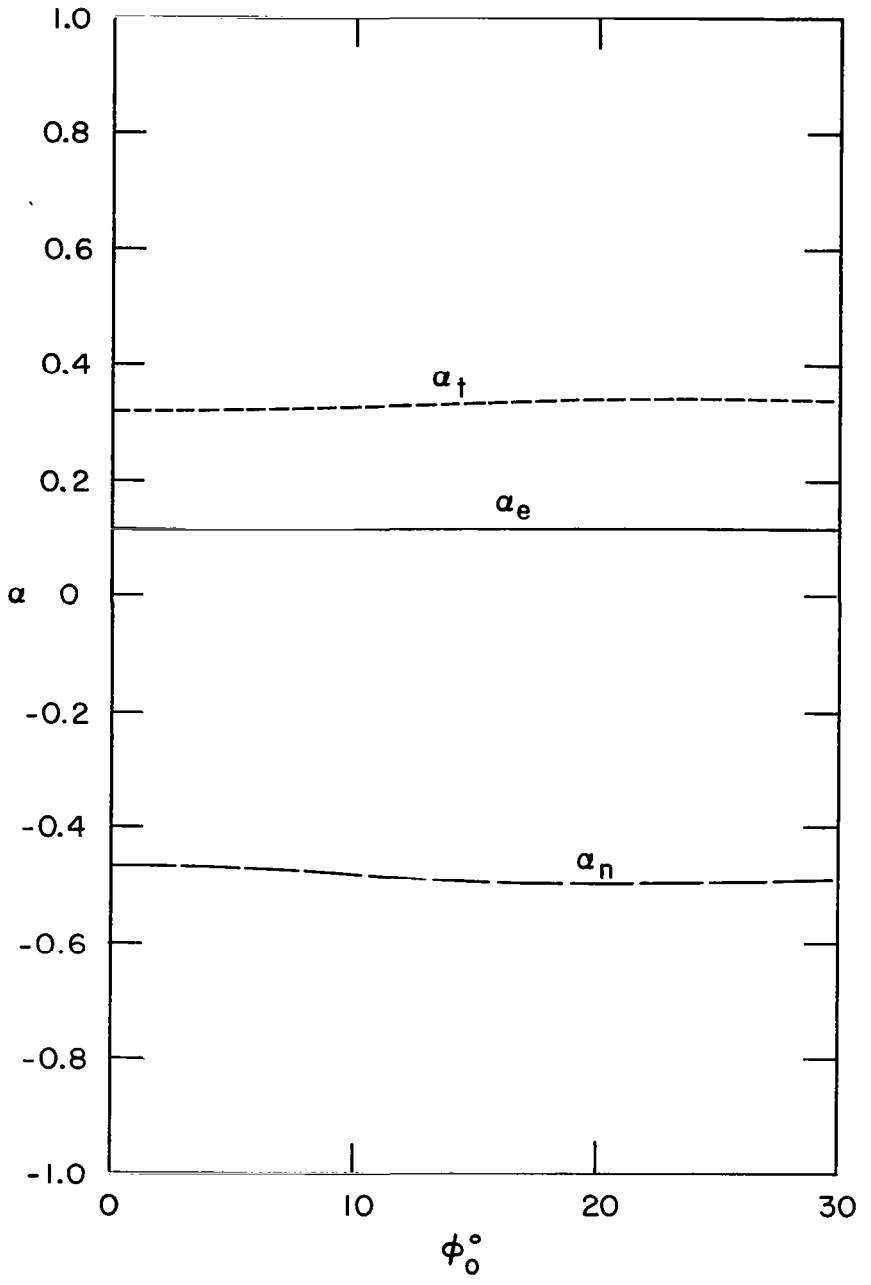

Fig. 6.29a $\alpha(\phi_o)$ for $\mu = 0.1$, $R = 0.9$, S = triangular, $\theta_o = 112.5°$

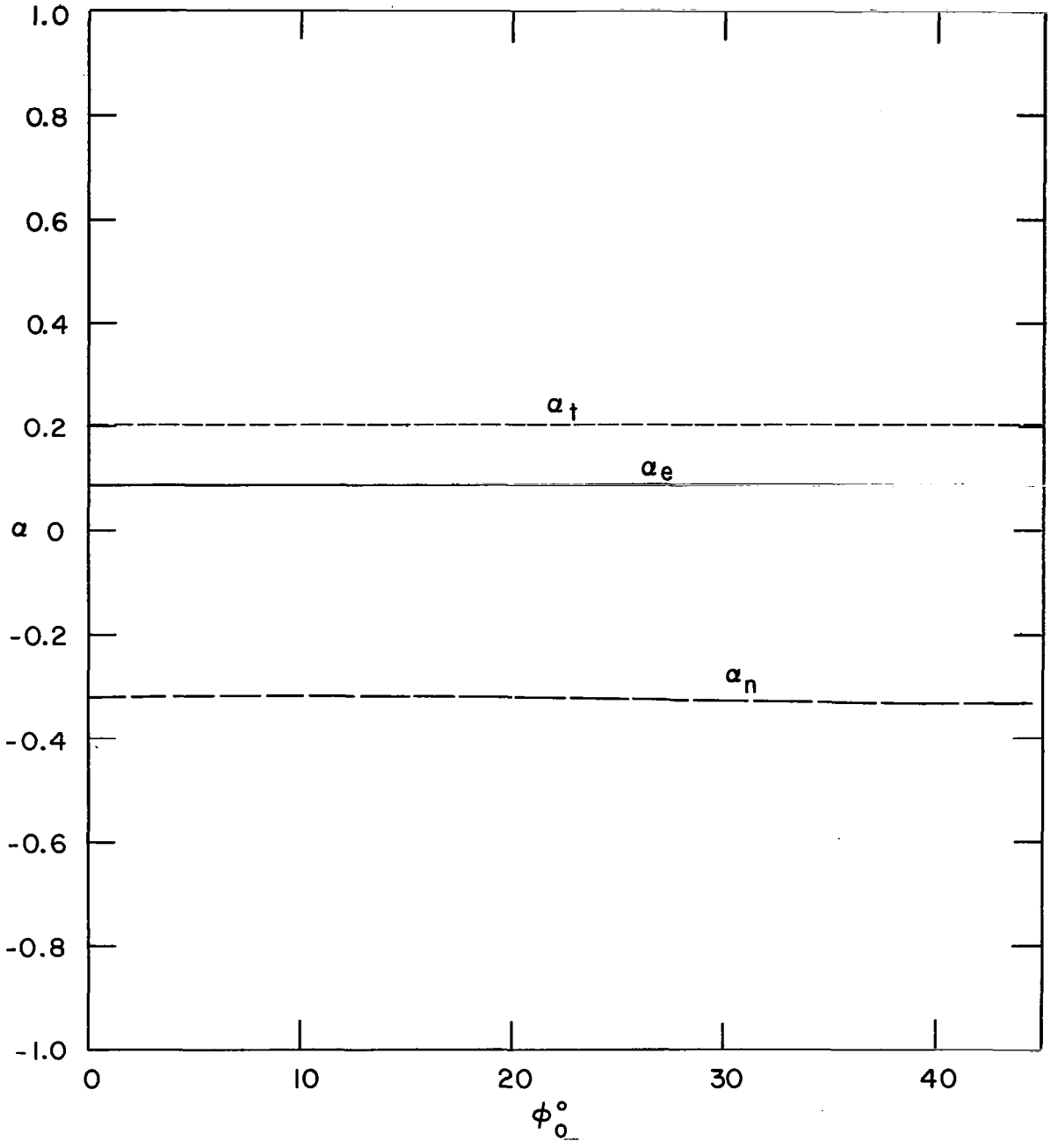

Fig. 6.30 $\alpha(\phi_o)$ for $\mu = 0.1$, $R = 1.3$, S = square, $\theta_o = 112.5°$

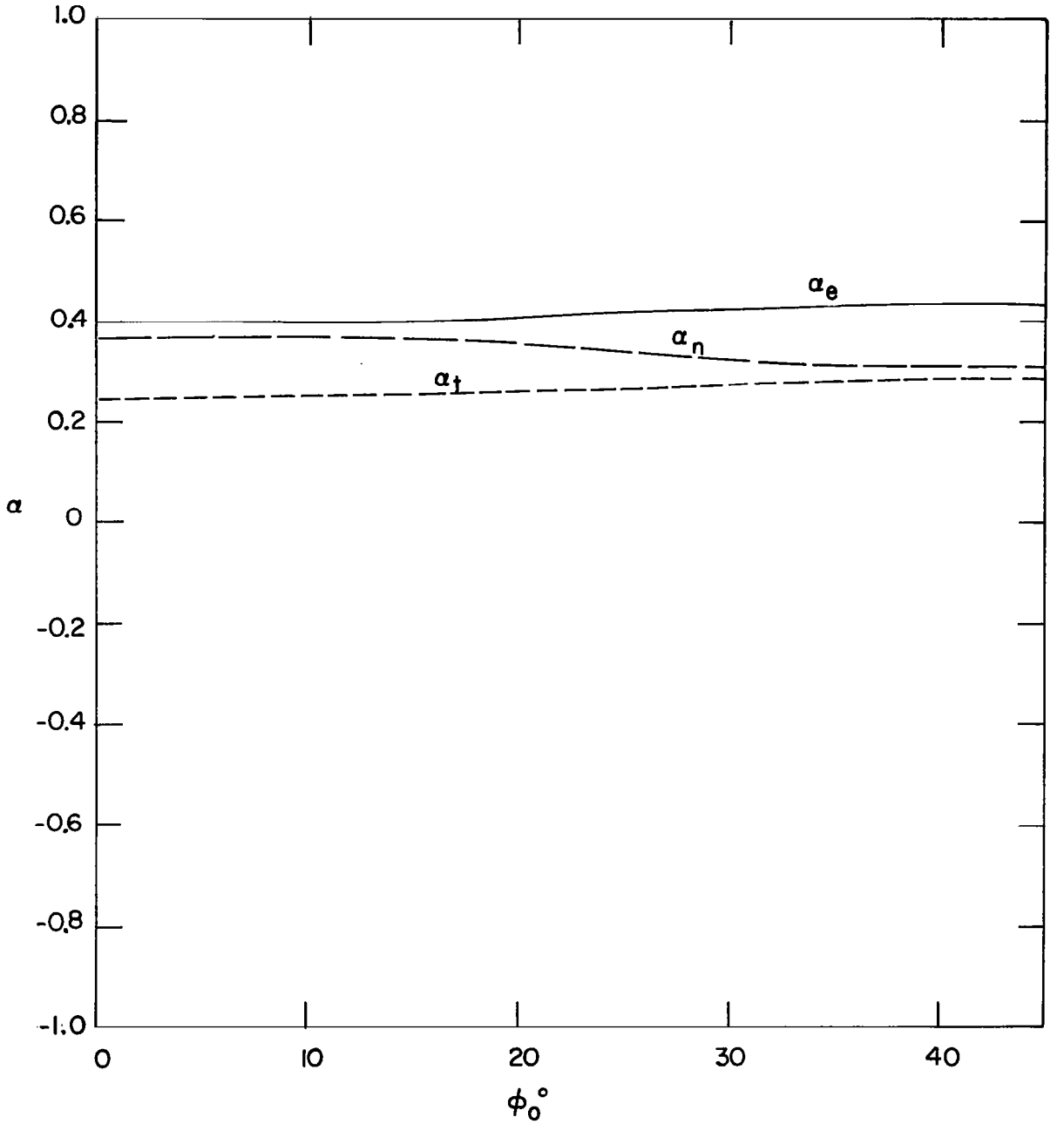

Fig. 6.31 $\alpha(\phi_o)$ for $\mu = 0.9$, $R = 0.9$, S = square, $\theta_o = 112.5°$

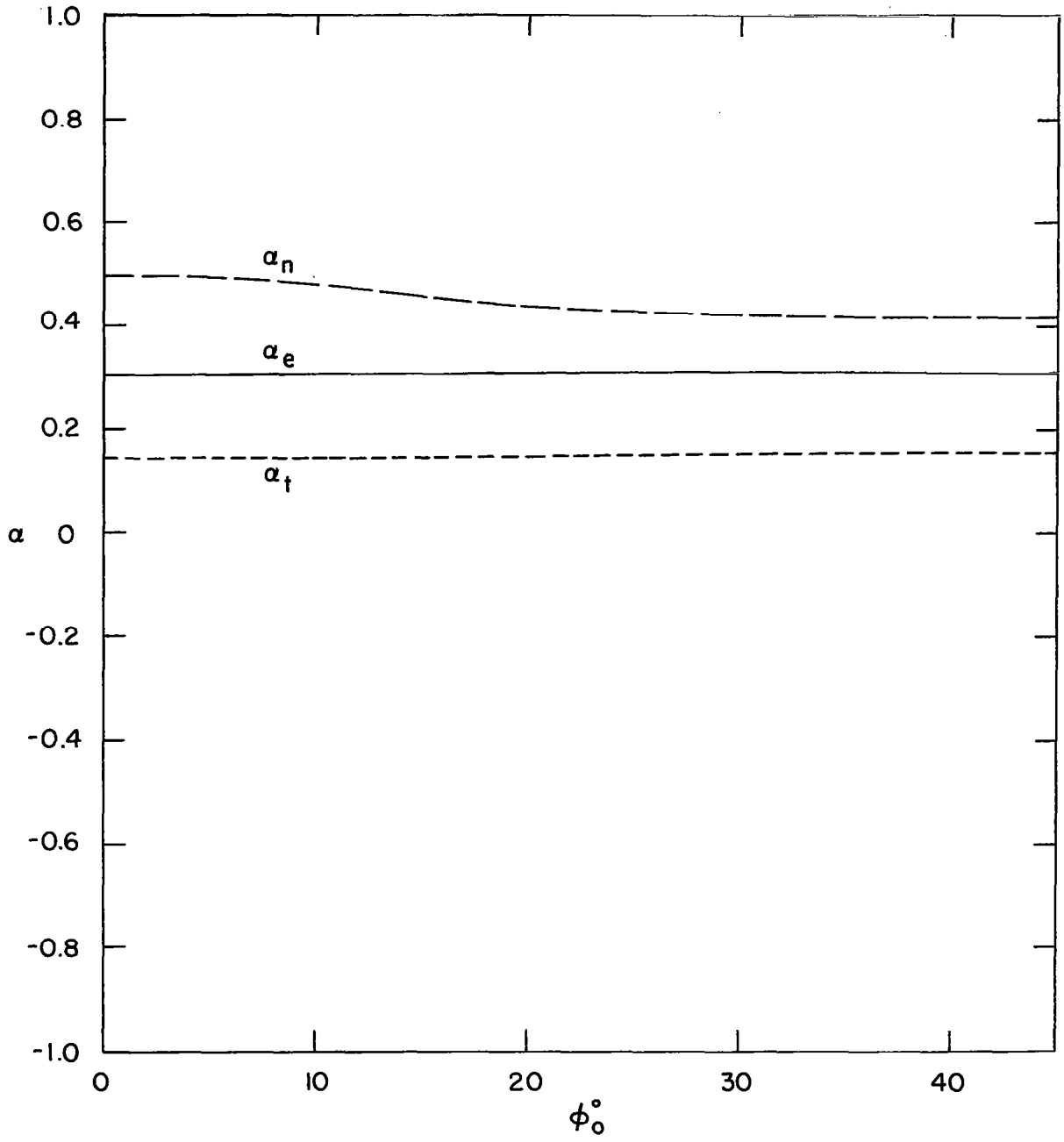

Fig. 6.32 $\alpha(\phi_o)$ for $\mu = 0.9$, R = 1.3, S = square, $\theta_o = 112.5°$

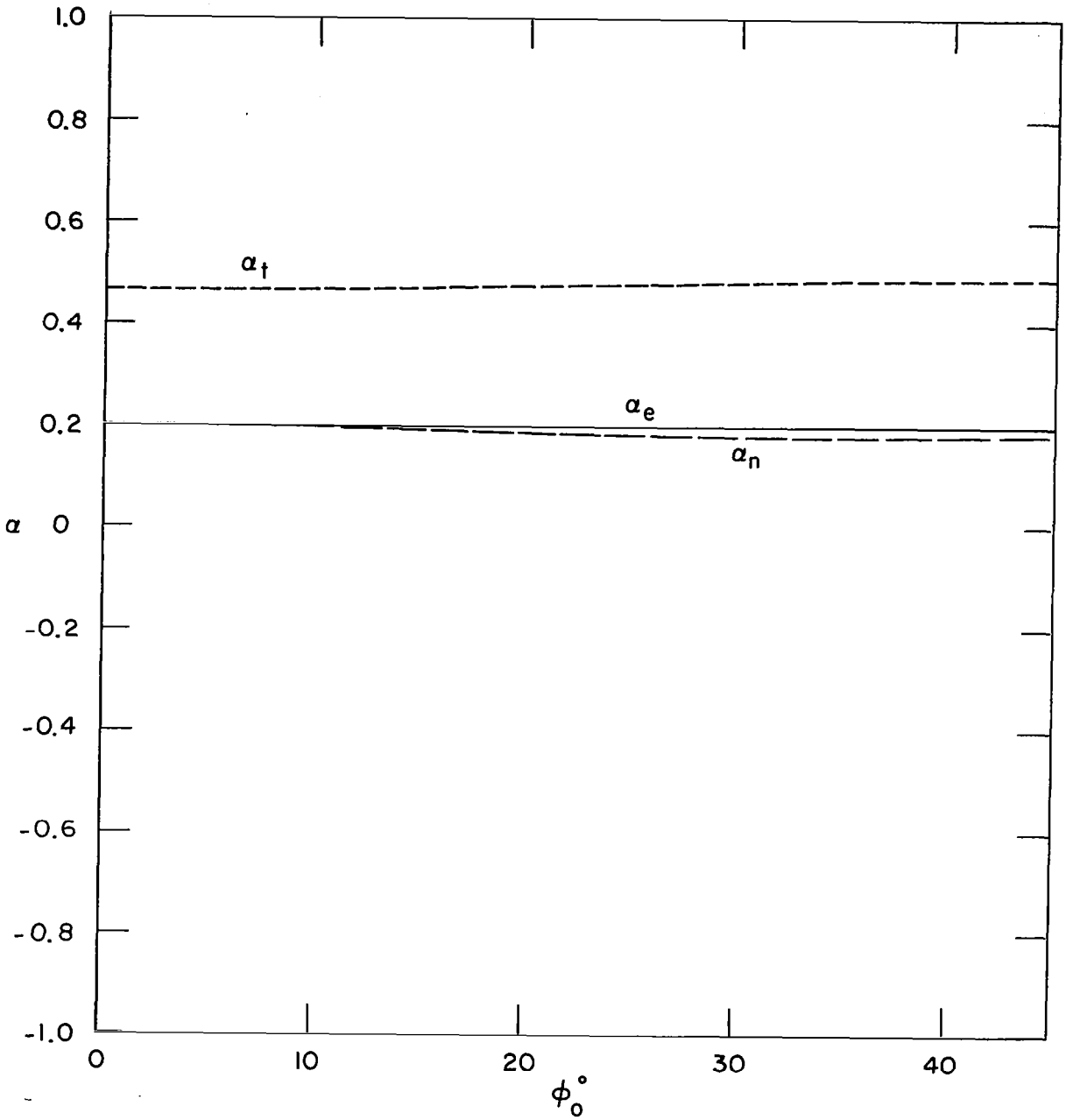

Fig. 6.33 $\alpha(\phi_0)$ for $\mu = 0.1$, $R = 0.9$, S = square, $\theta_0 = 135°$

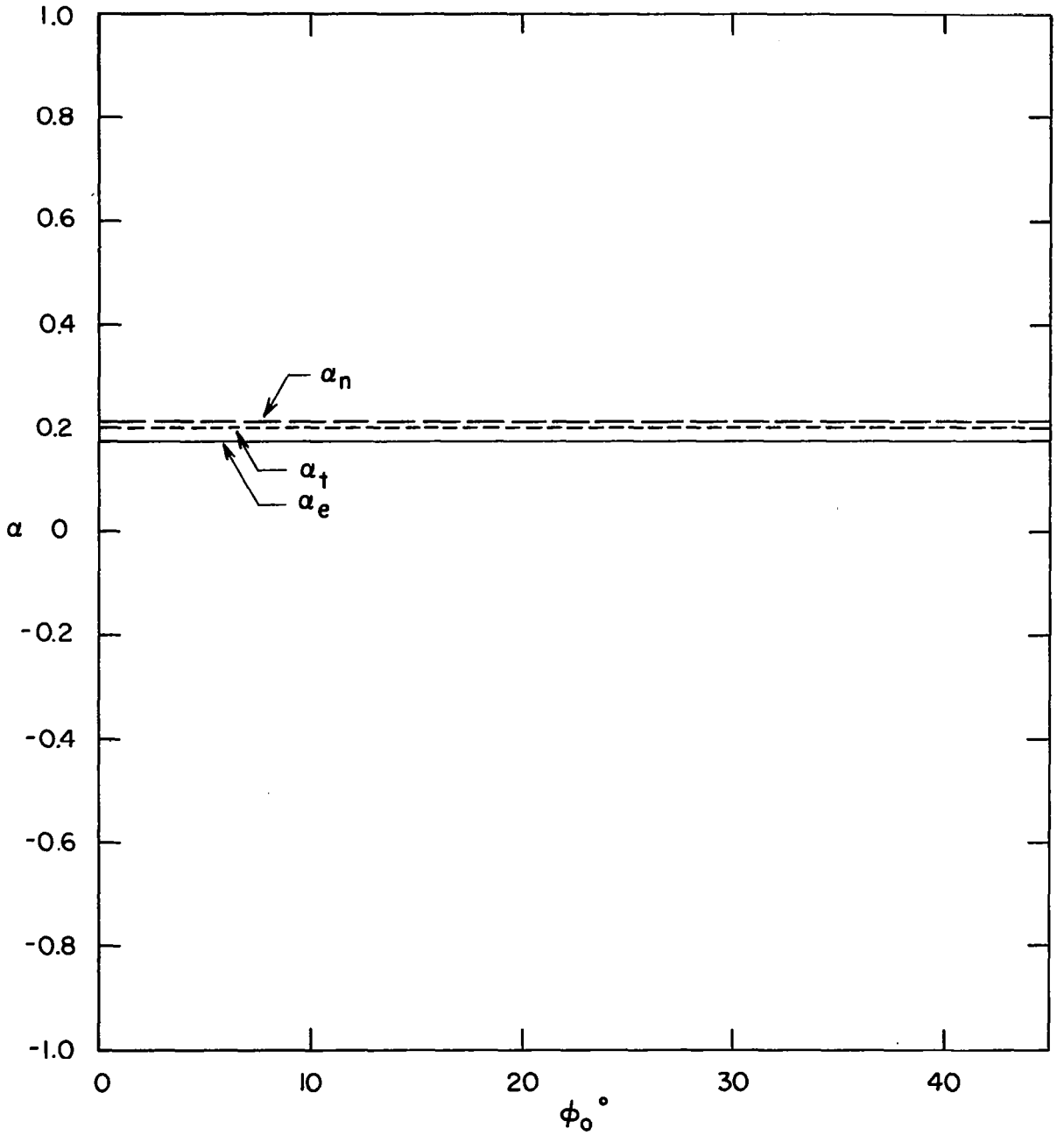

Fig. 6.34 $\alpha(\phi_o)$ for $\mu = 0.1$, R = 1.3, S = square, $\theta_o = 135°$

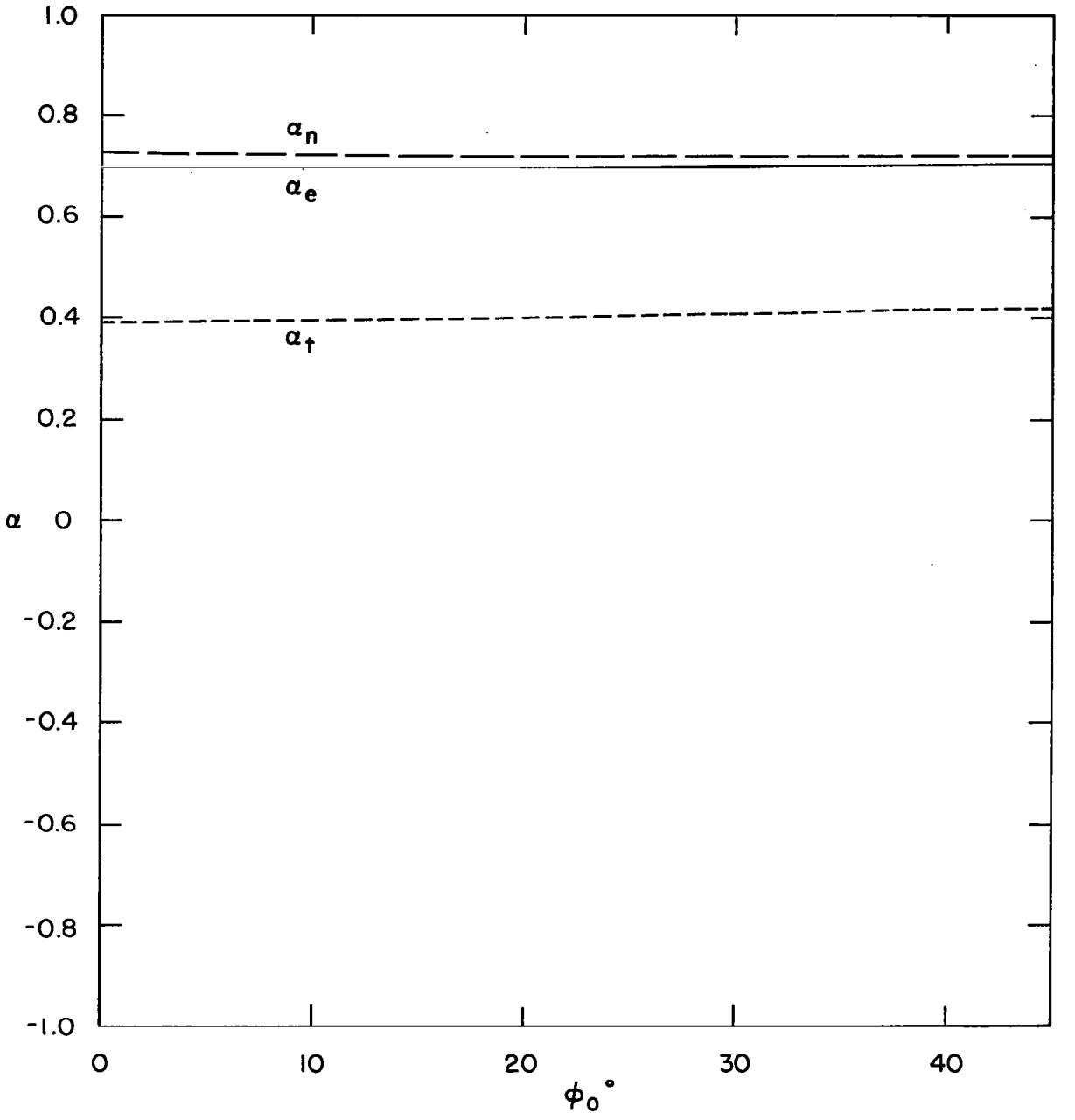

Fig. 6.35 $\alpha(\phi_0)$ for $\mu = 0.9$, R = 0.9, S = square, $\theta_0 = 135°$

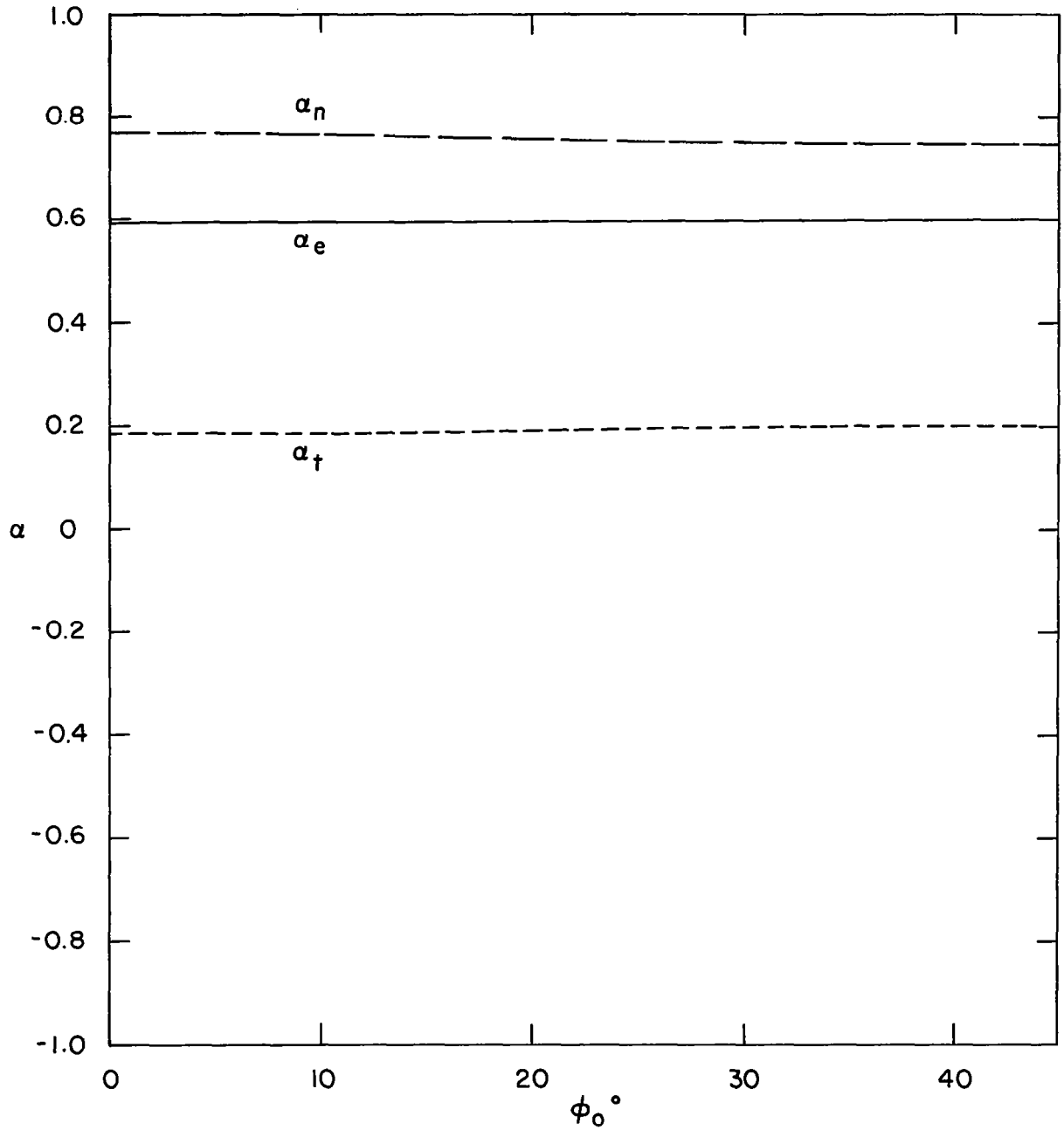

Fig. 6.36 $\alpha(\phi_o)$ for $\mu = 0.9$, $R = 1.3$, S = square, $\theta_o = 135°$

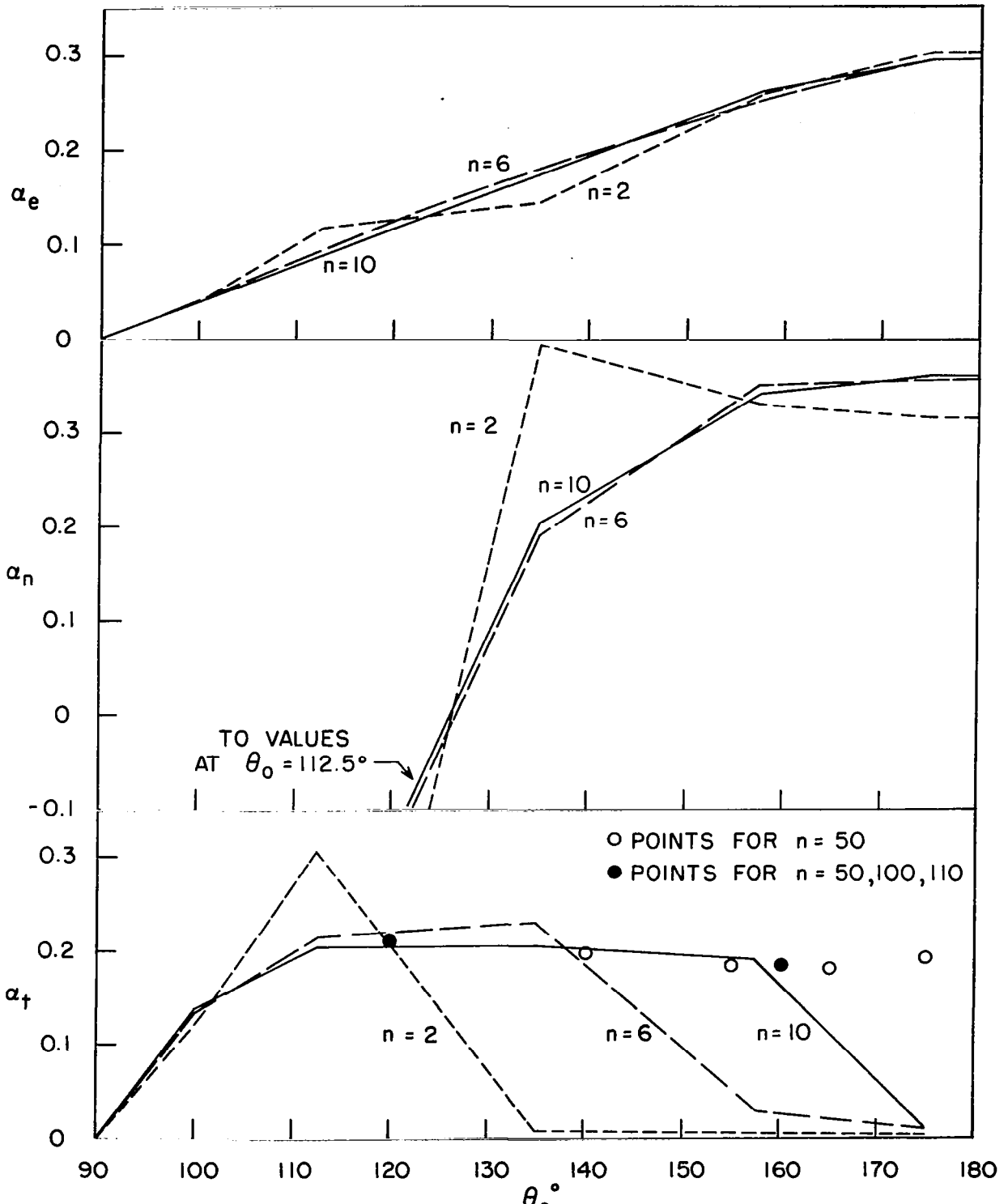

Fig. 7.1 $\alpha(\theta_0, n)$ for $\mu = 0.1$, $R = 1.3$, S = square, $\phi_0 = 0$

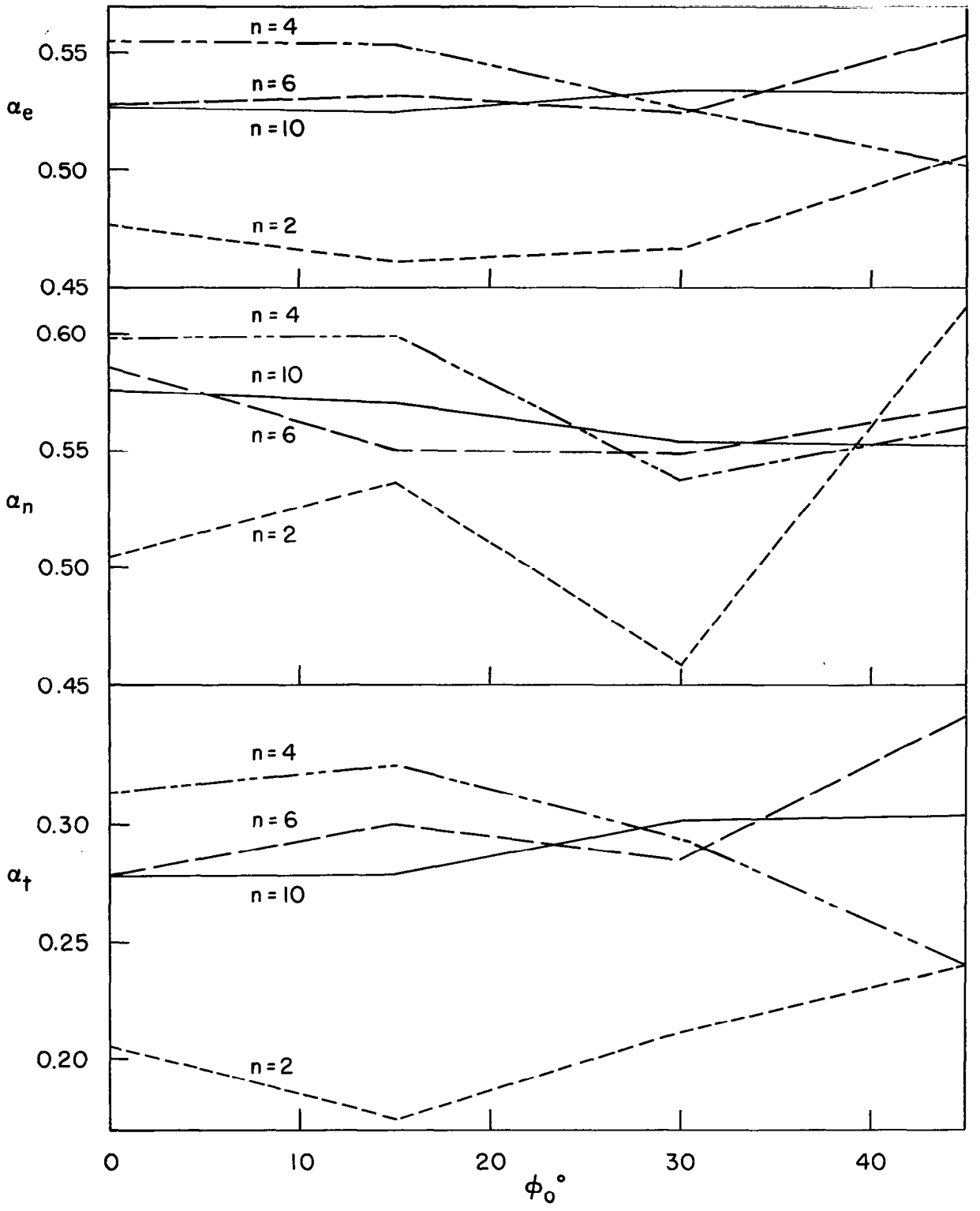

Fig. 7.2 $\alpha(\phi_0, n)$ for $\mu = 0.5$, $R = 1.06$, S = square, $\theta_0 = 135°$

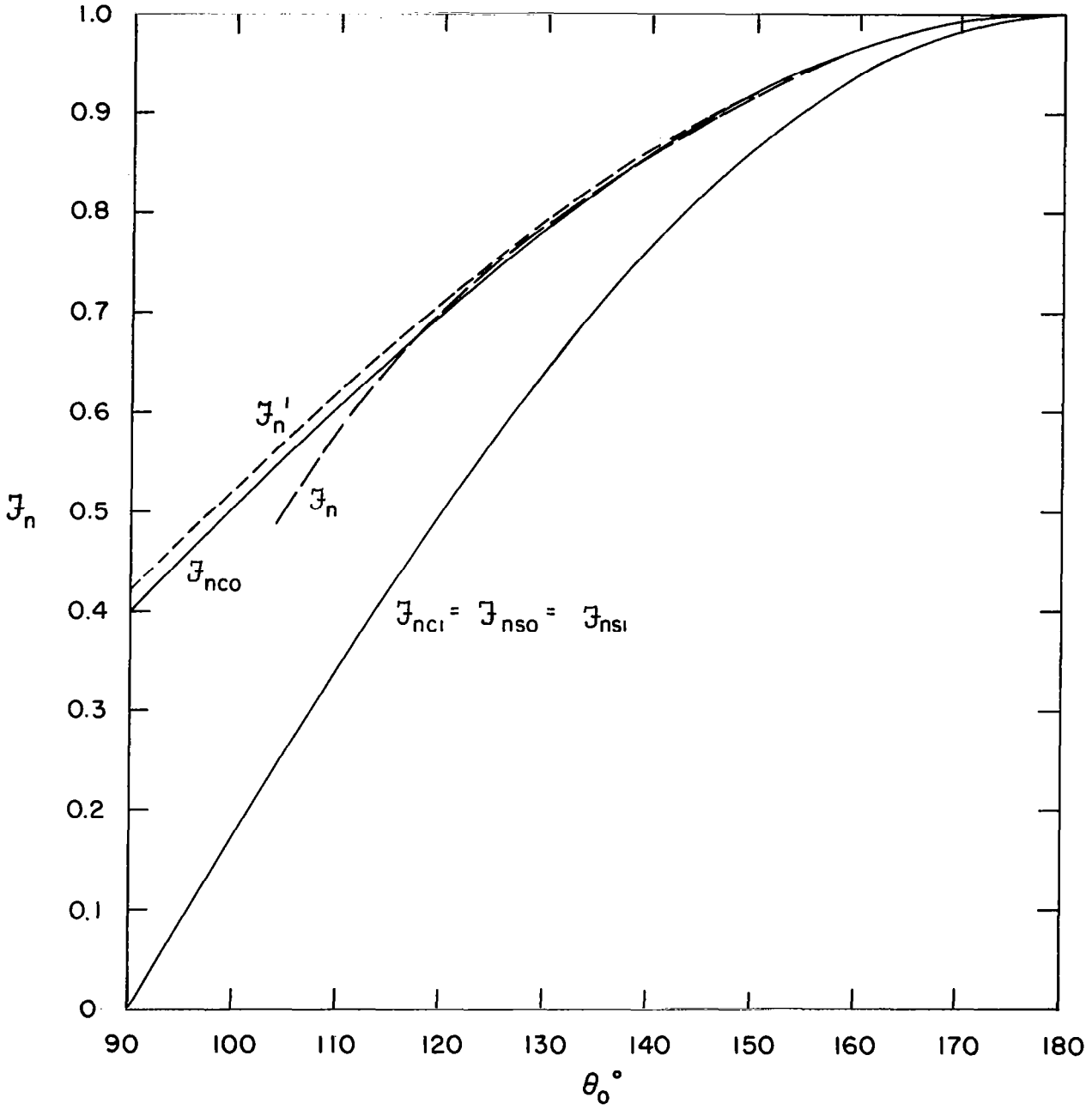

Fig. 8.1 $\mathcal{F}_n(\theta_o)$ for $\mu = 0.1$, R = 0.9, S = square, $\phi_o = 0$

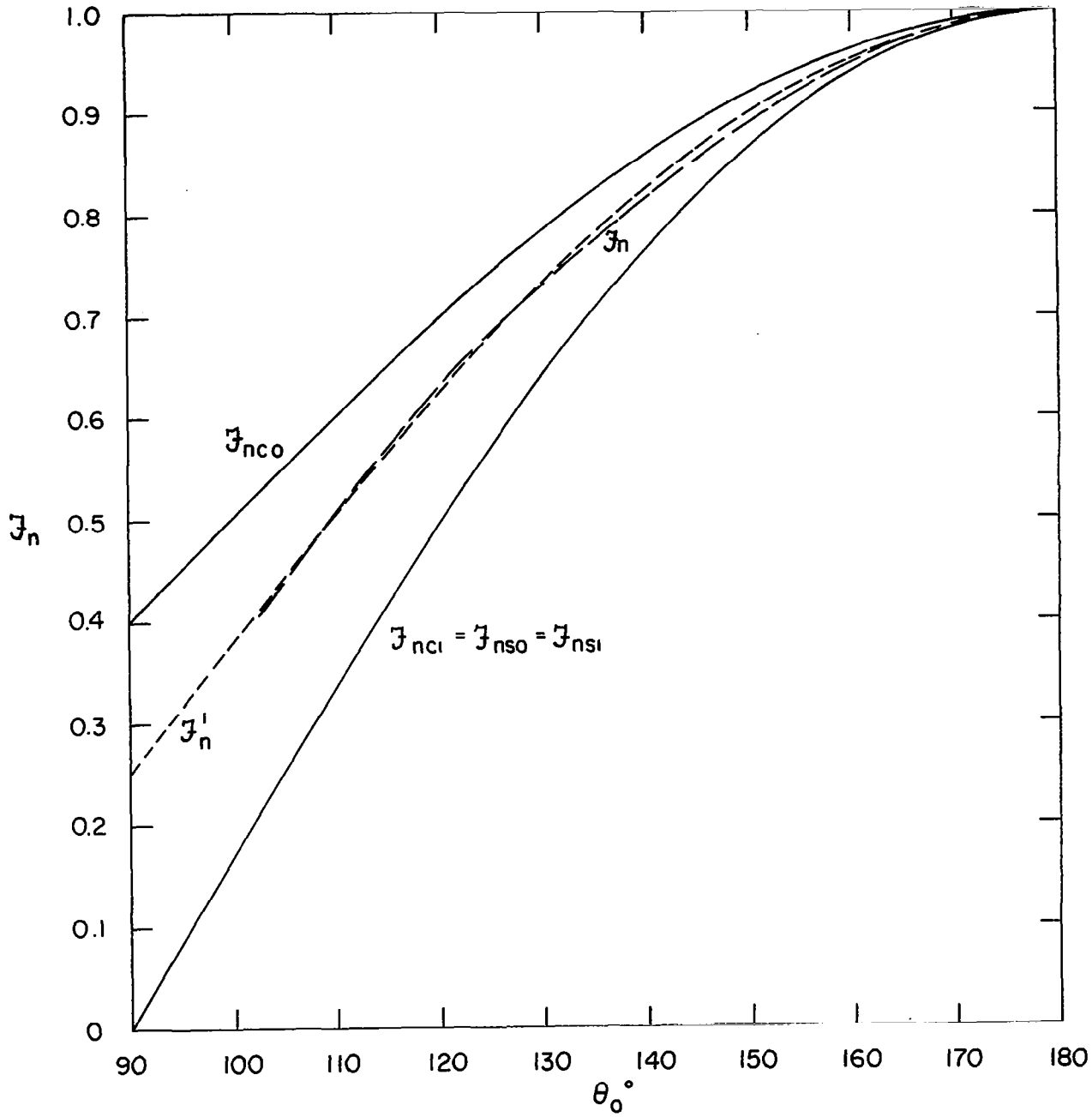

Fig. 8.2 $\mathcal{F}_n(\theta_o)$ for μ = 0.1, R = 1.3, S = square, ϕ_o = 0

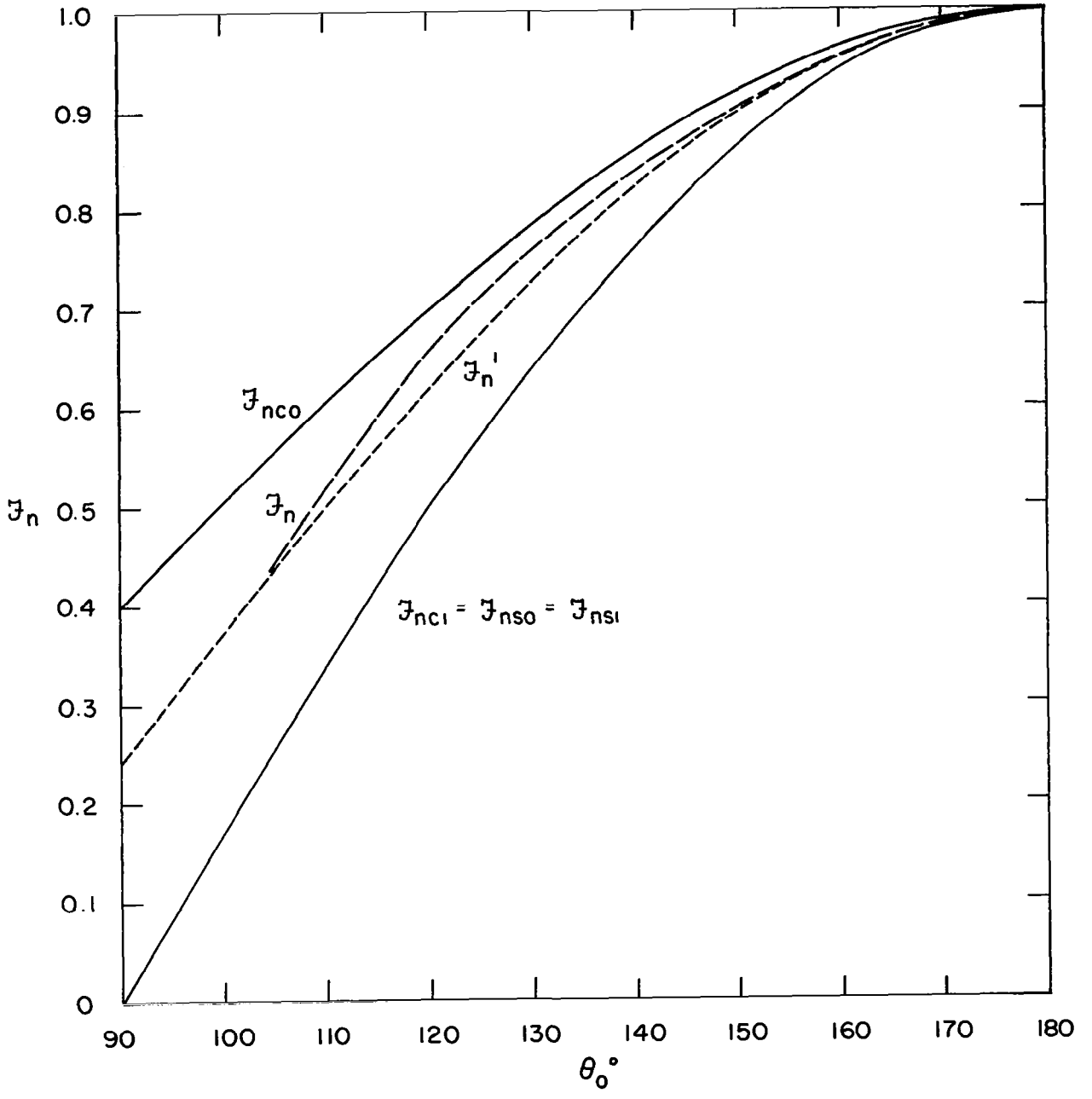

Fig. 8.3 $\mathcal{F}_n(\theta_o)$ for $\mu = 0.9$, R = 0.9, S = square, $\phi_o = 0$

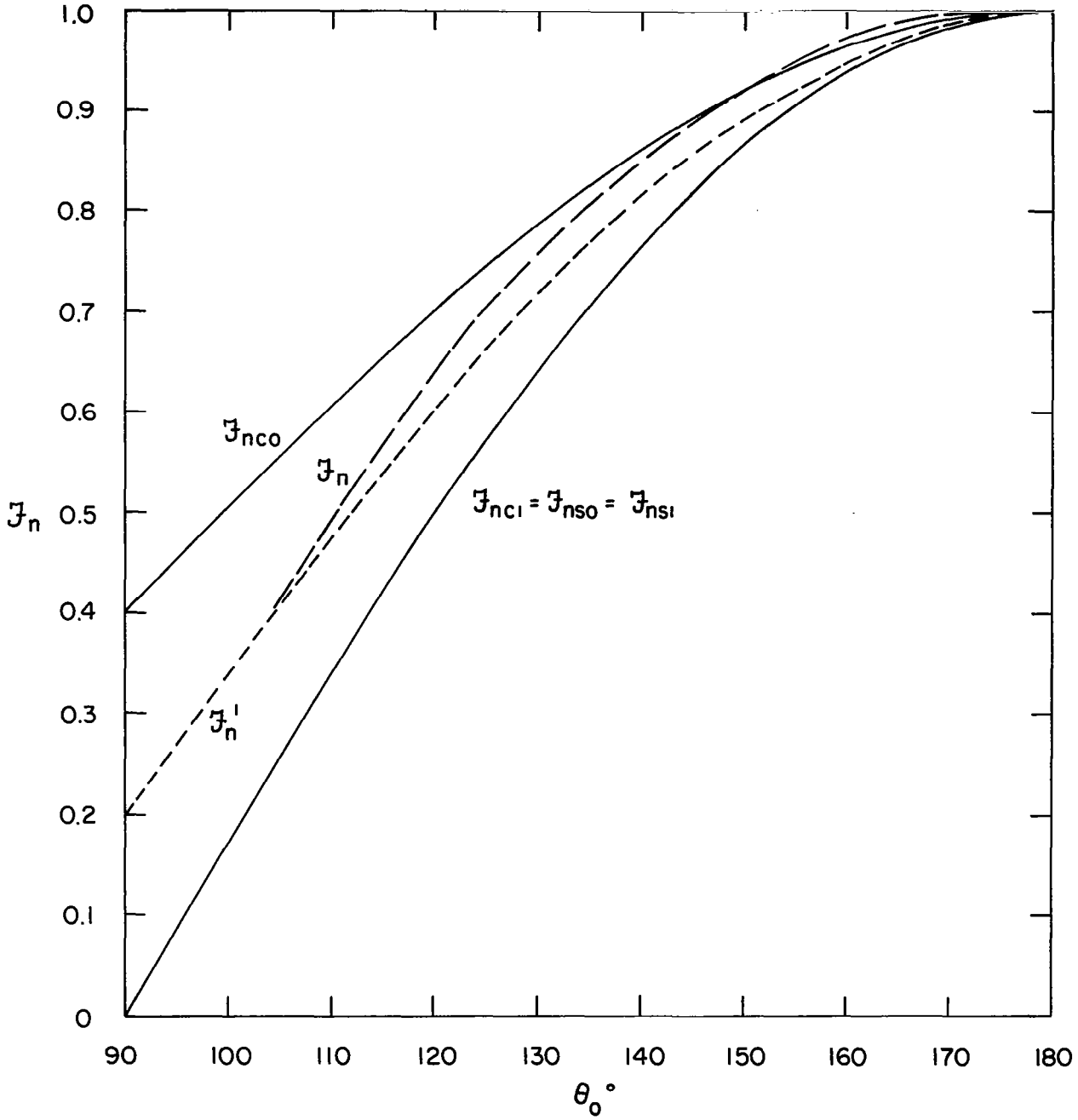

Fig. 8.4 $\mathcal{J}_n(\theta_o)$ for $\mu = 0.9$, R = 1.3, S = square, $\phi_o = 0$

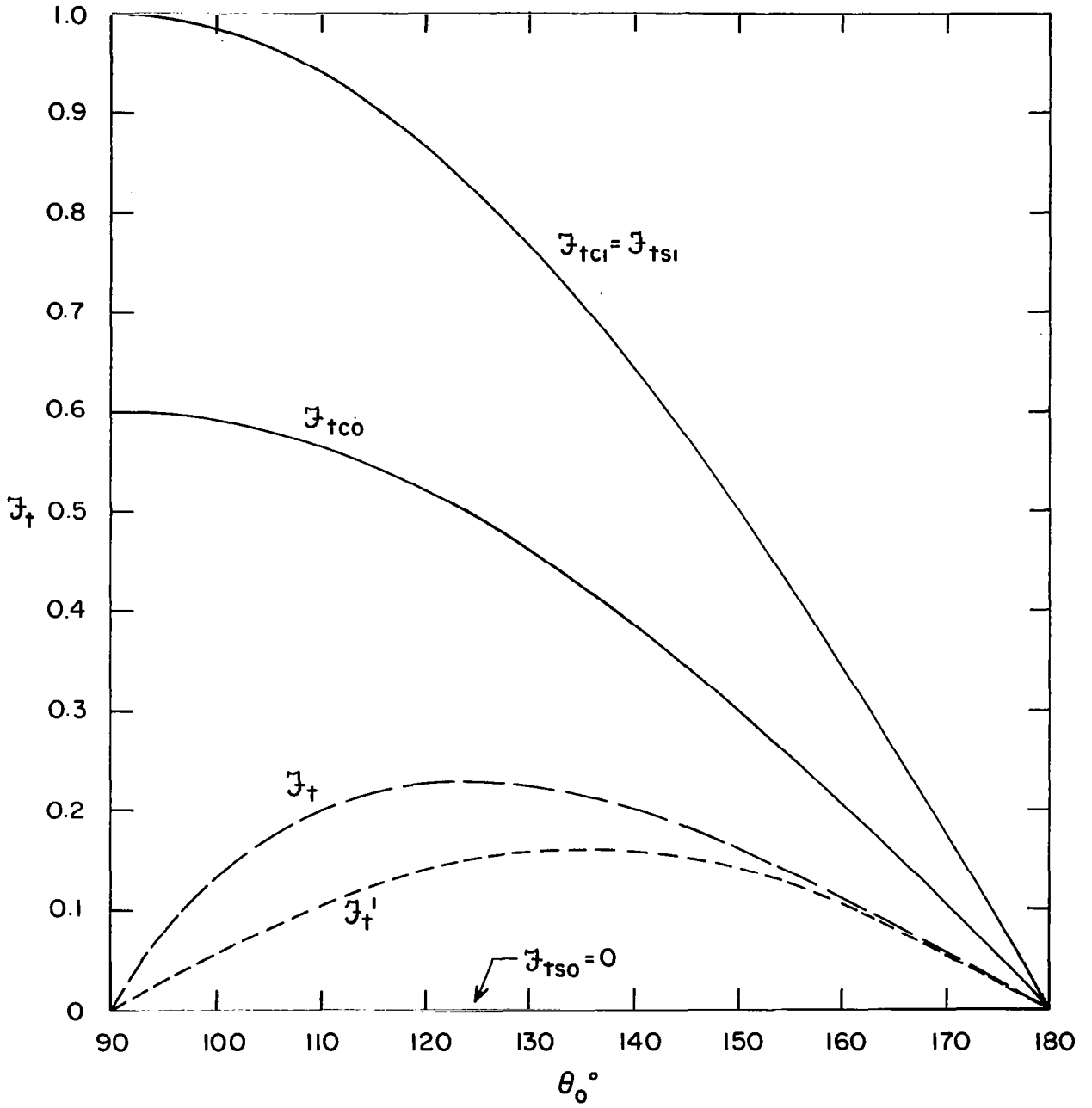

Fig. 8.5 $\mathfrak{F}_t(\theta_o)$ for $\mu = 0.1$, $R = 0.9$, S = square, $\phi_o = 0$

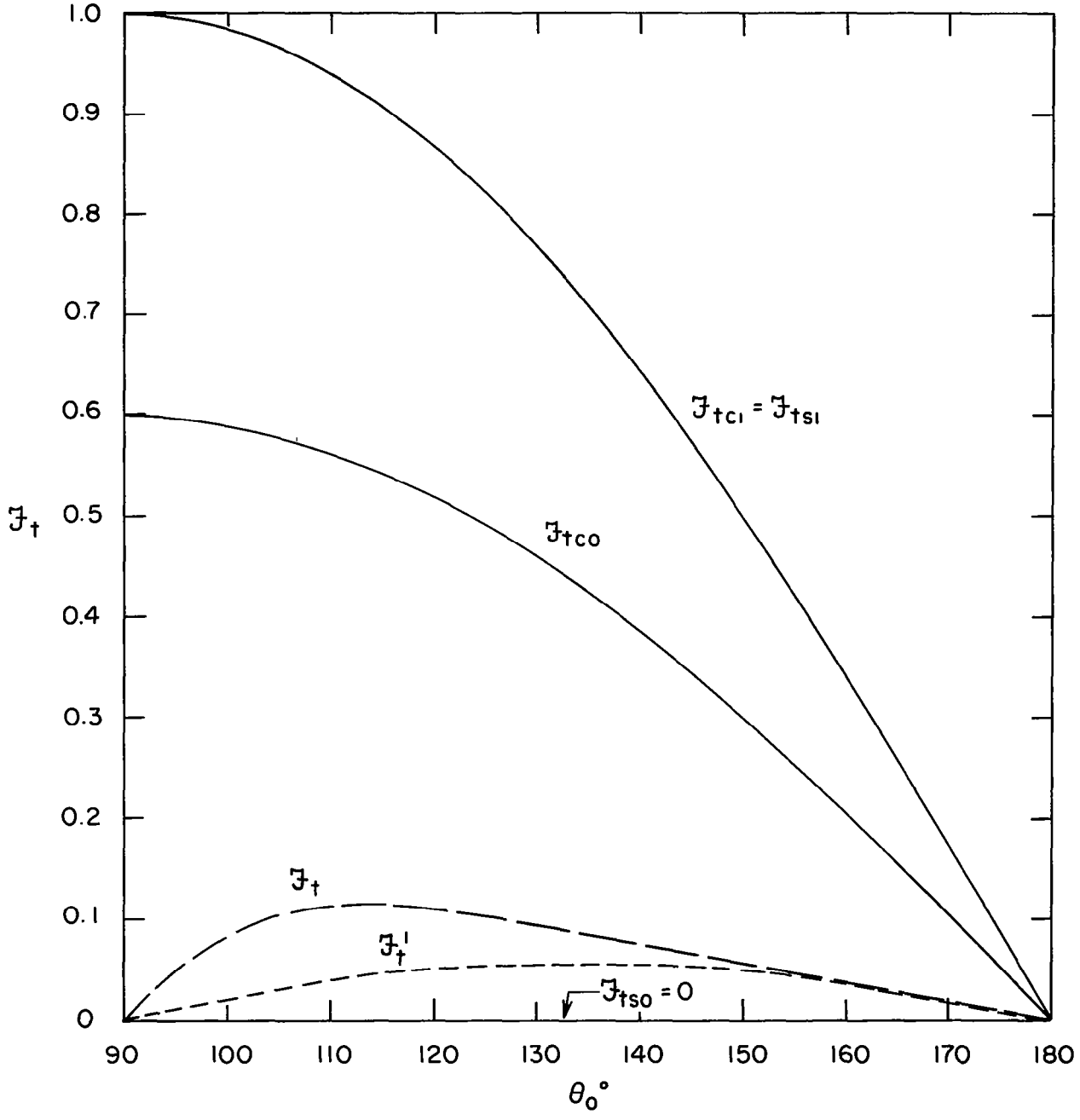

Fig. 8.6 $\mathcal{F}_t(\theta_o)$ for $\mu = 0.1$, R = 1.3, S = square, $\phi_o = 0$

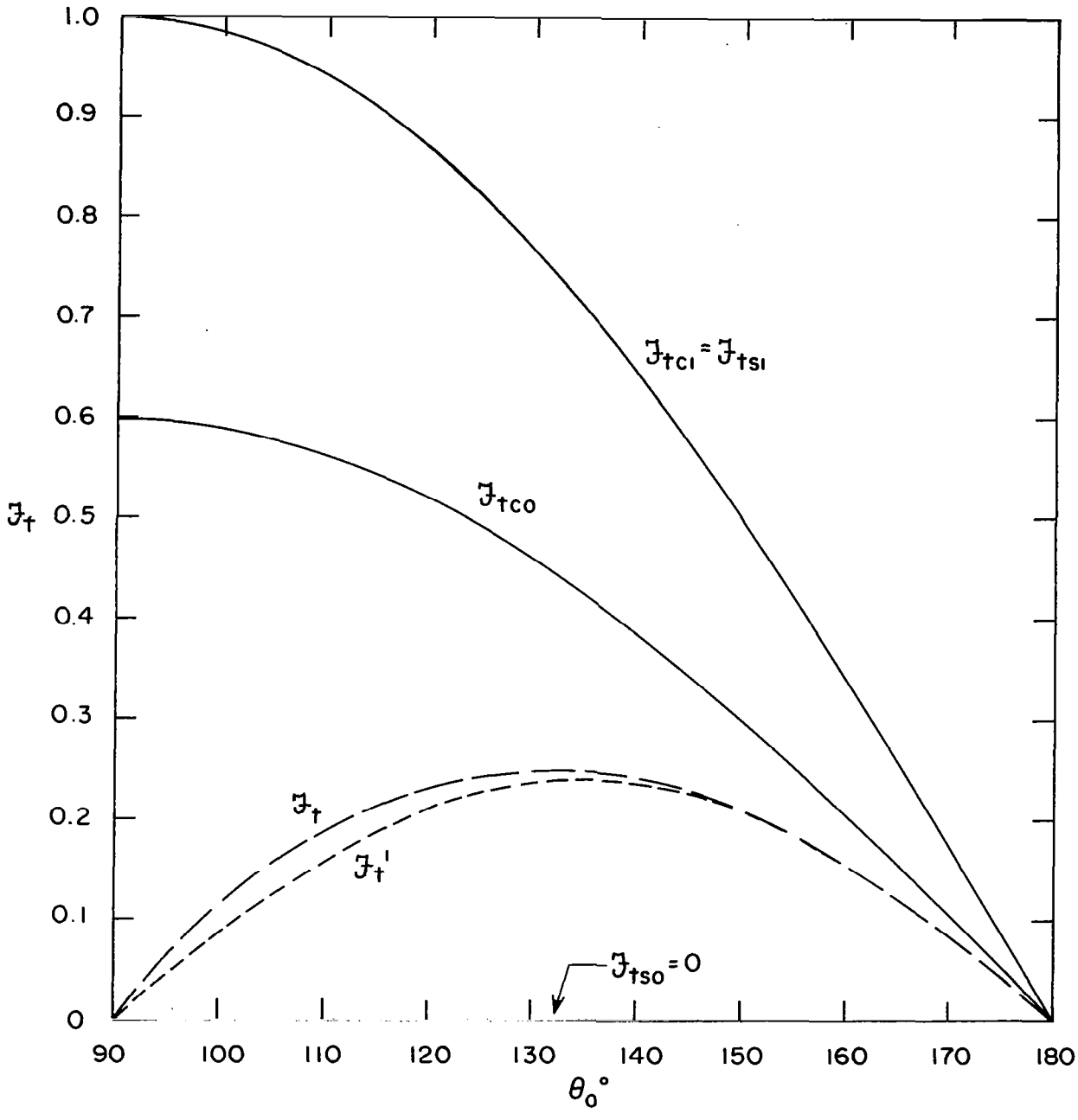

Fig. 8.7 $\mathcal{J}_t(\theta_o)$ for $\mu = 0.9$, $R = 0.9$, S = square, $\phi_o = 0$

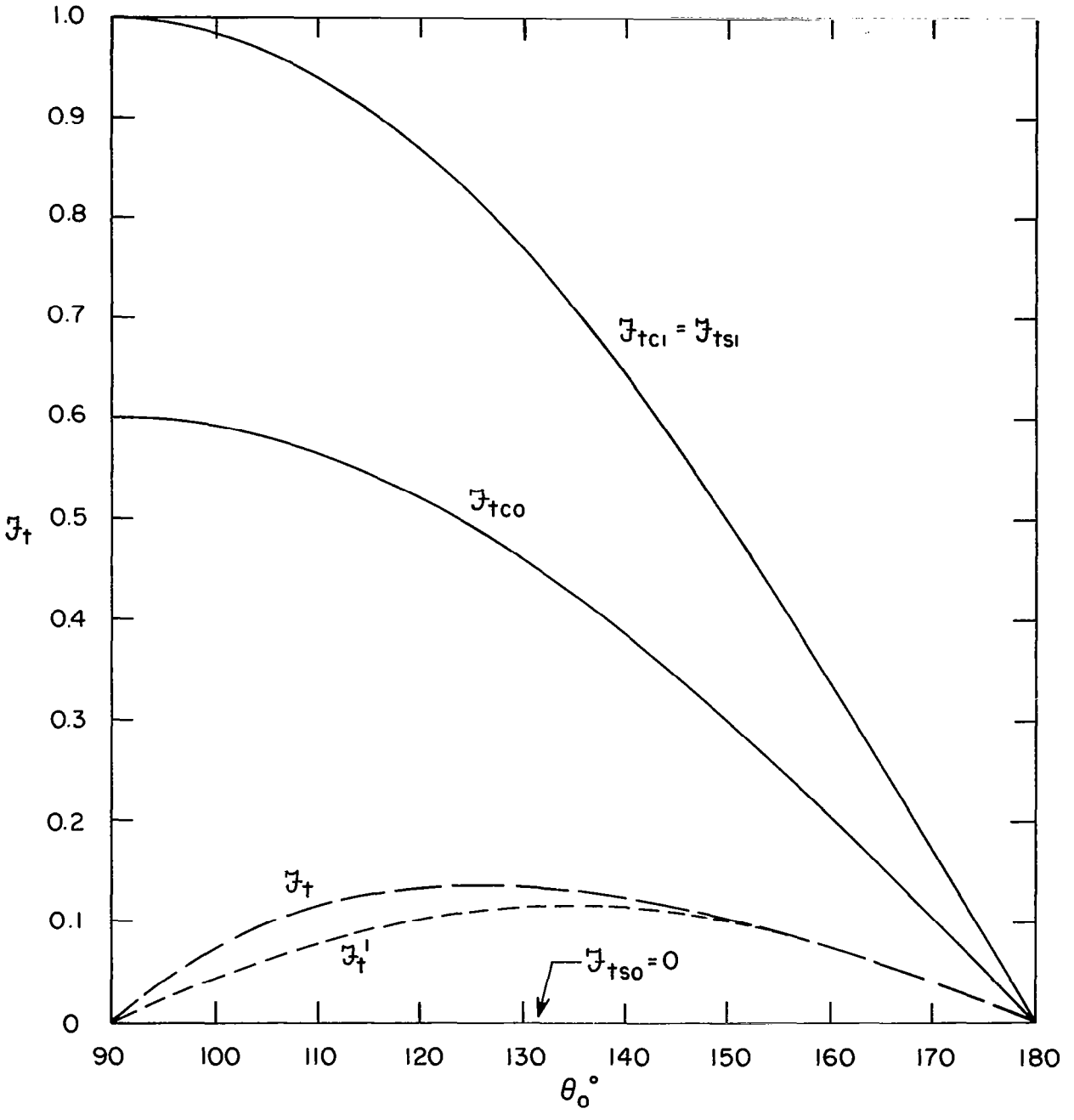

Fig. 8.8 $\mathcal{F}_t(\theta_o)$ for $\mu = 0.9$, R = 1.3, S = square, $\phi_o = 0$

NASA-Langley, 1967 —— 12 CR-933